UNIVERSITA' DEGLI STUDI DI NAPOLI
FEDERICO II

Fabrication And Development of innovative 3D platforms for cell biology by 2-photon lithography

PhD Program in Industrial product and process engineering
XXIX Cycle

Fabrizio Andrea Pennacchio

Supervisor
Prof. Paolo Antonio Netti
Advisor
Dr. Raffaele Vecchione
Coordinator
Prof. Giuseppe Mensitieri

March 2014-March 2017

Table of Contents

CHAPTER 1.
Introduction

In the living tissues cell functions are regulated by a complex set of signals principally provided by the extracellular matrix (ECM) [1][2]. These signals can be mainly divided in physical, chemical and topographic and their nature is strictly correlated to the physical and chemical properties of the ECM.

In order to get a deeper comprehension of the cell behavior and consequently to get a superior control over their fate, it is necessary to design artificial platforms able to replicate, in a biomimetic way, the complex signaling patterns provided by the ECM [1][3].

The creation of these platforms passes through the development of the cell instructive materials (CIMs), which simultaneously integrate multiple signals precisely organized in time and space that affect the cell fate [4]. In this context, a broad spectrum of materials has been processed and used (starting from inorganic materials to natural derived organic polymers). Among all the materials, the polymeric ones, due to their properties adjustability, have been the most widely employed. Thanks to the progresses in the material science and in the micro- and nano-fabrication techniques, nowadays it is in fact possible to modulate the polymers properties matching those of several living tissues. In cell engineering, synthetic, natural and nature derived polymers have been used. In principle, synthetic polymers allow to easier and independently modulate their properties and are then extensively used for the production of highly engineered platforms. On the other hand, even if natural and nature derived polymers intrinsically own some of the ECM properties (then resulting potentially more adequate for many cellular applications), their application is often limited by the difficulties related to their properties tuning [5].

Since the ECM is three dimensional, recent studies have demonstrated that experiments conducted on 2D platforms are not able to fully recapitulate the cell-ECM interactions.[6][7][8][9]. To overcome the limits of 2D platforms in the replication of the ECM 3D characteristics, several micro- and nano-fabrication techniques have been developed [10][11].

Among these techniques, the direct laser writing based on the two-photon polymerization principle (DLW-2PP), gives the possibility to mimic with good fidelity the ECM structures; by means of this technique, in fact, it is possible to realize with high accuracy complex 3D structures with features size also smaller than 100 nm [12]. Another advantage of the DLW-2PP technique is the possibility to process different types of materials and then fabricate 3D constructs resembling the structural and physical features of several tissues.

An important aspect to take into account in the design of cell-instructive platforms is the cell-ECM signaling dynamicity, which has been proved to affect cell behavior [13].For this reason in the last years several efforts have been spent for the development and integration into cell-instructive platforms of materials able to change their properties in response to specific stimuli (stimuli-responsive materials) [14][15][16][17][18].

Bearing in mind the number, specificity and complexity of the ECM signaling in the determination of the cell behavior, it is intuitive that the realization of platforms that comply with all the features of the cell living environment is one of the hardest challenges for bioengineering.

1.1 3D Microfabrication techniques

Processing biomaterials to replicate the complex 3D architecture of the ECM is of fundamental importance in cell engineering applications, where several 3D micro- and nano-fabrication techniques are currently being used

[6][7][8][9][10][11]. Nowadays the additive manufacturing (AM) techniques are the most promising ones, which are based on the layer-by-layer fabrication of 3D structures starting from the cross sections of a Computer Assisted Design (CAD) model [11].

Based on the specific fabrication system, the AM techniques can be classified in nozzle-, printer- and laser-based [19]. The latter is the most advanced, as it allows fabricating complex 3D structures with resolutions even down to 90 nm, while the other two are able to reach at most several micrometers in resolution.[11][20].

In the context of cell engineering, it is known that the ECM structural units show features size down to few nm [21][22][23]. Apparently cells feel and are influenced by structural dimensions down to 35 nm, making the laser-based AM the most suitable class of techniques [24][10].

However, the biggest limitation in using the laser-based techniques is represented by the fabrication time. In general, a higher resolution capability is in fact associated with a long process duration, which generally limits the use of these techniques to the fabrication of platforms covering only few millimiters.

The techniques belonging to the laser-based class are the selective laser sintering (SLS), stereolithography (SLA), micro-stereolithography (μSLA) and the 2PP. The SLS is a thermal technique in which a laser sinters powder materials. Using the actual SLS systems, to date it is impossible to produce components smaller than 500 μm [25].

SLA, μSLA and 2PP are optical techniques where a laser is used to photopolymerize or photocrosslink polymers. In the SLA and μSLA the fabrication of photosensitive materials takes place through the absorption of a single photon, while in the 2PP the simultaneously absorption of two photons occurs [26]. Thanks to the different optical processes involved, the 2PP has a better performance than SLA and μSLA, as it can produce structures with

resolution down to 90 nm, well below the resolution limit of about 1 μm shown by μSLA [11]. Furthermore, the 2PP process allows fabricating any 3D object without structural restrictions; this is due to the fact that the simultaneous absorption of two photons occurs only in the focal spot of the laser, which makes possible to freely structure a specific zone of the material volume [27]. In the SLA and μSLA processes, instead, the absorption of the single photon takes place at the material interface, forcing to build any structure following a layer-by-layer strategy [19]. The physical principles of the DLW-2PP process will be treated in the next sections.

1.2 Photo-polymerization

The photo-polymerization is a process in which a light source with a wavelength (λ) included between the ultraviolet (UV) and the infrared (IR) spectrum interacts with a photosensitive polymer-based material commonly called photoresist. This interaction excites the unsaturated polymer units (monomers or oligomers) that, as a consequence, start to polymerize or crosslink [28]. The widely used radical polymerization is a chain reaction in which reactive species are subsequently added to a molecule to form a polymer chain.

In the photoresist development, it is extremely important to evaluate the photopolymerization quantum yield; this parameter is defined as the ratio between the number of polymerized units and the number of photons needed for the polymerization process. Considering the radical photo-polymerization, because of the nature of the chain reaction, the quantum yield reaches also values of several thousands [29]. For practical purposes, because generally the polymer units are extremely difficult to excite with light, photoinitiators and/or photosensitizers are added to the photoresist

composition; these small molecules are more sensitive than the polymer units to the light sources and promote the photo-polymerization [30][31].

The photoinitiators are molecules that, consequently to the photon absorption, generate reactive species that initiate the polymerization attacking the polymer units. The photosensitizers, instead, transfer a portion of the energy derived from the photon absorption to the photoinitiators that, in turn, initiate the polymerization process [29].

In equation 1 the photo-initiations, polymerization propagation and polymerization termination (via combination or disproportionation) are schematically represented.

Equation 1

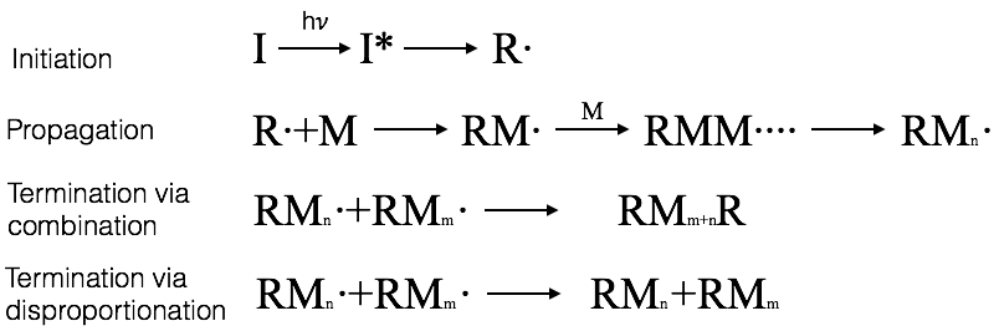

Here the symbols denote the photoinitiator (I), the radical unit (R·) and I* represents an intermediate state of the photoinitiator after the absorption of a photon (Initiation). M is the monomer or oligomer unit, and M_n, the macromolecule containing n monomer units. The photo-produced radicals react with monomers or oligomers producing monomer radicals that combine with new monomers and so on (Propagation); the monomer radicals expand in a chain reaction, until two radicals meet with each other and the reaction is then stopped (Termination).

1.3 2PP process

The 2PP is a process where the photo-polymerization takes place as a consequence of the quasi-simultaneous absorption of two photons. The two-photon absorption (TPA) was theoretically proposed by Göppert-Meyer in 1931 and experimentally demonstrated as a tool for the photo-polymerization only in the 1965, by Pao and Renztepis [29].

In the field of fabrication, both in one- and in two-photon absorption, photosensitive molecules that absorb photons are excited to an energetic state in which they can produce reactive species able to trigger the photo-polymerization. While in the one-photon absorption the excitation takes place in a single step, in the TPA it occurs in two stages, in each of which a single photon is absorbed: in the first step molecules are excited to a virtual energetic state and in the second step they could be further excited to the singlet state [20]. The passage to the singlet state takes place only if the absorption of the second photon occurs within the very short lifetime of the virtual state (10^{-15} s); otherwise molecules come back to the initial not excited energetic state [32] (ground state) (Fig. 1).

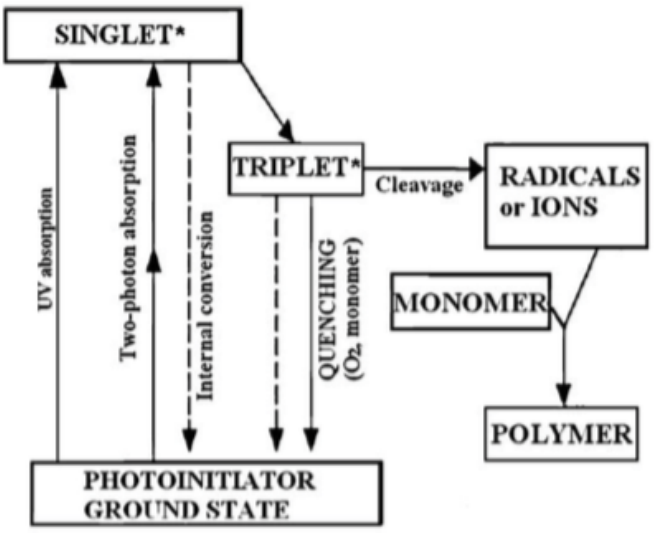

Figure 1: Diagram showing the activation and deactivation pathways of a photo initiator,

Wu et al. [32]. Both single-photon and 2-photon absorption is shown as well as various deactivation pathways and internal conversion to the triplet state via cleavage creating radicals or ions that can initiate polymerization.

Once excited to the singlet state, molecules can come back to the ground energetic state because of some deactivation mechanisms or can produce some reactive species that, passing through the triplet state, trigger the photopolymerization [32] (Fig. 1). To start the 2PP, molecules need to absorb a minimum quantity of energy called polymerization threshold, which value depends upon the photopolymerization quantum yield (see paragraph 1.2) and upon the 2-photon absorption cross section (δ), a parameter that estimates the initiator aptitude in the TPA.

The TPA is a non-linear phenomenon of the third order in which the molecule energy absorption rate, and thus the probability that the TPA takes place, is proportional to the square of the light intensity [33] (Eq.2).

Equation 2

$$\frac{dW}{dt} = \frac{8\pi^2\omega}{c^2n^2} I^2 Im\left[\chi^{(3)}\right]$$

Where ω is the angular frequency, C the speed of light in vacuum, n the refractive index of the medium, I the laser intensity and $[\chi^{(3)}]$ the imaginary part of the third order susceptibility tensor.

In the TPA each photon possesses approximately half of the total energy required to excite the molecules to the singlet state. Compared to the photons involved in the classic UV lithography (one photon absorption), photons used in the 2PP possess half of the energy and double of the λ, then belonging to the infrared (IR) region. Generally, the IR radiation used in the 2PP processes is provided by Ti:Sapphire lasers emitting photons between 700 and 800 nm. The low energy of the IR photons, combined to the quadratic dependence of

the TPA probability with the laser intensity, imply that in the 2PP processes it is necessary to reach very high photon densities and then huge radiation intensities to trigger the polymerization. IR lasers that work in continuous wave (CW) regime cannot achieve the necessary photon density values without thermal damaging the material [12]; due to this physical limitation and to the very limited lifetime of the virtual state, femtoseconds (fs) pulsed IR lasers are used.

Using IR radiations, the minimum photon density needed to trigger the 2PP is achieved only in the laser focal spot, while in the outer regions no radiation absorption occurs. This peculiarity allows selectively polymerizing any region in the photoresist volume simply changing the laser focus; thanks to this possibility, the structural fabrication restrictions related to the other AM techniques can be overpassed, and very complex 3D structures can be then fabricated [32] (Fig.2)

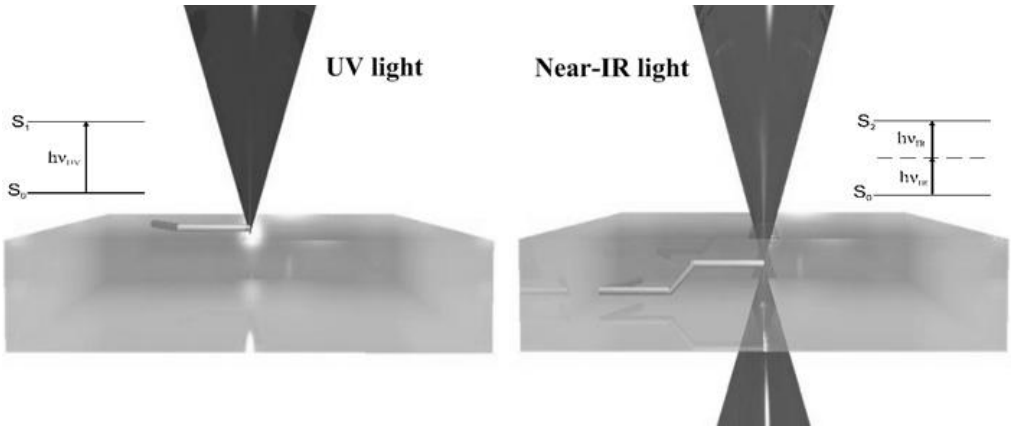

Figure 2: Left, UV light is absorbed at the surface of a photosensitive polymer and can only be used for fabrication of 2D structures. On the right NIR light is focused into the volume of the UV-sensitive resin allowing the 3D fabrication (2PP) [32].

Even though, theoretically, with the 2PP no limitations over the minimum achievable voxel size exist, practically the lowest dimensional limit is

determined by several parameters such as the photoresist photochemical properties, the two-photon system equipment specifications and the process parameters [34].

Furthermore, due to the differences between the axial and lateral components of the laser wave-vector, the voxel shape results elongated along the axial direction and presents an aspect ratio (AR) generally higher than 3 (Fig. 3) [34].

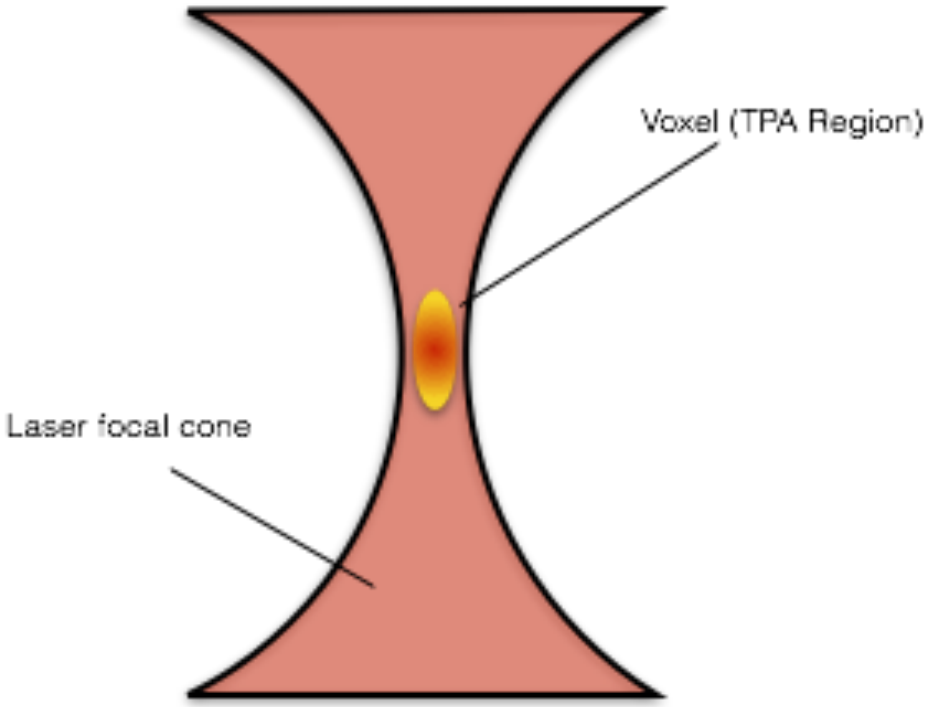

Figure 3: Schematic representation of voxel formed in the focal volume of the IR laser.

The analytical expressions that correlate in the three dimensions the voxel size with the polymer properties and the equipment specifications are reported in equations 3 and 4 [20].

Equation 3

$$\boldsymbol{d(P_t, t, NA)} = \frac{\boldsymbol{\lambda}}{\boldsymbol{\pi \tan\left(sin^{-1}(NA/n)\right)}} \times \left[\boldsymbol{ln}\left(\frac{\boldsymbol{4\pi^2 {P_t}^2 t\left[\tan\left(sin^{-1}\left(\frac{NA}{n}\right)\right)\right]^4}}{\boldsymbol{E_{th}\lambda^4}} \right) \right]^{\boldsymbol{1/2}}$$

Equation 4

$$\boldsymbol{l(P_t, t, NA)} = \frac{\boldsymbol{2\lambda}}{\boldsymbol{\pi\left[\tan\left(sin^{-1}(NA/n)\right)\right]^2}} \times \left[\left(\frac{\boldsymbol{4\pi^2 {P_t}^2 t\left[tan\left(sin^{-1}\left(\frac{NA}{n}\right)\right)\right]^4}}{\boldsymbol{\lambda^4 E_{th}}} \right)^{\boldsymbol{\frac{1}{2}}} - \boldsymbol{1} \right]^{\boldsymbol{\frac{1}{2}}}$$

Where d and l are respectively the voxel diameter and length. E_{th} is the threshold energy for polymerization, P_t the amount of laser power used, λ the laser wavelength, n the refractive index of the medium in which the objective is immersed in, t the exposure time and NA the numerical aperture of the objective used for the polymerization.

The previous equations clearly indicate that the axial voxel dimension is more sensitive to the laser power than to the exposure time; from these relations it is also evident that by opportunely choosing the process parameters it is possible to tune the voxel aspect ratio and, then, improve the 2PP process performance in terms of resolution or speed [20].

In order to decrease the minimum voxel size, more advanced versions of DLW-2PP process have been developed; here the principal ones are the stimulated-emission-depletion (STED) 2PP and the Resolution Augmentation through Photo-induced Deactivation [34]. Both these techniques are based on the concept of the depletion mechanism in which, simultaneously combining different laser sources, it is possible to stop the spatial advancement of the photo-polymerization then limiting the voxel dimensions; employing these innovative approaches voxel size down to 9 nm and resolutions of 52 nm have been achieved [35].

1.4 2PP bio-applications

The capability to produce 2D and 3D complex highly resolute structures and the possibility to process a broad variety of biomaterials in different conditions, have made the DLW-2PP an appealing technology for the development of several bioengineering systems [36][37][38]. DLW-2PP has been used for the fabrication of micro-needles, in microfluidic and micro-robotic applications, in tissue engineering and for the study of cell behavior.

Micro-needles are designed as painless transdermal drug delivery systems. Narayan et al. were the first to fabricate micro-needles by means of the DLW-2PP technology; in a first work they fabricated Ormocomp-based micro-needles able to penetrate the porcine skin [39] and, in a successive work, the human skin penetration was achieved [40].

In microfluidic the DLW-2PP has been used for many and different purposes; the introduction of actuator components [41] [42], the fabrication of entire 3D devices [43] or the insertion of complex 3D structures for the in-chip study of the cell behavior [44], are just some examples of the application of the DLW-2PP in this field. In a microfluidic chip it is possible to finely control several parameters, such as, for example, the fluid flow-rate, the temperature or the solution compositions. In the context of the cell behavior studies this capability could be used to better bio-mimic the cell-environment and then to get a precise control over the cell signaling [45][46]; here the insertion of 3D microstructures through the DLW-2PP technology represents an added value. Following this concept Olsen et al. have for example studied the migration of human dendritic cells in complex micro-topologies towards a chemo-attractant substance [44]. More specifically they have inserted in a commercial chip designed for the chemo-taxis analysis a complex woodpile structure and, varying its pores size, they have systematically evaluated the effect on cellular migration.

In the last years, the DLW-2PP technique has been used in the micro-robotic [47][48][49][50]. Here, because of the observed strong correlation between the object shape and motion, it is fundamental to precisely shape materials on the sub-micrometric scale. Huang et al. have realized magnetic-sensitive helical micro-swimmers demonstrating that very little design variations strongly affect the micro-objects motion [51]. These types of platforms have been used to transport and move different objects ranging from lipoplexes for gene delivery [49], to entire scaffolds for cells cultures [48].

Innovative cell-instructive platforms have been fabricated through the DLW-2PP technology [37]. Scheiwe et al. have for example realized a 2-component system to study the cell reactions to specific mechanical stimuli. First, they have controlled the cell shape precisely positioning cell adhesive sites on non-adhesive 3D structures trough a complex 2-steps lithography process [52]; once fixed the cell shape, they have employed an AFM tip to deform the structures and then evaluate the cell reactions (Fig.4) [53].

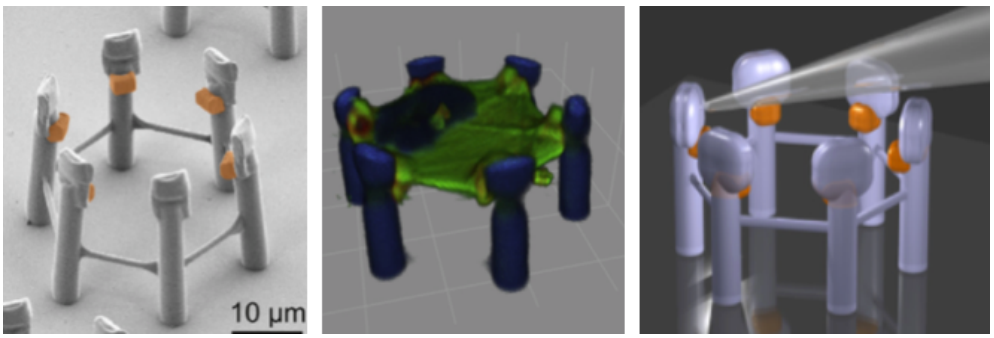

Figure 4: On the left an image of the 2-component scaffold: the grey pillars are made of Polyethilenglicole diacrylate (PEG-DA) and are cell-repellent, while the orange structures are made of Ormocomp, a photoresist able to adsorb fibronectin which then promotes cell-adhesion [53]. In the center a 3D reconstruction of a cell adhered selectively on the adhesive anchorage points is reported. In the image on the right is showed an AFM tip that deforms the structure in a controlled way.

Hohmann et al. have studied the influence of the 3D topography on the differentiation and proliferation of osteoblast-like cells [54]. Precisely controlling the 3D structures geometry they have identified the topographical parameters that in a 3D environment influence the cell shape and proliferation, thus providing important information useful for the design of *in-vivo* implants.

Marino et al. have fabricated a 3D scaffold replicating the natural trabecula architecture (Fig.5) [55] that, compared to the other scaffolds present in the literature, has strongly enhanced the cell proliferation and osteogenesis processes.

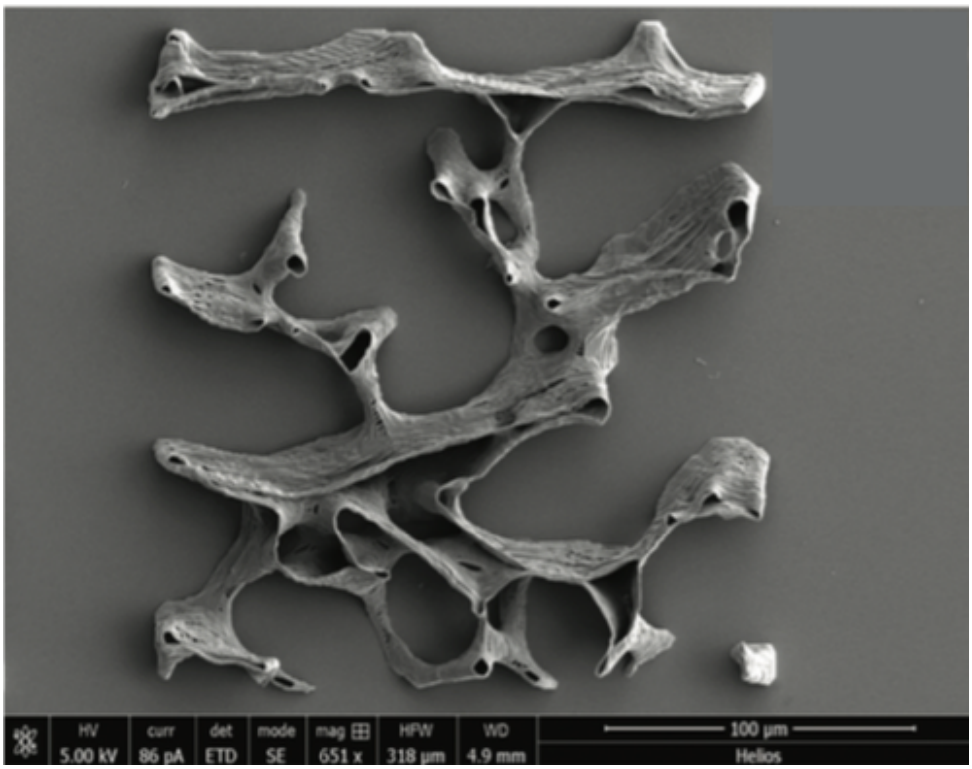

Figure 5: SEM image of the trabecula scaffold fabricated by Marino et al. [55]

1.5 Hydrogel for DLW-2PP

Hydrogels are polymeric materials formed by a 3D intricate network of hydrophilic units connected through chemical or physical crosslinks; as a consequence, hydrogels can absorb high quantities of water without dissolving [56][57].

Hydrogels are generally biocompatible, allow the diffusion of oxygen and nutrients and present tunable mechanical properties that often match with those of several living tissues [58].

Actually this class of materials, because of the capability to replicate several properties of the ECM, is considered as the most promising one for cell engineering applications [59][60]; basically hydrogels are divided in synthetic, natural and nature derived, which are obtained by chemical or physical treatment of natural polymers.

Natural hydrogels are biocompatible, biodegradable and generally encourage cell adhesion without the need of any specific treatment or functionalization. On the other hand natural hydrogels often suffer of low mechanical properties that limit their use in the fabrication of stable microstructures; moreover, generally, their chemical, mechanical and topographic properties cannot be independently tuned [61][62][63].

Synthetic hydrogels can be easily engineered and offer, unlike the natural ones, the opportunity to tune independently the spatio-temporal distribution of their physiochemical properties [5]. Generally, these materials lack of biodegradability and bioactivity, that could be however introduced through chemical functionalization [63].

In the last twenty years, the DLW-2PP technology has been frequently employed for the hydrogel processing [64][65], starting in most cases from natural hydrogels, due to their cell-friendly properties. The pioneering work conduced by Campagnola et al. [66][67] allowed for the first time to obtain

the photo-polymerization of Bovine Serum Albumine (BSA) by means of a 2PP system. The same group, later, optimized the 3D micro-fabrication of other natural hydrogels and proteins such as collagen I, fibrinogen, fibronectin and concavanalin A [68].

To overcome the limitations related to the fabrication and engineering of natural hydrogels, more advanced synthetic or nature derived ones have been developed [65].

Among synthetic hydrogels, PEG-DA has been one of the most used in its pure form or also in combination with other photosensitive polymers. As the greatest part of synthetic hydrogels, pure PEG-DA lacks bioactivity and biodegradability; to overcome these restrictions PEG-DA has been chemically doped with different cell adhesive and biodegradable peptides [69][63].

As an alternative to the realization of synthetic materials, nature derived hydrogels can be also specifically treated and modified to better match the requirements of the DLW-2PP fabrication processes [64]. Here, one of the most common strategies has been to increase the polymer cross-linking degree introducing photo-polymerizable functionalities in the polymer chain. One example of these modified materials is gelatin, which has been modified and for the first time fabricated with a DLW-2PP system by Ovsianikov et al. to obtain complex 3D scaffolds for the seeding of mesenchymal stem cells [70].

1.6 Gelatin

Gelatin is a hydrogel obtained from the partial hydrolysis and denaturation of collagen. During this process the collagen triple helix structure is broken and the polymer chains form a random coil [71] (Fig.6).

Because of its derivation, gelatin is an appealing material for several biomedical applications; it is in fact biodegradable, pro-angiogenic and non-immunogenic, it exhibits low levels of cytotoxicity and presents all the collagen cell adhesive motifs. In addition, compared to collagen, gelatin is more soluble, less antigenic and is less structurally polydisperse [72].

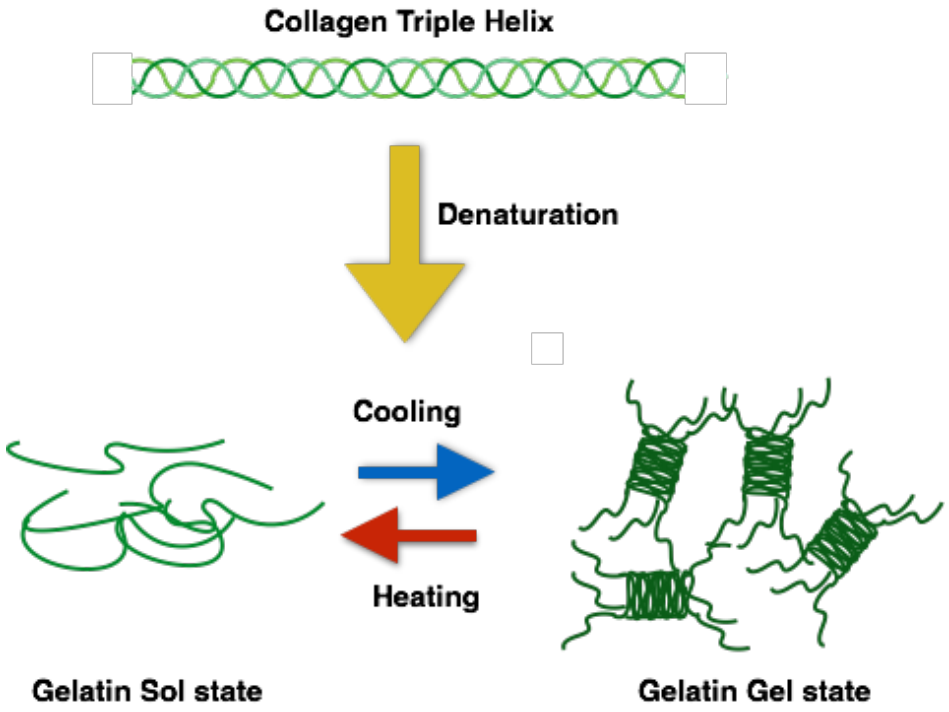

Figure 6: Schematic representation of the gelatin formation from collagen denaturation.

In its natural form, at 37°C, gelatin shows a sol-gel transition that prohibits its use as a scaffold for any cellular application. To solve this problem several crosslinking methods have been developed [73][74][75][76].

In this context, one of the possibilities is to photo-crosslink a chemically modified gelatin in which methacrylic or acrylic groups substitute a part (≤5%) of the native gelatin amino acids motifs ((Meth)acrylamide gelatin); because of the very low substitution degree, most of the native gelatin amino

acids related properties, such as for example the biodegradability and the cell adhesiveness, are preserved [72]. Differently from the other crosslinking methods, the photo-crosslinking allows to spatio-temporally control the polymerization reaction and then to create unique patterns and 3D structures to guide the cellular behavior [72].

In tissue engineering the (Meth)acrylamide gelatin has been used in many circumstances; it has been used, for example, to promote the cell vascularization in 3D environments [77], as a bone scaffold [78] and for the production of epidermis-type tissues [79].

To expand its spectrum of application, the (Meth)acrylamide gelatin has been used also as a composite material. As an example, in combination with gold nanoparticles, it has strongly influenced the regeneration of bone tissues and has promoted the differentiation of adipose derived stem cells towards the osteoblast lineage [80]. Shin et al. have added carbon nanotubes to the modified gelatin improving its electrical conductibility and then enhancing the cardiac cells adhesion, organization and cell-cell coupling [81]. Together with hyaluronic acid derivatives the (Meth)acrylamide gelatin has shown good potentialities also in promoting the development of scaffolds for cartilage tissues [82].

1.7 Aim of the work

The hard processing conditions of natural and nature-derived hydrogels, whose potential in cellular applications is well established, strongly limit their employment in the realization of advanced systems for guiding cells behavior.

In this thesis we aim to expand gelatin use by proposing new different approaches for the development of innovative platforms for specific cell engineering applications.

In Chapter 2 we define the composition of a gelatin-based photoresist to fabricate complex and high resolute microstructures with our 3D lithography system based on the DLW-2PP process (Nanoscribe Professional GT).

In Chapter 3 gelatin is engineered in order to fabricate instructive microstructures that undergo a deformation in response to a light stimulation; following this strategy we develop a gelatin-based platform for the positioning and mechanical stimulation of cells.

In Chapter 4 we fabricate gelatin instructive building blocks designed to guide, with specific topographic patterns, the production of anisotropic oriented microtissues for tissue engineering applications. To this end, because of its low fabrication speed, we use the Nanoscribe only as a rapid prototyping technique to test the efficiency of the aforementioned topographic signal. Once demonstrated the importance of the topography in determining the micro-tissue orientation, we propose a droplet microfluidic device for the massive production of tubular gelatin patterned emulsions.

Final conclusions and future perspectives, with some parameters that still need to be optimized, are synthetically presented and discussed in Chapter 5.

References

[1] E. S. Place, N. D. Evans, and M. M. Stevens, “Complexity in biomaterials for tissue engineering,” *Nat. Publ. Gr.*, vol. 8, no. 6, pp. 457–470, 2009.

[2] M. M. Stevens and J. H. George, “Exploring and Engineering the Cell Surface Interface,” 2005.

[3] A. M. Ross, Z. Jiang, M. Bastmeyer, and J. Lahann, “Physical aspects of cell culture substrates: Topography, roughness, and elasticity,” *Small*, vol. 8, no. 3, pp. 336–355, 2012.

[4] M. Ventre and P. A. Netti, “Engineering Cell Instructive Materials to Control Cell Fate and Functions through Material Cues and Surface Patterning,” *ACS Appl. Mater. Interfaces*, vol. 8, no. 24, pp. 14896–14908, 2016.

[5] M. Ventre and P. Netti, “Controlling Cell Functions and Fate with Surfaces and Hydrogels: The Role of Material Features in Cell Adhesion and Signal Transduction,” *Gels*, vol. 2, no. 1, p. 12, 2016.

[6] S. M. Oliveira, R. L. Reis, and J. F. Mano, “Towards the design of 3D multiscale instructive tissue engineering constructs: Current approaches and trends,” *Biotechnol. Adv.*, vol. 33, no. 6, pp. 842–855, 2015.

[7] F. Pampaloni, E. G. Reynaud, and E. H. K. Stelzer, “The third dimension bridges the gap between cell culture and live tissue,” vol. 8, no. october, pp. 839–845, 2007.

[8] L. G. Griffith and M. A. Swartz, “Capturing complex 3D tissue physiology in vitro,” vol. 7, no. March, pp. 211–224, 2006.

[9] C. Biosensors, R. Edmondson, J. J. Broglie, A. F. Adcock, and L. Yang, “Three-Dimensional Cell Culture Systems and Their Applications in Drug Discovery and Cell-Based Biosensors,” vol. 12,

no. 4, pp. 207–218, 2014.

[10] F. P. W. Melchels, J. Feijen, and D. W. Grijpma, “A review on stereolithography and its applications in biomedical engineering,” *Biomaterials*, vol. 31, no. 24, pp. 6121–6130, 2010.

[11] M. Vaezi, H. Seitz, and S. Yang, “A review on 3D micro-additive manufacturing technologies,” *Int. J. Adv. Manuf. Technol.*, vol. 67, no. 5–8, pp. 1721–1754, 2013.

[12] F. Jipa, Marian Zamfirescu, A. Velea, M. Popescu, and R. Dabu, “Femtosecond Laser Lithography in Organic and Non-Organic Materials,” *Updat. Adv. Lithogr.*, pp. 65–94, 2013.

[13] C. Bonnans, J. Chou, and Z. Werb, “Remodelling the extracellular matrix in development and disease I E r,” *Nat. Publ. Gr.*, vol. 15, no. 12, pp. 786–801, 2014.

[14] A. M. Rosales and K. S. Anseth, “The design of reversible hydrogels to capture extracellular matrix dynamics,” *Nat. Publ. Gr.*, vol. 1, no. February, pp. 1–16, 2016.

[15] H. Guo, Z. Li, S. Dong, W. Chen, L. Deng, Y. Wang, and D. Ying, “Colloids and Surfaces B : Biointerfaces Piezoelectric PU / PVDF electrospun scaffolds for wound healing applications,” *Colloids Surfaces B Biointerfaces*, vol. 96, pp. 29–36, 2012.

[16] C. 27 C.de Las Heras Alarcon, S. Pennadam, and C. Alexander, “Stimuli responsive polymers for biomedical applications.,” *Chem. Soc. Rev.*, vol. 34, no. 3, pp. 276–285, 2005.

[17] M. a C. Stuart, W. T. S. Huck, J. Genzer, M. Müller, C. Ober, M. Stamm, G. B. Sukhorukov, I. Szleifer, V. V Tsukruk, M. Urban, F. Winnik, S. Zauscher, I. Luzinov, and S. Minko, “Emerging applications of stimuli-responsive polymer materials.,” *Nat. Mater.*, vol. 9, no. 2, pp. 101–113, 2010.

[18] B. Jeong and A. Gutowska, “Lessons from nature: Stimuli-responsive polymers and their biomedical applications,” *Trends Biotechnol.*, vol. 20, no. 7, pp. 305–311, 2002.

[19] T. Billiet, M. Vandenhaute, J. Schelfhout, S. Van Vlierberghe, and P. Dubruel, “A review of trends and limitations in hydrogel-rapid prototyping for tissue engineering,” *Biomaterials*, vol. 33, no. 26, pp. 6020–6041, 2012.

[20] K. S. Lee, R. H. Kim, D. Y. Yang, and S. H. Park, “Advances in 3D nano/microfabrication using two-photon initiated polymerization,” *Prog. Polym. Sci.*, vol. 33, no. 6, pp. 631–681, 2008.

[21] D. H. Kim, P. P. Provenzano, C. L. Smith, and A. Levchenko, “Matrix nanotopography as a regulator of cell function,” *J. Cell Biol.*, vol. 197, no. 3, pp. 351–360, 2012.

[22] K. Kulangara and K. W. Leong, “Substrate topography shapes cell function,” *Soft Matter*, vol. 5, no. 21, pp. 4072–4076, 2009.

[23] M. Nikkhah, F. Edalat, S. Manoucheri, and A. Khademhosseini, “Engineering microscale topographies to control the cell-substrate interface,” *Biomaterials*, vol. 33, no. 21, pp. 5230–5246, 2012.

[24] F. P. W. Melchels, M. A. N. Domingos, T. J. Klein, J. Malda, P. J. Bartolo, and D. W. Hutmacher, “Additive manufacturing of tissues and organs,” *Prog. Polym. Sci.*, vol. 37, no. 8, pp. 1079–1104, 2012.

[25] D. W. Hutmacher, “Scaffold-based Tissue Engineering – Design and Fabrication of Matrices Using Solid Freeform Fabrication Techniques,” *Adv. Manuf. Technol. Med. Appl.*, 2006.

[26] M. T. Raimondi, S. M. Eaton, M. M. Nava, M. Laganà, G. Cerullo, and R. Osellame, “Two-photon laser polymerization: from fundamentals to biomedical application in tissue engineering and regenerative medicine.,” *J. Appl. Biomater. Funct. Mater.*, vol. 10, no. 1, pp. 55–65, 2012.

[27] A. Selimis, V. Mironov, and M. Farsari, “Direct laser writing: Principles and materials for scaffold 3D printing,” *Microelectron. Eng.*, vol. 132, pp. 83–89, 2014.

[28] W. Schnabel, *Part III Light-induced synthesis of polymers*. 2007.

[29] H. B. Sun and S. Kawata, “Two-photon photopolymerization and 3D lithographic microfabrication,” *Adv. Polym. Sci.*, vol. 170, pp. 169–273, 2004.

[30] B. M. Monroe and G. C. Weed, “Photoinitiators for free-radical-initiated photoimaging systems,” *Chem. Rev.*, vol. 93, no. 1, pp. 435–448, 1993.

[31] J. P. Fouassier, D. Ruhlmann, B. Graff, and F. Wieder, “New insights in photosensitizers-photoinitiators interaction,” *Prog. Org. Coatings*, vol. 25, no. 2, pp. 169–202, 1995.

[32] S. Wu, J. Serbin, and M. Gu, “Two-photon polymerisation for three-dimensional micro-fabrication,” *J. Photochem. Photobiol. A Chem.*, vol. 181, no. 1, pp. 1–11, 2006

.

[33] J. D. Bhawalkar, G. S. He, and P. N. Prasad, “Nonlinear multiphoton processes in organic and polymeric materials,” *Reports Prog. Phys.*, vol. 60, no. 6, p. 689, 1997.

[34] J. Fischer and M. Wegener, “Three-dimensional optical laser lithography beyond the diffraction limit,” *Laser Photonics Rev.*, vol. 7, no. 1, pp. 22–44, 2013.

[35] Z. Gan, Y. Cao, R. a Evans, and M. Gu, “Three-dimensional deep sub-diffraction optical beam lithography with 9 nm feature size,” *Nat. Commun.*, vol. 4, no. May, p. 2061, 2013.

[36] K. C. Hribar, P. Soman, J. Warner, P. Chung, and S. Chen, “Light-assisted direct-write of 3D functional biomaterials.,” *Lab Chip*, vol. 14, no. 2, pp. 268–75, 2014.

[37] A. Marino, C. Filippeschi, V. Mattoli, B. Mazzolai, and G. Ciofani, “Biomimicry at the nanoscale: current research and perspectives of two-photon polymerization,” *Nanoscale*, vol. 7, no. 7, pp. 2841–2850, 2015.

[38] C. M. B. Ho, S. H. Ng, K. H. H. Li, and Y.-J. Yoon, “3D printed microfluidics for biological applications,” *Lab Chip*, vol. 15, no. 18, pp. 3627–3637, 2015.

[39] A. Doraiswamy, C. Jin, R. J. Narayan, P. Mageswaran, P. Mente, R. Modi, R. Auyeung, D. B. Chrisey, A. Ovsianikov, and B. Chichkov, “Two photon induced polymerization of organic-inorganic hybrid biomaterials for microstructured medical devices,” *Acta Biomater.*, vol. 2, no. 3, pp. 267–275, 2006.

[40] L. Z. Hannover, P. Mente, N. Carolina, a Doraiswamy, and R. J. Narayan, “Two Photon Polymerization of Polymer – Ceramic Hybrid Materials for Transdermal Drug Delivery,” *Int. J. Appl. Ceram. Technol*, vol. 29, pp. 22–29, 2007.

[41] Y. Ding, F. Qiu, X. Casadevall i Solvas, F. W. Y. Chiu, B. J. Nelson, and A. De Mello, “Microfluidic-based droplet and cell manipulations using artificial bacterial flagella,” *Micromachines*, vol. 7, no. 2, pp. 1–13, 2016.

[42] J. van ‘t Oever, N. Spannenburg, H. Offerhaus, D. van den Ende, J. Herek, and F. Mugele, “In-chip direct laser writing of a centimeter-scale acoustic micromixer,” *J. Micro/Nanolithography, MEMS, MOEMS*, vol. 14, no. 2, p. 23503, 2015.

[43] B.-B. Xu, Y.-L. Zhang, H. Xia, W.-F. Dong, H. Ding, and H.-B. Sun, “Fabrication and multifunction integration of microfluidic chips by femtosecond laser direct writing,” *Lab Chip*, vol. 13, pp. 1677–1690, 2013.

[44] M. H. Olsen, G. M. Hjortø, M. Hansen, Ö. Met, I. M. Svane, N. B.

Larsen, “In-chip fabrication of free-form 3D constructs for directed cell migration analysis,” *Lab Chip*, vol. 13, no. 24, p. 4800, 2013.

[45] S. N. Bhatia and D. E. Ingber, “Microfluidic organs-on-chips,” *Nat. Biotechnol.*, vol. 32, no. 8, pp. 760–772, 2014.

[46] S. M. Kim, S. H. Lee, and K. Y. Suh, “Cell research with physically modified microfluidic channels: A review,” *Lab a Chip - Miniaturisation Chem. Biol.*, vol. 8, no. 7, pp. 1015–1023, 2008.

[47] H. Zeng, P. Wasylczyk, C. Parmeggiani, D. Martella, and M. Burresi, “Light-Fueled Microscopic Walkers,” pp. 3883–3887, 2015.

[48] S. Kim, F. Qiu, S. Kim, A. Ghanbari, C. Moon, L. Zhang, B. J. Nelson, and H. Choi, “Fabrication and characterization of magnetic microrobots for three-dimensional cell culture and targeted transportation,” *Adv. Mater.*, vol. 25, no. 41, pp. 5863–5868, 2013.

[49] F. Qiu, S. Fujita, R. Mhanna, L. Zhang, B. R. Simona, and B. J. Nelson, “Magnetic Helical Microswimmers Functionalized with Lipoplexes for Targeted Gene Delivery,” *Adv. Funct. Mater.*, vol. 25, no. 11, pp. 1666–1671, 2015.

[50] C. Peters, O. Ergeneman, P. D. W. García, M. Müller, S. Pané, B. J. Nelson, and C. Hierold, “Superparamagnetic twist-type actuators with shape-independent magnetic properties and surface functionalization for advanced biomedical applications,” *Adv. Funct. Mater.*, vol. 24, no. 33, pp. 5269–5276, 2014.

[51] T. Y. Huang, F. Qiu, H. W. Tung, X. B. Chen, B. J. Nelson, and M. S. Sakar, “Generating mobile fluidic traps for selective three-dimensional transport of microobjects,” *Appl. Phys. Lett.*, vol. 105, no. 11, 2014.

[52] F. Klein, B. Richter, T. Striebel, C. M. Franz, G. Von Freymann, M. Wegener, and M. Bastmeyer, “Two-component polymer scaffolds for controlled three-dimensional cell culture,” *Adv. Mater.*, vol. 23, no. 11, pp. 1341–1345, 2011.

[53] A. C. Scheiwe, S. C. Frank, T. J. Autenrieth, M. Bastmeyer, and M. Wegener, “Subcellular stretch-induced cytoskeletal response of single fibroblasts within 3D designer scaffolds,” *Biomaterials*, vol. 44, pp. 186–194, 2015.

[54] J. K. Hohmann and G. Von Freymann, “Influence of Direct Laser Written 3D Topographies on Proliferation and Differentiation of Osteoblast-Like Cells: Towards Improved Implant Surfaces,” *Adv. Funct. Mater.*, vol. 24, no. 42, pp. 6573–6580, 2014.

[55] A. Marino, C. Filippeschi, G. G. Genchi, V. Mattoli, B. Mazzolai, and G. Ciofani, “The Osteoprint: A bioinspired two-photon polymerized 3-D structure for the enhancement of bone-like cell differentiation,” *Acta Biomater.*, vol. 10, no. 10, pp. 4304–4313, 2014.

[56] N. Annabi, A. Tamayol, J. A. Uquillas, M. Akbari, L. E. Bertassoni, C. Cha, G. Camci-Unal, M. R. Dokmeci, N. A. Peppas, and A. Khademhosseini, “25th anniversary article: Rational design and applications of hydrogels in regenerative medicine,” *Adv. Mater.*, vol. 26, no. 1, pp. 85–124, 2014.

[57] J. L. Drury and D. J. Mooney, “Hydrogels for tissue engineering: Scaffold design variables and applications,” *Biomaterials*, vol. 24, no. 24, pp. 4337–4351, 2003.

[58] A. Sivashanmugam, R. Arun Kumar, M. Vishnu Priya, S. V. Nair, and R. Jayakumar, “An overview of injectable polymeric hydrogels for tissue engineering,” *Eur. Polym. J.*, vol. 72, pp. 543–565, 2015.

[59] S. R. Caliari and J. A. Burdick, “A practical guide to hydrogels for cell culture.,” *Nat. Methods*, vol. 13, no. 5, pp. 405–14, 2016.

[60] D. Seliktar, “Designing Cell-Compatible Hydrogels,” *Science (80-.).*, vol. 336, no. June, pp. 1124–1129, 2012.

[61] I. Jun, S. J. Kim, E. Choi, K. M. Park, T. Rhim, J. Park, K. D. Park, and H. Shin, “Preparation of Biomimetic Hydrogels with Controlled Cell Adhesive Properties and Topographical Features for the Study of

Muscle Cell Adhesion and Proliferation," *Macromol. Biosci.*, vol. 12, no. 11, pp. 1502–1513, 2012.

[62] S. Park and K. M. Park, "Engineered polymeric hydrogels for 3D tissue models," *Polymers (Basel).*, vol. 8, no. 1, 2016.

[63] J. Zhu, "Bioactive modification of poly(ethylene glycol) hydrogels for tissue engineering," *Biomaterials*, vol. 31, no. 17, pp. 4639–4656, 2010.

[64] J. Torgersen, X. H. Qin, Z. Li, A. Ovsianikov, R. Liska, and J. Stampfl, "Hydrogels for two-photon polymerization: A toolbox for mimicking the extracellular matrix," *Adv. Funct. Mater.*, vol. 23, no. 36, pp. 4542–4554, 2013.

[65] A. I. Ciuciu and P. J. Cywiński, "Two-photon polymerization of hydrogels-versatile solutions to fabricate well-defined 3D structures," *RSC Adv.*, vol. 4, no. 85, pp. 45504–45516, 2014.

[66] S. Multiphoton, F. Fabrication, J. D. Pitts, P. J. Campagnola, G. A. Epling, and S. L. Goodman, "Submicron Multiphoton Free-Form Fabrication of Proteins and Polymers: Studies of Reaction Efficiencies and Applications in Sustained Release," pp. 1514–1523, 2000.

[67] J. Pitts, a Howell, R. Taboada, I. Banerjee, J. Wang, S. Goodman, and P. Campagnola, "New Photoactivators for Multiphoton Excited Three-dimensional Submicron Cross-linking of Proteins: Bovine Serum Albumin and Type 1 Collagen¶†," *Photochem. Photobiol.*, vol. 76, no. 2, pp. 135–144, 2002.

[68] K. Gomi, M. Kanazashi, D. Lickorish, T. Arai, and J. E. Davies, "Bone marrow genesis after subcutaneous delivery of rat osteogenic cell-seeded biodegradable scaffolds into nude mice," *J. Biomed. Mater. Res. - Part A*, vol. 71, no. 4, pp. 602–607, 2004.

[69] M. W. Tibbitt, A. M. Kloxin, K. U. Dyamenahalli, and K. S. Anseth, "Controlled two-photon photodegradation of PEG hydrogels to study

and manipulate subcellular interactions on soft materials," *Soft Matter*, vol. 6, no. 20, p. 5100, 2010.

[70] A. Ovsianikov, A. Deiwick, S. Van Vlierberghe, P. Dubruel, L. Möller, G. Drager, and B. Chichkov, "Laser fabrication of three-dimensional CAD scaffolds from photosensitive gelatin for applications in tissue engineering," *Biomacromolecules*, vol. 12, no. 4, pp. 851–858, 2011.

[71] M. E. Hoque, T. Nuge, T. K. Yeow, N. Nordin, and R. G. S. V Prasad, "Gelatin Based Scaffolds for Tissue Engineering – a Review," *Polym. Res. J.*, vol. 9, no. 1, 2014.

[72] K. Yue, G. Trujillo-de Santiago, M. M. Alvarez, A. Tamayol, N. Annabi, and A. Khademhosseini, "Synthesis, properties, and biomedical applications of gelatin methacryloyl (GelMA) hydrogels," *Biomaterials*, vol. 73, pp. 254–271, 2015.

[73] W. E. Hennink and C. F. van Nostrum, "Novel crosslinking methods to design hydrogels," *Adv. Drug Deliv. Rev.*, vol. 64, no. SUPPL., pp. 223–236, 2012.

[74] H. C. Liang, W. H. Chang, H. F. Liang, M. H. Lee, and H. W. Sung, "Crosslinking structures of gelatin hydrogels crosslinked with genipin or a water-soluble carbodiimide," *J. Appl. Polym. Sci.*, vol. 91, no. August, pp. 4017–4026, 2004.

[75] J. Y. Lai, "Biocompatibility of chemically cross-linked gelatin hydrogels for ophthalmic use," *J. Mater. Sci. Mater. Med.*, vol. 21, no. 6, pp. 1899–1911, 2010.

[76] J. Y. Lai and Y. T. Li, "Evaluation of cross-linked gelatin membranes as delivery carriers for retinal sheets," *Mater. Sci. Eng. C*, vol. 30, no. 5, pp. 677–685, 2010.

[77] Y. C. Chen, R. Z. Lin, H. Qi, Y. Yang, H. Bae, J. M. Melero-Martin, and A. Khademhosseini, "Functional human vascular network generated in photocrosslinkable gelatin methacrylate hydrogels," *Adv.*

Funct. Mater., vol. 22, no. 10, pp. 2027–2039, 2012.

[78] H. Kang, Y.-R. V Shih, Y. Hwang, C. Wen, V. Rao, T. Seo, and S. Varghese, "Mineralized gelatin methacrylate-based matrices induce osteogenic differentiation of human induced pluripotent stem cells.," *Acta Biomater.*, vol. 10, no. 12, pp. 4961–70, 2014.

[79] X. Zhao, Q. Lang, L. Yildirimer, Z. Y. Lin, W. Cui, N. Annabi, K. W. Ng, M. R. Dokmeci, A. M. Ghaemmaghami, and A. Khademhosseini, "Photocrosslinkable Gelatin Hydrogel for Epidermal Tissue Engineering," *Adv. Healthc. Mater.*, vol. 5, no. 1, pp. 108–118, 2016.

[80] D. N. Heo, W.-K. Ko, M. S. Bae, J. B. Lee, D.-W. Lee, W. Byun, C. H. Lee, E.-C. Kim, B.-Y. Jung, and I. K. Kwon, "Enhanced bone regeneration with a gold nanoparticle–hydrogel complex," *J. Mater. Chem. B*, vol. 2, no. 11, p. 1584, 2014.

[81] S. R. Shin, S. M. Jung, M. Zalabany, K. Kim, P. Zorlutuna, S. B. Kim, M. Nikkhah, M. Khabiry, M. Azize, J. Kong, K. T. Wan, T. Palacios, M. R. Dokmeci, H. Bae, X. Tang, and A. Khademhosseini, "Carbon-nanotube-embedded hydrogel sheets for engineering cardiac constructs and bioactuators," *ACS Nano*, vol. 7, no. 3, pp. 2369–2380, 2013.

[82] W. Schuurman, P. A. Levett, M. W. Pot, P. R. van Weeren, W. J. A. Dhert, D. W. Hutmacher, F. P. W. Melchels, T. J. Klein, and J. Malda, "Gelatin-methacrylamide hydrogels as potential biomaterials for fabrication of tissue-engineered cartilage constructs," *Macromol. Biosci.*, vol. 13, no. 5, pp. 551–561, 2013

.

CHAPTER 2.
DLW-2PP of Photosensitive Gelatin

2.1 Introduction

The most common micro-fabrication techniques used to process (Meth)acrylamide gelatin are photopatterning [1], microfluidic [2], micromolding [3] and bioprinting [4]. Among these techniques, the DLW-2PP lithography, as photopatterning technique, offers the possibility to create the most complex and resolute 3D geometries (see paragraph 1.4) and, because of these potentialities, its application in the fabrication of hydrogel is in continuous development [5][6].

Ovsianikov et al. have applied for the first time the 2PP technology to pattern the methacrylate gelatin, showing the remarkable potentialities of this approach in a cellular study [7]. In their first work, by defining the material porosity and micro-topography, they developed a complex instructive 3D scaffold that supported the adhesion, proliferation and differentiation of porcine mesenchimal stem cells towards the osteogenic lineage.

Up to now, only Billiet et al. have modified gelatin with acrylic functionalities instead of the methacrylic ones [8]; in their work they have demonstrated that the acrylic motifs improve the mechanical properties and UV reactivity of the obtained material. However, acrylic functionalities are potentially more toxic than the methacrylic ones, even though they did not reduce too much cell viability (>90%) in the cell-laden constructs.

On the other hand, because of its nature derivation, the photopatterning of gelatin by means of the DLW-2PP technique presented several critical issues [5]; one of these in particular is the low CAD reproducibility due to the

resolution losses and to the swelling related deformations. In this context, Hoorick et al. have presented a new approach in which the methacrylate gelatin is further modified to increase its crosslinking degree [9]; more specifically, they substituted a part of the carboxylic acid motifs with amino-ethyl-methacrylate functionalities that, in turn, are involved in the photo-polymerization process. The results showed an evident improvement of the CAD reproducibility, also when employing low percentage of gelatin solution; furthermore the material resulted more reactive to the light, completely biodegradable and apparently cytocompatible.

These studies demonstrate the importance to engineer the material according to the specific process and application. In line with this observation here we have adapted an in-house synthetized acrylate gelatin-based photoresist to the Nanoscribe system for the fabrication of complex 3D innovative platforms for cell or tissue engineering applications. In this section we show the characterization of the material, the optimization of the photoresist composition and of the process writing parameters for the fabrication of complex 3D microstructures with feature sizes down to 1μm.

2.2 Materials and methods

2.2.1 Acrylamide Gelatin Synthesis

Gelatin type B (Bloom strength of 225 g, Sigma) isolated from bovine skin, acrylic acid N-hydroxysuccinimide ester (Aldrich) and 4-Methoxyphenol (MeHQ) (Sigma-Aldrich) were used as received. Starting from a protocol reported by Billiet at al. [8], gelatin was chemically modified with acrylic side groups. After dissolution of 1 g of gelatin in phosphate buffer (pH 7.8) at 40 °C, 0.19, 0.38, 0.57 and 0.76 mmol of acrylic acid *N*-hydroxysuccinimide (NHS)-ester and 46 ppm of MeHQ were added while vigorously stirring. After 1 h, the reaction mixture was diluted and dialyzed for 48 h against

distilled water at 40 °C. The reaction product was then freeze-dried leading to a white fluffy solid. The degree of functionalization was verified using ^{1}H-NMR spectroscopy at 40 °C.

2.2.2 Azobenzene synthesis

Azobenzene 1 was synthesized by an already reported protocol [10][11]. Azobenzene 1 (30 mg, 0.111 mmol) was dissolved in dichloromethane (CH_2Cl_2) and 74 µl of triehtylamine (TEA) at room temperature. Then 2.4 equiv. of 1-Hydroxybenzotriazole hydrate (HOBt·H_2O), 2.4 equiv. of *N*-(3-dimethylaminopropyl)-*N*′-ethylcarbodiimide hydrochloride (EDC·HCl) and 2.4 equiv. of compound 2 were added and left reacting overnight (Figure 1). The reaction was followed by thin layer chromatography (TLC) and the product was extracted in dichloromethane. The product was purified by column chromatography. The product formation was confirmed by Mass Spectrometry. MS (ESI): m/z calculated for $C_{36}H_{54}N_6O_{10}$: 731.39 $[M+H]^+$; found: 731.40. After that, compound 3 was treated for 2 hours with a solution of 50/50 v/v trifluoroacetic acid (TFA) in CH_2Cl_2 to remove the Boc protecting group, then co-evaporated with toluene and treated with TEA. Finally, Boc-deprotected compound 3 was reacted with 2.4 equiv. of acrylic acid (197 mmol, 14.2 mg), 2.4 equiv. of HOBt·H_2O, 2.4 equiv. of EDC·HCl and 4.8 equiv. of TEA. The reaction was followed by thin layer chromatography (TLC). The product was purified by column chromatography. The product formation was confirmed by Mass Spectrometry and characterized by UV/Vis spectrophotometry (see Chapter 3, paragraph 3.3.2) MS (ESI): m/z calculated for $C_{32}H_{42}N_6O_8$: 639.39 $[M+H]^+$; found: 639.31.

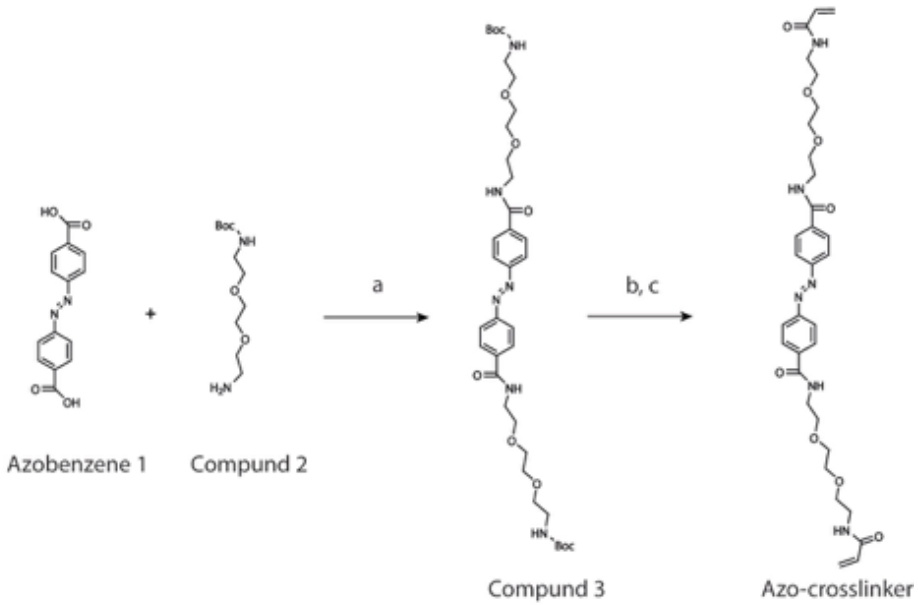

Figure 1: Synthetic scheme of Azo-crosslinker. Reaction conditions: a) 0.111 mmol of azobenzene 1, 4.8 equiv. of TEA, 2.4 equiv. of HOBt·H_2O, 2.4 equiv. EDC·HCl and 2.4 equiv. of compound 2, overnight at room temperature. b) TFA/CH_2Cl_2 50/50 v/v for 2 hours to remove the Boc protecting group. After the reaction it was treated with TEA and co-evaporated with toluene. c) Boc-deprotected compound 3 was reacted with 2.4 equiv. of acrylic acid, 2.4 equiv. of HOBt·H_2O, 2.4 equiv. of EDC·HCl and 4.8 equiv. of TEA overnight at room temperature.

2.2.3 Gelatin-based Photoresist Preparation

Acrylamide-mofied gelatin B (20 % w/v) was dissolved in a citrate buffer (pH 3.1) at 40 °C for 24 h. When the solution becomes clear, 4 wt% (12.5 mM) of azo-crosslinker and 3 wt% (16.4 mM) of Irgacure 369 ($\lambda max \approx 325$ nm) were added.

2.2.4 Photolithography Process

2PP was performed on a Nanoscribe Photonic Professional GT system (Nanoscribe GmbH). The Nanoscribe system uses a 780 nm Ti-Sapphire laser emitting ≈100 fs pulses at 80 MHz with a maximum power of 150 mW and is equipped with a 63x, 1.4 NA oil immersion objective. The substrate is

placed in a holder that fits into a piezoelectric x/y/z stage. A galvo scanner determines the laser trajectories. The aforementioned objective could work either in oil- (Fig. 2A) or photoresist-immersion configuration (Dip-in Laser Lithography, DiLL) (Fig. 2B). In the oil-immersion configuration the lens is immersed in an oil with a refractive index matching that of the glass on which the photoresist is placed; here, because of the refractive index difference between the glass and the photoresist, a laser scattering takes place at the glass-photoresist interface then worsening the fabrication performances of the system. In the DiLL configuration, instead, the objective is directly immersed in the photoresist and, because the laser does not cross any interface, the system fabrication performances are preserved compared to the case of the oil immersion configuration; however this configuration could be used only with free-solvent photoresist.

In this work, because of the gelatin-based photoresist composition (gelatin is dissolved in a solvent) the oil immersion configuration was used.

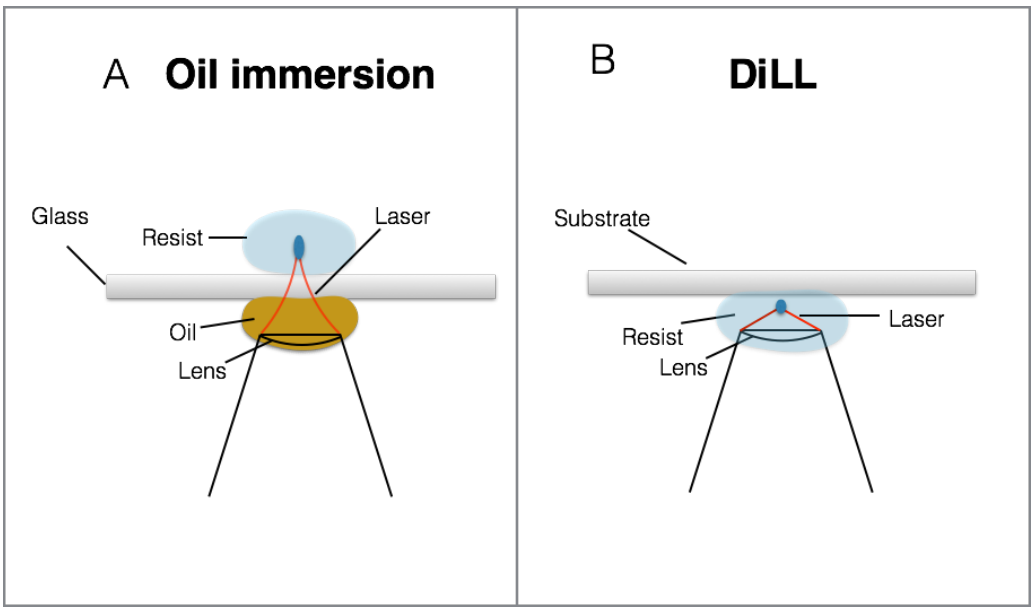

Figure 2: Schematic representation of the two Nanoscribe working cofigurations. A) Oil immersion configuration. B) DiLL configuration.

For the process, gelatin was first heated at 40 °C and then dropped on a circular cover glass (30 mm diameter, 0.17 mm thickness) previously washed with 2-propanol and dried with nitrogen. To minimize solvent evaporation from the photoresist, gelatin was dropped in a closable homemade polydimethylsiloxane (PDMS) reservoir carefully placed on the cover glass surface (Fig. 3). Gelatin was photo-crosslinked at room temperature (solid state) and, as process parameters, output powers ranging from 24 to 60 mW and writing-speed ranging from 3000 to 7500 μm/s were used, in dependence of the z-writing coordinate inside the photoresist. To minimize the optical aberrations caused by the already polymerized gelatin, the structures were written in a "Top-Down" sequence (the first layer was the furthest away from the substrate). Thanks to the solid state of the resist during the fabrication, this writing sequence could be used without recurring to pre-fabricated supporting structures.

After exposure, gelatin was developed in water at 45 °C for 20 min; immediately after development, the sample was immersed in water at room temperature to prevent the distortions of the structures derived from the solvent evaporation. The structures were observed in a water environment using a Leica system confocal microscope (Leica Microsystems).

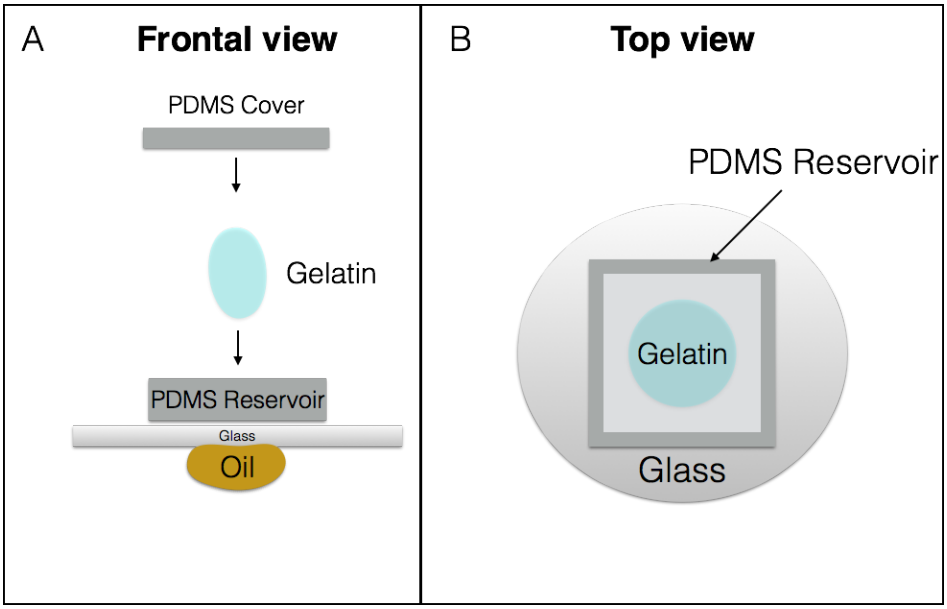

Figure 3: Schematic representation of the system used for avoiding the gelatin solvent evaporation during the process. A) Frontal view. B) Top view.

2.2.6 Degradation tests

Enzymatic degradation of the crosslinked gelatin was carried out using collagenase (Sigma Chemical Co.) with an activity of 0.625 U/mg solid. All the samples were photopolymerzed under an UV lamp (λ=365 nm) for 4h and then treated with the degradation solution. More specifically triplicate samples of dry crosslinked disks (2 mm thickness, 1 cm diameter) for each time point were weighted (W_1) and then well immersed in a 0.020 U/ml and 80 mg/ml collagenase solution (pH 7.5) and incubated at 37 °C. Degradation of the material was stopped at three time points (60, 180, and 360 min), by withdrawing the supernatant collagen solution and adding water to eliminate all the collagenase residuals. As a control, we treated other samples in the same conditions but in absence of the collagenase enzyme. To prevent falsified results, after the photopolymerization and before the first dehydration step, all the samples were incubated in milliQ water at 40 °C for 2h; in this way possible weight losses due to non polymerized material were

avoided**.** Weight loss of the disks due to degradation with or without collagenase was quantified as follows:

Equation 5 $$\text{weight loss } [\%] = \frac{W2\text{-}W1}{W2} \times 100\%$$

where W_2 is the weight of degraded disks at each time point after dehydration by means of an incremental series of ethanol solutions (75%, 85%, 95% and 100%, and 100% again, each step 20 min at room temperature) and dried in oven at 45 C for 24 h.

2.2.7 AFM analysis

The local elasticity of gelatin was probed with a commercial AFM (JPK Instruments, Germany) mounted on the stage of an Axio Observer Z1 microscope (Carl Zeiss GmbH). Material stiffness was quantified testing gelatin parallelepipeds opportunely fabricated on a glass substrate by means of the Nanoscribe system; more specifically, the parallelepipeds were fabricated with a thickness of 20 μm and an area of 900 μm^2. A force mapping was obtained by indenting each sample at 64 distinct points covering an area of 100 μm^2; the substrate stiffness was defined as the average of 6 measurements. A statistical analysis was performed using an Anova test. We used glass sphere cantilevers with a force constant of 0.05 N/m (Novascan, USA). Cantilevers were calibrated by measuring the free fluctuations when unloaded. To quantify the Young Modulus (E), the Hertz model was employed [12].

2.3 Results and discussion

2.3.1 Gelatin modification results

To obtain a photo-crosslinkable gelatin we adapted the protocol described by Billiet et al. [8] to substitute, as schematically represented in Figure 4, part of the free amines of lysine, one of the proteins of gelatin, with acrylic functionalities.

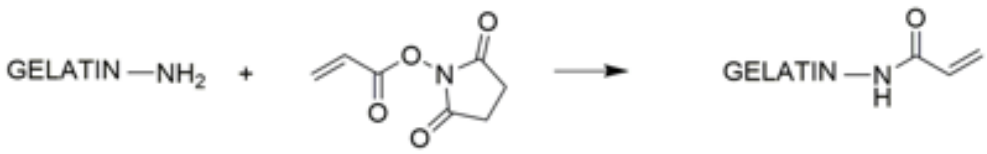

Figure 4: Synthetic scheme of the gelatin modification.

Varying the acrylic acid amount we obtained four different degrees of functionalization, which were proportional to the percentage of the substituted lysine free amines and that strongly affected the final mechanical properties of the polymerized material, as its stiffness increases with the functionalization degree. To characterize the acrylamide gelatin, a ^{1}H NMR analysis (Fig. 5A) was conducted. The presence of the two peaks relative to the acrylamide groups (5.83, 6.25 ppm) indicates the success of the substitution reaction. Moreover, the ratio between the integration of this peak (5.83 ppm) with that relative to the alkyl side chains (1.2 ppm) provides a measurement of the functionalization degree. The relation between the functionalization degree and the added reagent amount is represented in Fig. 5B; optimizing the reaction conditions the highest functionalization degree was obtained using 2 equivalents of reagent amount. Differently from the work of Billiet et al., to evaluate the substitution reaction here we have defined the functionalization degree instead of the substitution degree (DS), a

parameter that quantifies the substitution reaction taking into account the aminoacid composition of the starting gelatin and the ratio between the two previously mentioned ^{1}H NMR peaks. This choice was done just for seek of clarity and justified by the fact that we did not analyze the aminoacid composition of our gelatin that, because of its derivation (bovine skin) and mechanical properties (Bloom number), should possess a composition quite similar to that presented by Billiet et al. (that is conform to those presented in literature). Moreover, because our purpose was just to use the most functionalized gelatin, the reaction with 2 equivalents was the only one performed in duplicate. In the two accomplished synthesis the depicted degree of functionalization did not significantly varied (0.085,0.083) confirming the reproducibility of the process. Using these results with the formula reported by Billiet et al. the DS would be 83 and 80%.

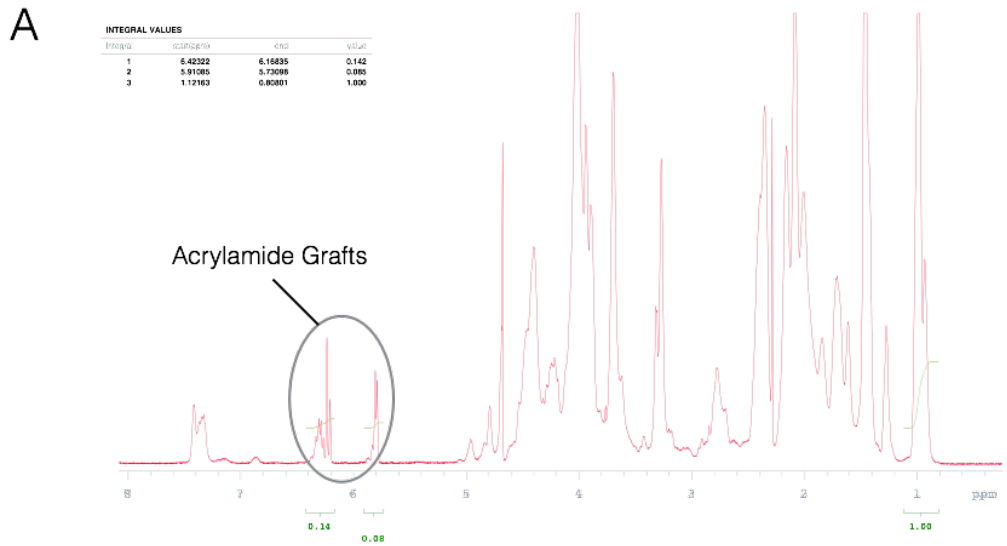

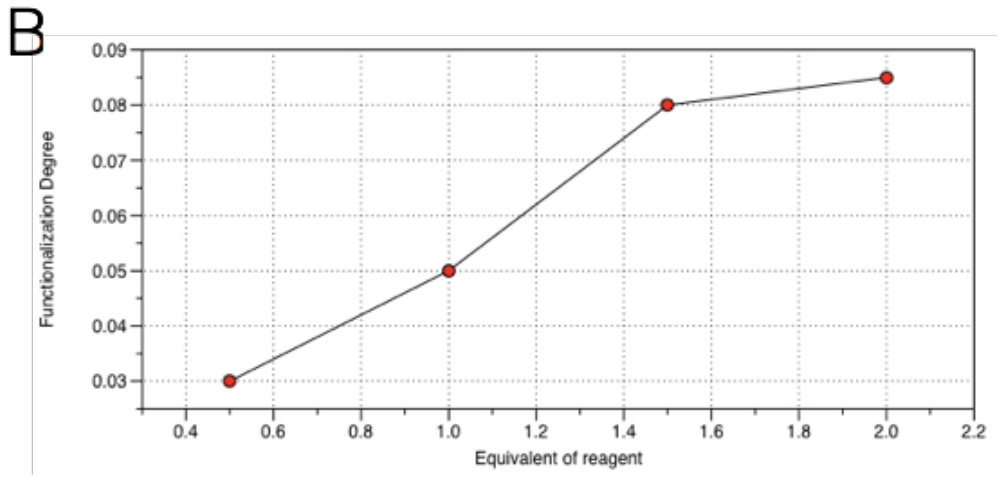

Figure 5: A) NMR spectrum of the acrylamide gelatin synthetized using 2 equivalent of acrylic acid; the highlighted peaks are relative to the presence of the acrylate groups in the polymer chain. B) Gelatin functionalization degree vs equivalent used in the reaction.

2.3.2 Gelatin fabrication

In this work we have processed an acrylate gelatin with the Nanoscribe system to create 3D structures to be used for cell or tissue engineering. The choice of the acrylate gelatin was justified by its reported higher photo-reactivity and structural properties after the photopolymerization, as compared to the methacrylate gelatin [8].

Inspired by the pioneering work of Ovsianikov et al. [7], the photosensitive gelatin was fabricated with the DLW-2PP technology by dissolving it in a suitable solvent and in presence of a photoinitiator. As photoiniator molecule we used the Irgacure 369 (Fig. 6A), even though for biological applications the more biocompatible Irgacure 2959 is generally preferred [13]; this choice was dictated by the laser wavelength of our system (390 nm in the TPA region) that, among these two molecules, is absorbed and can activate only the Irgacure 369. Because of the low photoinitiator water solubility, we used a phosphate buffer (pH of 3.1) as solvent for both gelatin and photoinitiator; for the fabrication process we selected the most functionalized gelatin to

ensure the best mechanical properties (see previous paragraph). Gelatin was prepared at 20% wt/v in phosphate buffer and the photoinitiator was added at 3% wt of the solid gelatin.

Moreover, we added to the photosensitive mixture an acrylate azobenzene moiety (4% wt) that plays a double role: it participates to the photoreaction acting as an additional crosslinker (Fig. 6A) [14] and it gives also the possibility to deform the material by means of specific light stimulations (see chapter 3).

In the fabrication context it is important to underline that, because of its absorption valley at 390 nm (Fig.6B), the azobenzene molecule can be embedded in the photoresist mixture without decreasing significantly the photoinitiator absorbed radiation and then the photoreactivity of the material [14]. The final goal of the writing parameters optimization is to fabricate structurally stable constructs in the shortest time. Basically, the writing parameters to tune in our system are slicing and hatching distance, the laser power and the scan speed; the dwell time parameter can be ignored in our system because of the presence of the galvo scanner.

The Nanoscribe software offers the possibility to automatically divide a 3D CAD file in a series of lines which represent the trajectories that the laser should follow to build the final structure; here the user can fix the distance between lines in the 3 dimensions (slicing and hatching distance), the exposure power and the scanning speed for each line. The laser polymerizes successive voxels which, overlapping in the 3 dimensions, compose the final structure; to get the structural stability it is then necessary to ensure an adequate connection between voxels controlling both their dimension and positioning.

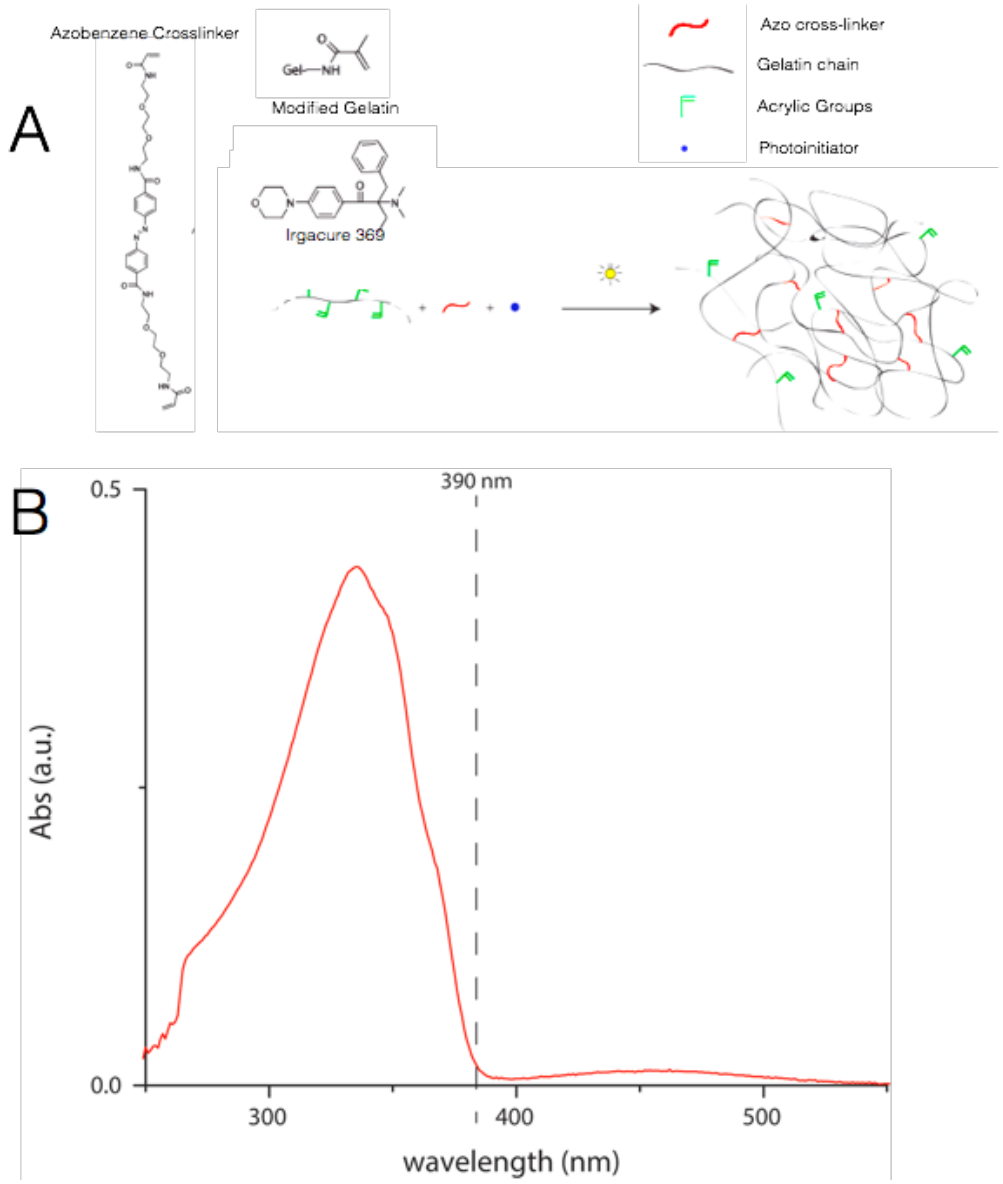

Figure 6: A) Chemical structures of photoinitiator, gelatin and azobenzene molecules are represented and the schematic photopolymerization scheme is reported. B) UV adsorption spectrum of the azobenzene molecule.

Voxel dimension is proportional to the exposure dose which results from the combination of the laser power and exposure time (reciprocal of scan speed) [15]. However the highest achievable voxel dimension is limited; in particular over the polymerization threshold (see chapter 1) it could be

identified an energetic range called "polymerization range" within a normal polymerization is obtained, but over which an incontrollable polymerization takes place. Too high exposure doses (overcoming the polymerization range) trigger in fact a phenomenon called "laser-induced breakdown", which causes the formation of micro-explosions on the material surface that irreversibly damage the material and definitely compromise the fabrication process [16][17]. More specifically the laser-induced breakdown is a thermal process where a plasma is generated consequently to a strong interaction of light with the electrons that, in turn, strongly increase their density causing a vaporization and atomization of the sample constituents [16].

The limits over the voxel dimensions then dictate the maximum distance allowed to ensure the voxel overlapping. Therefore, to obtain stable structures with the fastest process, it is necessary to increase the exposure dose, combining the highest powers with the highest scan speeds (lowest exposure time) and spacing as much as possible adjacent voxels.

However, the suitable voxel dimension and, then, the maximum dose, depend upon the desired structure resolution: higher is the resolution smaller is the allowed voxel dimension.

To test our capability to fabricate gelatin and to evaluate the role played by the azobenzene in the fabrication process, we optimized the writing parameters to build the two structures represented in figure 7.

These two structures were designed to test our capability to fabricate on the micrometric scale high resolute (down to 1μm**)** 3D complex structures, also presenting freestanding features (Fig. 7A).

For both gelatins the optimized parameters were:

- Slicing and hatching distance 0.3 μm
- Output laser power 24 mW
- Scan speed 7500 μm/s.

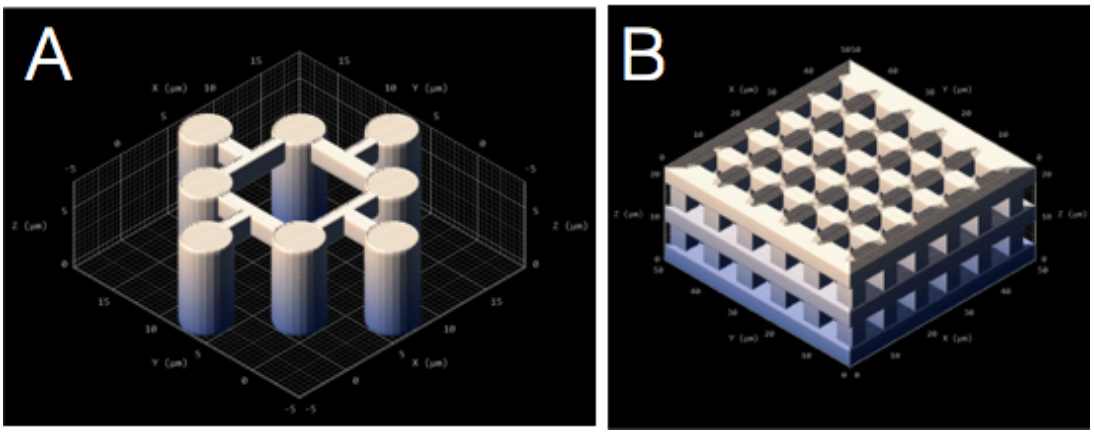

Figure 7: Nanoscribe software representation of the two fabricated structures: A) Pillar height =7µm, diameter = 3µm; free standing structures width=1µm. B) Woodpile structure, beams distance = 5 µm, beam width = 3µm, structure height = 20 µm.

To fabricate gelatin it was necessary to follow a top-down writing sequence (from the highest to the lowest z) because of the optical aberration caused by the already polymerized material; it was in particular noticed that the polymerized gelatin altered the transmitted radiation dose, preventing the polymerization of structures higher than 15 µm using a bottom-up writing sequence. In our protocol, gelatin was fabricated at room temperature and then in its gel state (solid); this condition allowed overcoming the shortcomings of the more common liquid resins top-down writing sequences, in which the fabrication of supporting anchorage structures is necessary to fabricate the final construct.

Comparing the confocal images of the structures fabricated with the optimized parameters, the role of the azobenzene in the fabrication could be easily evaluated (fig. 8 C and E, Fig. 8 B and F). As predicted, the azobenzene moieties did not change the material polymerization threshold and consequently the highest usable dose was the same for both gelatins based photoresists. However, because of the molecule crosslinking role,

using equal doses, higher crosslinking degree was obtained; as it is evident from the images, thanks to the higher crosslinking degree, very complex 3D structures faithful to the original CAD design were fabricated.

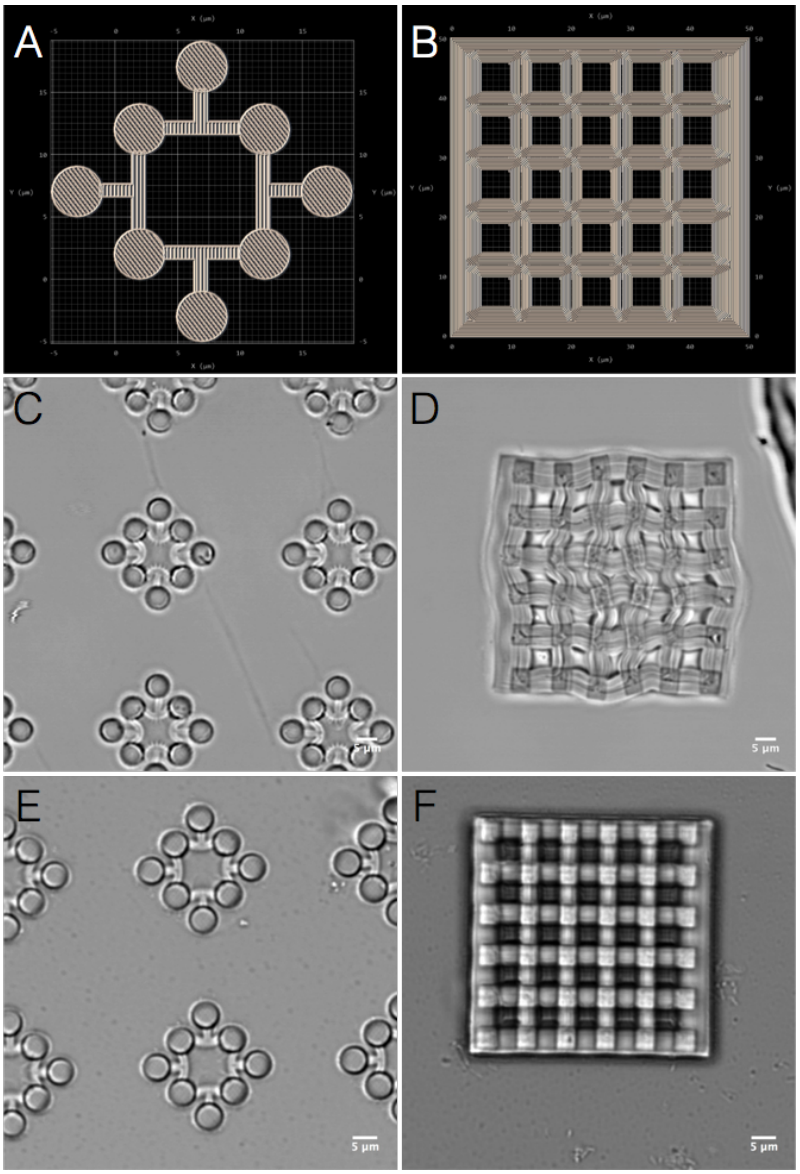

Figure 8: A-B) Top view Nanoscribe software representation of the fabricated structures. Confocal images of the gelatin structures fabricated without (C-D) and with (E-F) the azobenzene crosslinker. Scale Bars: 5µm.

However, for what concerns the parameters optimization, it is fundamental to specify that the performances of the DLW-2PP process depend also upon the combination of the photoresist composition and the lithography equipment specifications and not only on the process parameters [18][19][20]. As a consequence, for a fixed photoesist composition, it is then questionable to compare the fabrication results of two different systems. The aforementioned optimized process parameters are then only relative to our Nanoscribe system.

The mechanical properties of the polymerized azobenzene-doped gelatin were evaluated in terms of stiffness of the microstructured material by means of an AFM analysis; the measured Young Modulus was of 6.55 ±0.447 kPa, a value belonging to a range of interest for several cell phenotypes studies [21]. Analyzing the mechanical properties of the non-doped gelatin, a Young Modulus of 2.7 ±0.754 kPa was measured, further confirming the role of the azobenzene in the modulation of the material mechanical properties. Moreover, as it will be shown in the experiments reported in the following chapters, the polymerized gelatin did not show particular cytotoxic effects on cultured cells.

2.3.3 Degradation

A fundamental property of cellular scaffolds, especially in tissue engineering applications, is the capability to undergo enzymatic degradation in the physiological environment [22].

To investigate if the azobenzene molecule inhibited the typical enzymatic degradability of gelatin, macroscopic material samples were incubated in a PBS collagenase solution with an activity of 0.020 U/ml at 37 °C. The rate of enzymatic degradation *in vitro* was evaluated with the gravimetric method (Fig. 9). After 6 h of incubation, gelatin samples lost about 85% of their

original weight. The loss weight of the control (gelatin incubated in the collagenase-free solution) are ascribable to measurements errors related to the very small quantity of gelatin (≈13 mg) used to perform the test; however our results indicate that the material preserve its degradability.

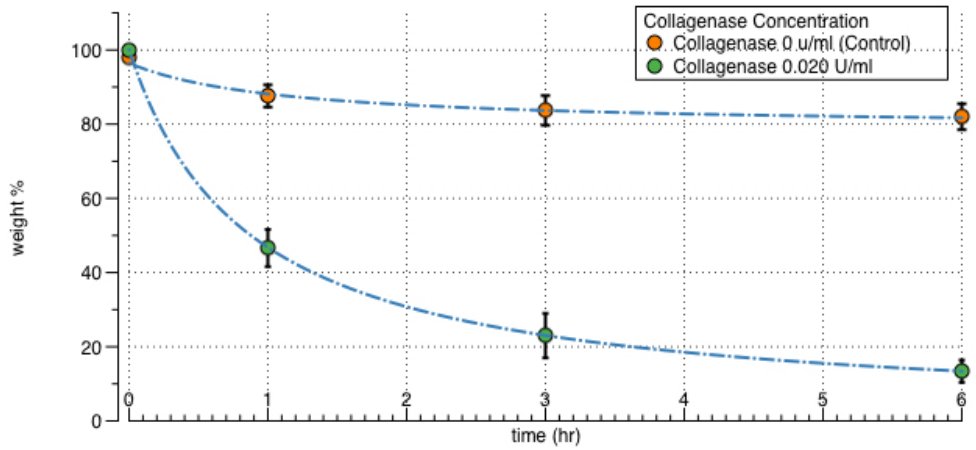

Figure 9: Weight loss curves of the enzymatic degradation of the acrylate gelatin.

2.4 Conclusions and future perspectives

An acrylate gelatin was synthetized and fabricated on the microscale with a 3D lithography system. The photosensitive mixture was adapted to the Nanoscribe system and an optimization of the writing parameters was performed.

To address the typical gelatin DLW-2PP fabrication issues, such as the low mechanical properties or the low resolutions, an azobenzene-based crosslinker was added to the photosensitive mixture in order to increase the crosslinking degree of the material without changing its photoreactivity; thanks to this addition, evident structural improvements were obtained, allowing the fabrication of complex and stable 3D structures on a dimensional scale potentially interesting for several cell engineering applications (down also to 1µm).

Despite the addition of the azobenzene functionality, the polymerized material showed interesting mechanical properties and preserved its enzymatic degradability, a fundamental characteristic for tissue engineering applications.

To match the characteristics of the laser wavelength, as photoinitiator it was used the Irgacure 369 and consequently an acid substance was employed as solvent. This composition did not compromise material biocompatibility. Of course in case of more sensitive applications such as, for example, the fabrication of cell-laden constructs, the biocompatibility should be reassessed. A possible alternative strategy could be the use of crosslinking thiolen-based reactions or other water soluble and more biocompatible photoinitiators with an appropriate TPA [23], in order to preserve the resolution standards obtained.

Reference

[1] J. W. Nichol, S. T. Koshy, H. Bae, C. M. Hwang, S. Yamanlar, and A. Khademhosseini, "Cell-laden microengineered gelatin methacrylate hydrogels," *Biomaterials*, vol. 31, no. 21, pp. 5536–5544, 2010.

[2] X. Shi, S. Ostrovidov, Y. Zhao, X. Liang, M. Kasuya, K. Kurihara, K. Nakajima, H. Bae, H. Wu, and A. Khademhosseini, "Microfluidic spinning of cell-responsive grooved microfibers," *Adv. Funct. Mater.*, vol. 25, no. 15, pp. 2250–2259, 2015.

[3] B. W. Lee, B. Liu, A. Pluchinsky, N. Kim, G. Eng, and G. Vunjak-Novakovic, "Modular Assembly Approach to Engineer Geometrically Precise Cardiovascular Tissue," *Adv. Healthc. Mater.*, vol. 5, no. 8, pp. 900–906, 2016.

[4] L. E. Bertassoni, J. C. Cardoso, V. Manoharan, A. L. Cristino, N. S. Bhise, W. A. Araujo, P. Zorlutuna, N. E. Vrana, A. M. Ghaemmaghami, M. R. Dokmeci, and A. Khademhosseini, "Direct-write bioprinting of cell-laden methacrylated gelatin hydrogels," *Biofabrication*, vol. 6, no. 2, p. 24105, 2014.

[5] J. Torgersen, X. H. Qin, Z. Li, A. Ovsianikov, R. Liska, and J. Stampfl, "Hydrogels for two-photon polymerization: A toolbox for mimicking the extracellular matrix," *Adv. Funct. Mater.*, vol. 23, no. 36, pp. 4542–4554, 2013.

[6] A. I. Ciuciu and P. J. Cywiński, "Two-photon polymerization of hydrogels-versatile solutions to fabricate well-defined 3D structures," *RSC Adv.*, vol. 4, no. 85, pp. 45504–45516, 2014.

[7] A. Ovsianikov, A. Deiwick, S. Van Vlierberghe, P. Dubruel, L. Möller, G. Drager, and B. Chichkov, "Laser fabrication of three-dimensional CAD scaffolds from photosensitive gelatin for applications in tissue engineering," *Biomacromolecules*, vol. 12, no. 4, pp. 851–858, 2011.

[8] T. Billiet, B. Van Gasse, E. Gevaert, M. Cornelissen, J. C. Martins, and P. Dubruel, “Quantitative contrasts in the photopolymerization of acrylamide and methacrylamide-functionalized gelatin hydrogel building blocks,” *Macromol. Biosci.*, vol. 13, no. 11, pp. 1531–1545, 2013.

[9] J. Van Hoorick, P. Gruber, K. H?lzl, M. Markovic, M. Tromayer, J. Van Erps, A. Ovsianikov, H. Thienpont, P. Dubruel, and S. Van Vlierberghe, “Two-photon polymerization of gelatin hydrogels: carboxylic acid modification as the key to success,” *Front. Bioeng. Biotechnol.*, no. 627.

[10] E. Vaselli, C. Fedele, S. Cavalli, and P. A. Netti, “‘On-Off’ RGD Signaling Using Azobenzene Photoswitch-Modified Surfaces,” *Chempluschem*, vol. 80, no. 10, pp. 1547–1555, 2015.

[11] D. Liu, Y. Xie, H. Shao, and X. Jiang, “Using azobenzene-embedded self-assembled monolayers to photochemically control cell adhesion reversibly,” *Angew. Chemie - Int. Ed.*, vol. 48, no. 24, pp. 4406–4408, 2009.

[12] J. Domke and M. Radmacher, “Measuring the elastic properties of thin polymer films with the atomic force microscope,” *Langmuir*, vol. 14, no. 12, pp. 3320–3325, 1998.

[13] C. G. Williams, A. N. Malik, T. K. Kim, P. N. Manson, and J. H. Elisseeff, “Variable cytocompatibility of six cell lines with photoinitiators used for polymerizing hydrogels and cell encapsulation,” *Biomaterials*, vol. 26, no. 11, pp. 1211–1218, 2005.

[14] L. H. Nguyen, M. Straub, and M. Gu, “Acrylate-based photopolymer for two-photon microfabrication and photonic applications,” *Adv. Funct. Mater.*, vol. 15, no. 2, pp. 209–216, 2005.

[15] T. Baldacchini, S. Snider, and R. Zadoyan, “Two-photon polymerization with variable repetition rate bursts of femtosecond laser pulses.,” *Opt. Express*, vol. 20, no. 28, pp. 29890–9, 2012.

[16] H. B. Sun and S. Kawata, “Two-photon photopolymerization and 3D lithographic microfabrication,” *Adv. Polym. Sci.*, vol. 170, pp. 169–273, 2004.

[17] M. G. Guney and G. K. Fedder, “Estimation of line dimensions in 3D direct laser writing lithography,” *J. Micromechanics Microengineering*, vol. 26, no. 10, p. 105011, 2016.

[18] G. Witzgall, R. Vrijen, E. Yablonovitch, V. Doan, and B. J. Schwartz, “Single-shot two-photonexposure of commercial photoresist for the production of three-dimensionalstructures,” *Opt. Lett.*, vol. 23, no. 22, pp. 1745–1747, 1998.

[19] B. Tan, K. Venkatakrishnan, and A. Makaronets, “Effects of pulsewidth on two-photon polymerization,” *Des. Monomers Polym.*, vol. 16, no. 2, pp. 145–150, 2013.

[20] M. Malinauskas and P. Danileviˇ, “Three-dimensional micro- / nano-structuring via direct write polymerization with picosecond laser pulses,” *Opt. Express*, vol. 19, no. 6, p. 5602, 2011.

[21] D. E. Discher, P. Janmey, and Y.-L. Wang, “Tissue cells feel and respond to the stiffness of their substrate.,” *Science*, vol. 310, no. 5751, pp. 1139–43, 2005.

[22] K. T. Nguyen and J. L. West, “Photopolymerizable hydrogels for tissue engineering applications,” *Biomaterials*, vol. 23, no. 22, pp. 4307–4314, 2002.

[23] E. Blasco, M. Wegener, and C. Barner-Kowollik, “Photochemically Driven Polymeric Network Formation: Synthesis and Applications,” *Adv. Mater.*, p. 1604005, 2017.

CHAPTER 3
Gelatin based 3D photo-actuators for confinement and deformation of cells

3.1 Introduction

Cell behavior is determined by chemical, mechanical and topographic signals provided by the cell-surrounding microenvironment.

Mechanical signals which can be either associated to the mechanical properties of the aforementioned microenvironment [1] or to the forces directly applied on cells [2], are fundamental in the regulation of many cell functions and in the progress of several physiological and pathological processes. Hypertension, osteoporosis, atherosclerosis and some forms of cancer are only a few examples of diseases related to the alteration of cell-environment mechanical interactions [3][4][5].

Cells convert mechanical stimuli into biochemical information through a mechano-transduction process. Indeed, mechanical stimuli are transmitted through the cytoskeleton force-bearing elements from the adhesion complexes to mechanosensitive macromolecules that, once stressed, change their functions and impact cellular behavior [3][6]. For example, the mechanical force transmission can lead to the deformation of the cell nucleus activating molecular pathways which regulate important cells functions such as the differentiation [7]. Moreover, mechano-transduction can result in the induction of different cell behaviors, depending on the temporal and spatial dynamics of the mechanical stimuli perceived [8][9][10][11][12], a process not yet fully understood from a functional point of view [3].

To fill this gap of knowledge, it would be highly desirable to develop platforms enabling the fine tuning of the mechanical signals and an easy detection of the induced changes of cell behavior.

The development of new microfabrication techniques and the advancements in the material science have significantly fostered research in this direction [13][14][15]. Among all the approaches, the employment of biocompatible responsive-materials, systems able to change their properties in response to specific stimuli, has offered the most adequate solutions [16][17][18]. Nowadays, platforms with chemical-tunable properties are the most advanced [19], but only few examples of biomaterials with mechanical [20][21] or topographic-tunable [22] features are present in the literature. In these two latter cases, a complete control of the properties, especially for what concerns their variation in time (e.g. frequency or rate), still remains a critical issue to address.

An important factor to take into account in the design of stimuli-responsive systems is the stimuli source to employ. The ideal source should be finely tunable in time and space to precisely control the material properties, and should operate without changing the environmental parameters that could alter cell-scaffold interactions. Among all the stimuli used so far, light, lasers and magnetic fields are those with best performances [23][20].

Here, we have contributed to this research area by developing a platform to selectively deform the nuclei of living cells. This goal has been achieved introducing photo-deformable gelatin microstructures, fabricated with the Nanoscribe system, and opportunely designed to position cells through specific topographic signals; more specifically we have fabricated patterned 3D instructive microstructures which, irradiated with an adequate light source, undergo a deformation which directly stresses the cells.

The material photo-deformability was achieved thanks to the light-sensitivity of the azobenzene molecules introduced in the gelatin-based photoresist (see

Chapter 2) [24][25]. As stimuli source to induce the deformations, the laser of a confocal microscope was employed; this setup allowed to observe in real time cell reactions in a cell-friendly environment.

3.2 Materials and Methods

3.2.1 Cell cultures (NIH-3T3)

NIH−3T3 fibroblasts were cultured in low glucose DMEM and incubated at 37°C in a humidified atmosphere of 95% air and 5% CO_2. Prior to cell seeding, substrates were sterilized in Pennicillin-Streptomycin solution in PBS (Phosphate Buffered Saline) (1:2 v:v) for 4 h. On each sample, a number of cells varying from 40,000 to 80,000 were seeded and left to adhere overnight in the incubator, set at the temperature indicated above. The day after, cells were treated with vital Cell Tracker Deep Red (1:1000 in cell culture medium without FBS) for 30 minutes in the incubator and then the nuclei were stained with HOECHST (100 µl of a solution 1:10000 v:v in the culture medium). (Invitrogen) for the actin filament and nucleus live staining, respectively. Cells were, then, fixed with 4% paraformaldehyde for 20 min.

3.2.2 Cell cultures (HUVECs)

Human umbilical vein endothelial cells (HUVECs) were purchased from LONZA. Cells were cultured in gelatin-coated flasks in an incubator at 37 °C and humidified atmosphere with 5% of CO_2. Cell medium M200 supplemented with LSGS Kit (fetal bovine serum 2% v/v, hydrocortisone 1 µg/ml, human epidermal growth factor 10 ng/ml, basic fibroblast growth factor 3 ng/ml, heparin 10 µg/ml) was used. Prior to cell seeding, substrates were sterilized in Pennicillin-Streptomycin solution in PBS (Phosphate Buffered Saline) (1:2 v:v) for 4 h. On each sample a number of cells of

80,000 were seeded and left adhering overnight in the incubator. After the overnight cells were stained with vital CellTracker Deep Red and observed with the confocal microscope (Leica Microsystems, Germany).

3.2.3 Staining protocol

After fixation, cells were permeabilized with 0.1% Triton X−100 in PBS for 3 min. Actin filaments were stained with rhodamin−phalloidin. Samples were incubated for 30 min at room temperature in the phalloidin solution (dilution 1:200). Finally, cells were incubated for 15 min at 37°C in HOECHST solution (dilution 1:200) to stain cells nuclei. A TCS SP5 multiphoton microscope (Leica Microsystems) was used to collect fluorescent images of cells.

3.2.4 Confocal stimulation

A multiphoton (MP) confocal microscope (Leica Microsystems, Germany) was used to photo-actuate the 3D structures. The azobenzene isomerization and the consequent structure deformation were activated by using an MP laser, tuned at 700 and 840 nm wavelength (TPA wavelength 350 and 420 nm respectively). The structures were immersed in water and photo-stimulated by controlling the laser beam focusing and position; the exposed area was determined through the region−of−interest (ROI) editor of the microscope software. The deformation of the structures was live monitored and recorded via software, by time-lapse function.

3.2.5 AFM analysis

The AFM analysis was performed to evaluate Young Modulus (E) variations of the gelatin after the photo-stimulation; each measurement was performed as described in the materials and methods section of the chapter 2 (paragraph

2.2.6). Gelatin stiffness was first measured before the stimulation; after the stimulation the variation of E was monitored after 15 min, successively every h for 4 h, and reevaluated after an overnight interval (24 h).

3.2.6 3D lithography process

The microstructures presented here were fabricated by means of our 3D lithography system (Nanoscribe Professional GT (GmbH)) following the same procedure described in the chapter 2 (paragraph 2.2.4).

3.3 Results and Discussion

The aim of this work has been to build up a system which potentially allows studying the reaction of cells in response to mechanical forces. To this end, we have transferred the concept of photo-actuation to the CIMs. More specifically, adding azobenzene functionalities to a photo-crosslinkable gelatin, we have fabricated a microstructured instructive and photo-actuable platform capable to confine and selectively stress cells by using the Nanoscribe system.

Basically, the aforementioned platform is constituted by an array of micro-patterned gelatin parallelepipeds (Fig.1) that, through a topographic signal, confine cells between their lateral walls. Once cells are confined, the surrounding structures are selectively photo-deformed and, by expanding, act like a press that stresses and deforms cells.

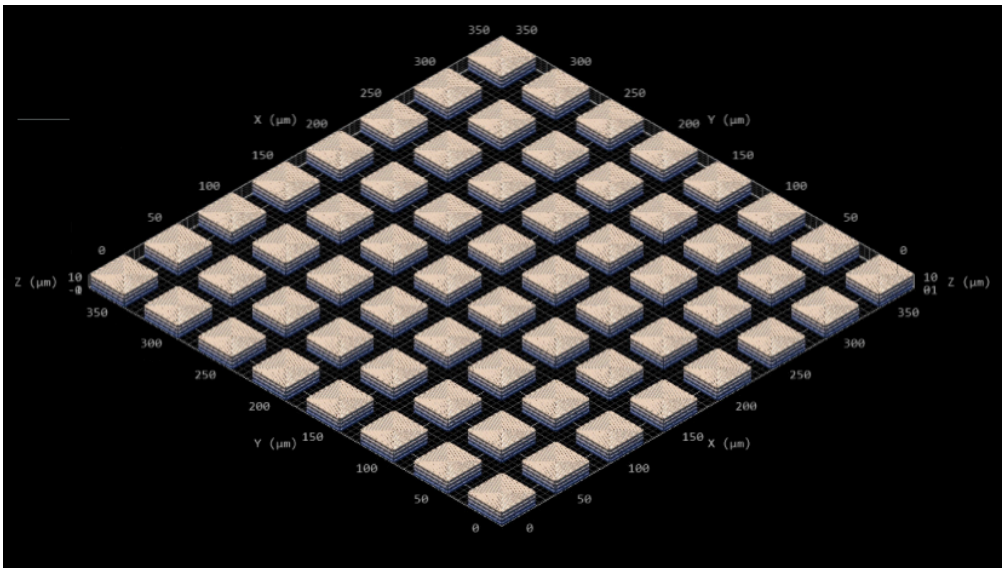

Figure 1: Nanoscribe software representation of the parallelepipeds array. Parallelepipeds dimensions = 30x30x10 µm (xyz); distance wall-to-wall = 10 µm.

As a light source we have employed the laser of a confocal microscope. This choice has allowed stressing living cells and simultaneously observes their reactions in real time; moreover, thanks to the ROI editor of the microscope software, it has been possible to control with high accuracy (micrometric precision) the stimulus in space (Fig.2).

In the first part of this section, the photo-actuation experiments are discussed, while in the second and third part cells confinement and deformation results are respectively showed.

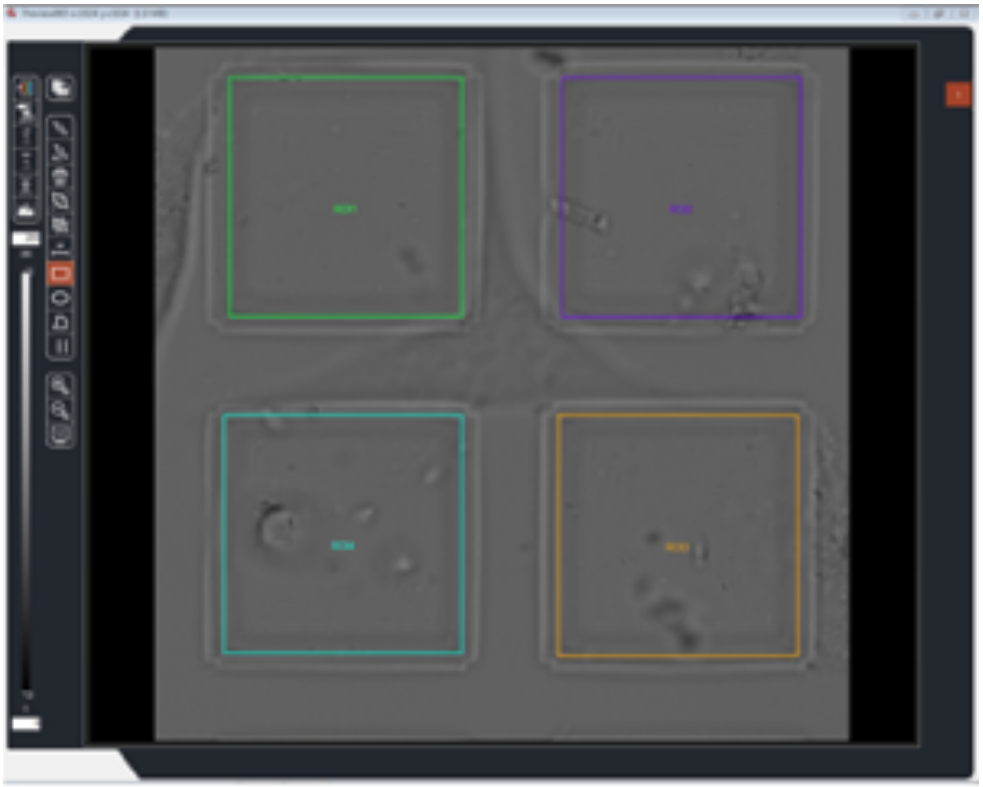

Figure 2: Screenshot of the ROI editor of the confocal microscope; the colored squares represent the region to expose with a specific radiation.

3.3.1 Stimulation results

Light-deformable materials have shown great potentialities in various scientific and technological fields and provide cutting edge solutions in material science research.

Nowadays, among all the light-sensitive materials, the azobenzene-based ones represent the gold standard [24]. Azobenzene are extremely versatile moieties which can be directly polymerized, embedded in polymeric matrices or processed to form liquid crystal elastomers (LCEs) [26]; furthermore, differently from the other developed light-sensitive materials, only with the azobenzene-based ones a reversible deformation can be obtained. The photo-deformation of azobenzene-based materials is basically driven by the

reversible isomerization of the azobenzene molecules triggered by the interaction with light.

In this work, in order to develop a photo-deformable platform for cells deformation, an in-house synthetized azobenzene (Fig.3) molecule was added to an acrylate photo-crosslinkable gelatin (for materials and methods information, see paragraph 2.2.3).

First, the azo-molecule isomerization behavior was studied by UV-Vis spectroscopy. The isomerization mechanism of azobenzene molecules in solution can be monitored by UV-Vis spectroscopy, thanks to the fact that each isomer presents a characteristic absorption spectrum [27].

Azobenzene undergoes a trans-cis isomerization when irradiated with a UV light (365 nm) and a cis-trans back isomerization when illuminated with blue light (420 nm) (Fig. 3). Moreover, the isomerization rate is strongly influenced by the type of light source employed. Because of the higher thermodynamic stability of the trans isomer, the cis-trans isomerization could take place also spontaneously; to characterize this behavior the sample was left in a dark environment at room temperature and its UV spectrum monitored. In these conditions a complete cis-trans back isomerization was observed after 3 days.

Once identified the isomerization wavelengths, the photo-deformation process of gelatin microstructures was studied. To this end gelatin parallelepipeds (square section of 900 μm^2, thickness of 10 μm) fabricated with the Nanoscribe on a glass substrate were tested.

The multiphoton laser of a confocal microscope was employed as stimulus. Then, the microscope was used as stimuli source and as a tool to observe, record and evaluate in real time the micro-deformations. With this system, it was also possible, by opportunely tuning the microscope control settings, to spatio-temporally modulate the stimulus with extreme accuracy. All the

stimulation experiments were conducted under water immersion of the samples.

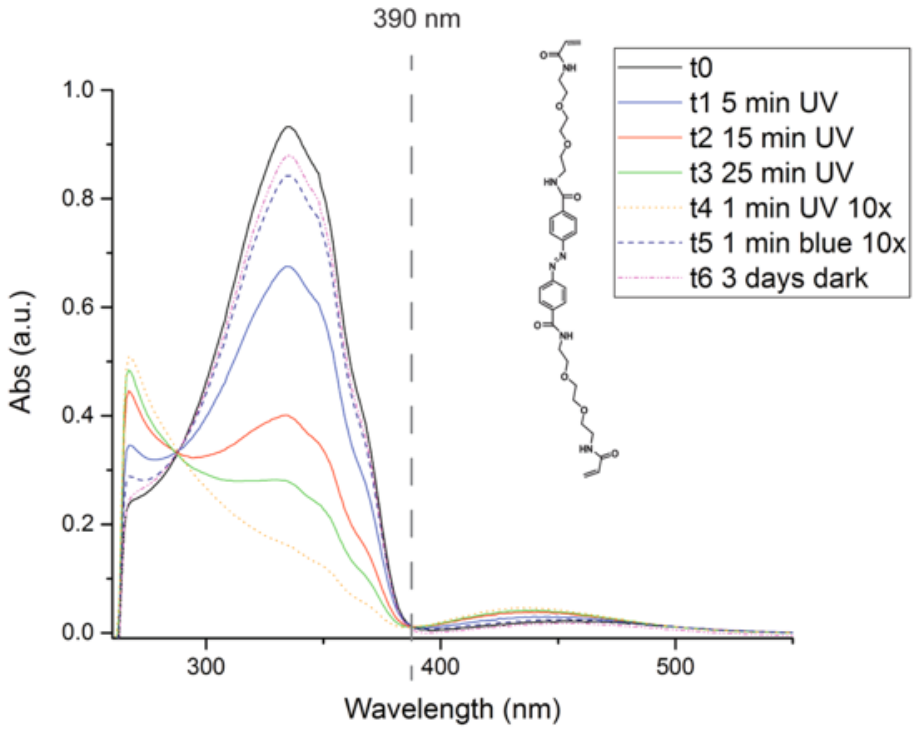

Figure 3 UV-Vis spectrum of the azobenzene dissolved in dimethylformamide (DMF). Studying the spectrum after different sample light exposures, the molecule isomerization can be evaluated. In the legend the exposure time (t_i), the type of illumination (UV or blue light) and the light source (UV=desk lamp, UV and blue 10x= mercury lamp focalized with a 10x objective) are reported for each curve.

Exposing the structures to a 700 nm laser (voxel wavelength 350 nm) with the output power fixed at 13 ±0.5 mW, an expansion rate of approximately 0.3µm/min was recorded, leading to deformation values up to ≈10% (Fig.4). Using power higher than 15±0.5 mW the material was instead irreversibly damaged.

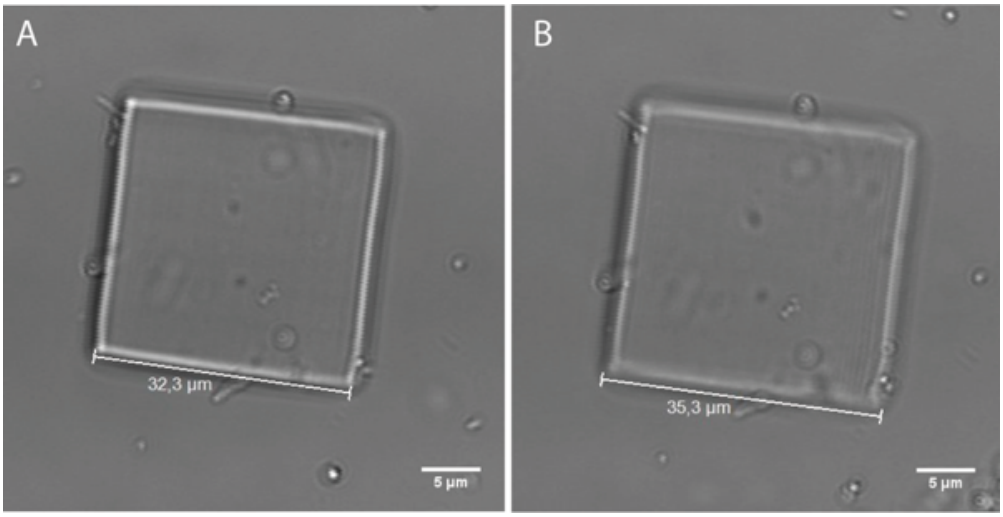

Figure 4: Confocal bright field images of the gelatin parallelepipeds before (Fig. A) and after (Fig. B) the photo-actuation. Scale bars: 5µm.

As a negative control, we performed the same experiment tuning the laser at 780 nm, a wavelength at which the azobenzene presents a light absorption valley (Fig. 3), and fixing the output power at 13 mW. In these conditions no deformations were observed, confirming the role of the azobenzene in the process.

Once obtained the trans-cis driven photo-deformation, the back cis-trans isomerization was tested tuning the laser at 840 nm (voxel wavelength 420 nm); surprisingly no shape recovery was observed.

Structures were then left in a dark environment and monitored for 1 week and, also in this case, no shape recovery was observed. The missing of spontaneous and light-driven back isomerizations may be due to local relaxation of the polymer chain, as we will explain later in the chapter.

The photo-deformation of the azobenzene-based hydrogels has been analyzed only in few studies but the mechanisms involved in this process are not completely clear, even though it was demonstrated that the mechanical properties of the polymer strongly affect the photo-deformation process [28] [29].

Here, we have tried to elucidate the role played by the polymer chains by monitoring with an AFM the effects of the stimulation on the material stiffness. The collected data indicate the occurrence of a change of the material stiffness over time (Fig.5 and Table 1) that could be divided in 3 principal phases.

The first phase (from t0 to t1) is developed in approximately 15 min after the photo-stimulation: during this period E decreases, changing its value from ≈6.5 to ≈3.9 kPa. In our opinion this behavior is directly attributable to the azobenzene molecules that, undergoing to a trans-cis isomerization, increase the material hydrophilicity [30]; the increase of hydrophilicity, in turn, (because the structures are immersed in water) causes an increase of the swelling and a consequent reduction of the material stiffness.

In the second phase (from t1 to t3), E increases and reaches its maximum about 2 h after the stimulation, passing from ≈3.9 to ≈9.6 kPa. The trans-cis isomerization causes a bending of the azobenzene molecules moving gelatin chains closer and then leading to an increase in the number of polymer entanglements, which, in turn, causes an augmentation of E [28].

During the third phase (from t3 to t6) another significant decrease of E takes place; we associate this behavior to the relaxation and to the spatial reconfiguration of the polymer chains consequent to the stiffening of the previous phase. The extremely high variance observed in t5 describes a spatial inhomogeneity of the material mechanical properties, probably associated to the transient nature of the relaxation phenomenon.

After 24 h from the photo-stimulation (t6), E reaches again its original value decreasing the variance, but a shape recovery is not yet observed. We associate the lack of shape recovery to a viscous and non-reversible deformation that limits the possibility to cyclically deform the structures. To overcome this problem, we are currently trying to reduce the material viscous

component with the introduction of more elastic azobenzene based crosslinkers, which allow increasing the range of reversible deformations.

In parallel, to further investigate on the mechanisms involved in the photoactuation, we are developing an experimental protocol to correlate the isomerization state of the molecules with the material deformation. More in detail, we are trying to follow the isomerization-related fluorescence emission variations of the azobenzene, during and after the photoactuation process.

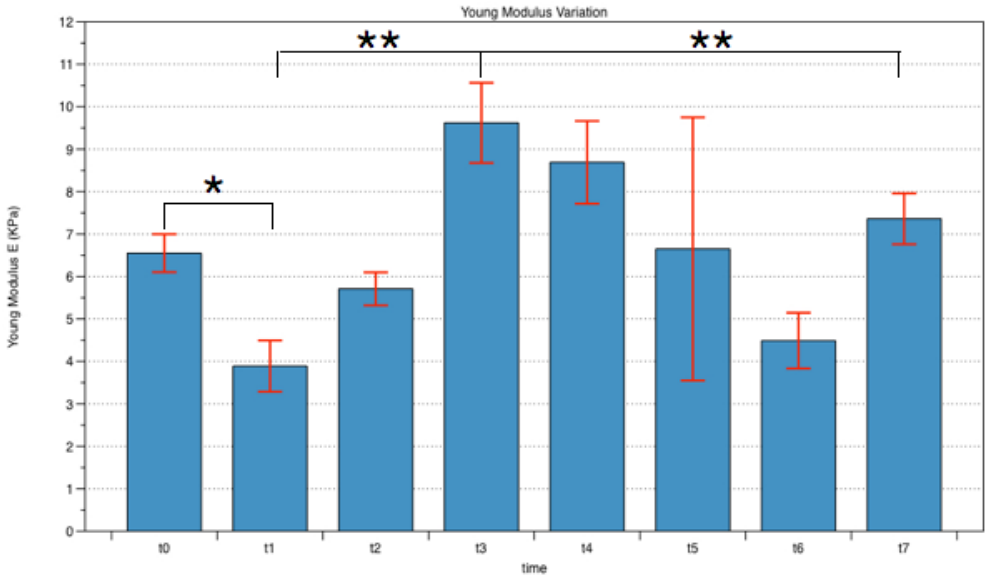

Figure 7: Evolution of the material Young modulus before (t0) and after (from t1 to t6) the photo-actuation. t1= 0.25h, t2=1h, t3=2h, t4=3h, t5=4h, t6=24h. The asterisks in the graph represent the statistical significance between groups: "*" means significant difference ($p<0.05$), "**" means highly significant difference ($p<0.01$).

Table 1: Reported data are referred to the Figure 5. E is the Young modulus and σ the variance.

	E (kPa)	σ (kPa)
t0 (b.s.)	**6.55**	**0.447**
t1 (0.25 h a.s.)	**3.89**	**0.604**
t2 (1 h a.s.)	**5.71**	**0.389**
t3 (2h a.s.)	**9.62**	**0.944**

t4 (3h a.s.)	**8.69**	**0.975**
t5 (4h a.s.)	**6.65**	**3.100**
t6 (24 h a.s.)	**7.36**	**0.60**

b.s.= before stimulation
a.s.= after stimulation

3.3.2 Cells Confinement

The capability to selectively deform cells by means of the afore-described photo-actuable platform depends upon the control over cell positioning in space. In the strategy adopted in this work, cells were positioned and confined between adjacent blocks, which compress cells upon photo-expansion.

To obtain the cell confinement we have used the well known contact guidance, phenomenon for which nano- or micro-patterns (topological and/or chemical) influence the cell orientation and morphology [31][32][33][34][35].

More in details, following a strategy similar to that described by Annabi et al. [36], we produced with the Nanoscribe a network of interconnected 10X10 μm channels, fabricating an array of acrylate gelatin parallelepipeds directly attached on a glass substrate (figure 1).

Additionally, we used our 3D lithography system to enhance the platform confinement efficiency then increasing the percentage of confined cells that, in the work of Annabi et al. [36] reached values of ≅54%. To this end we patterned the lateral walls of the gelatin microstructures with a linear topography composed by 3μm pitch gratings with a square section of 1 μm^2 (Fig. 6A). The pattern size was not optimized, but it was chosen starting from literature data that have highlighted the capability of micrometric linear topographies to align fibroblasts [37].

To evaluate the influence of the lateral micro-topography on the cell positioning, NIH-3T3 cells were used as model and seeded with a density of 140 cells/mm^2. Comparing the acquired confocal images (figures 6C and 6D) it is easy to observe that the cells seeded on the µpatterned structures (Fig. 6C), contrary to those seeded on the flat ones (Fig. 6D), are systematically confined between adjacent blocks. From figure 6D it seems that the weak tendency of cells to be confined between adjacent blocks (comparable with that reported in literature) is strongly enhanced by the presence of the linear topography on the lateral gelatin surfaces.

It is also noteworthy that with this approach a notable cell confinement is obtained without recurring to any additional chemical functionalization step. In many platforms designed to precisely shape cells, in fact, it is common to introduce patterns of cell-adhesive chemical moieties (cell adhesive islands) opportunely positioned on cell-repellent surfaces [38][35].

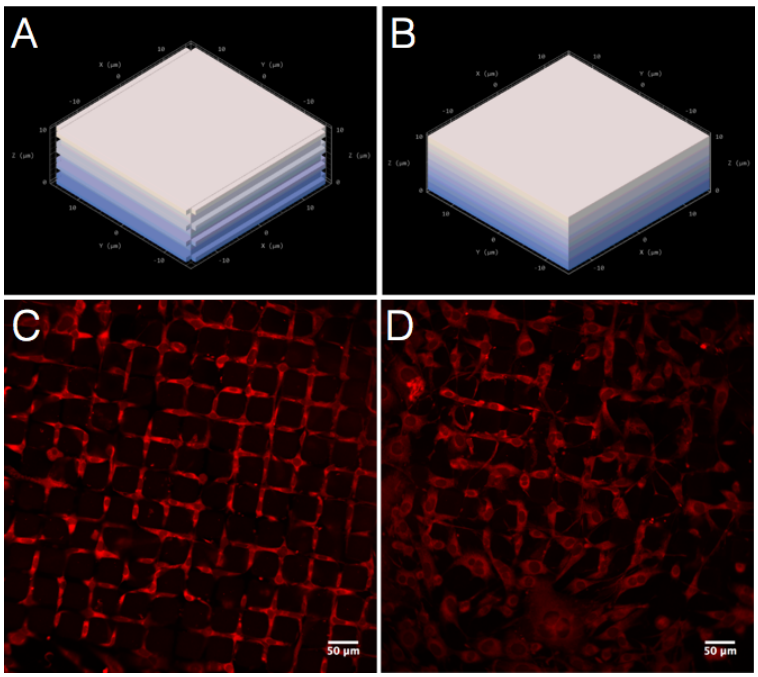

Figure 6: Nanoscribe software representation of the patterned (A) and flat (B) gelatin parallelepipeds. In figures C and D confocal images of living NIH 3T3 stained with the vital Cell Tracker Deep Red and seeded on the patterned (C) and flat (D) structures are reported. Scale bars: 50µm.

The strong influence on the cell adhesion of this topographic signal is further highlighted by the images of the fixed cells (Fig.7A-C); the confined cells tend in fact to follow the lateral micropattern surrounding many parallelepipeds and, at the same time, assuming very intricate shapes which are associated with a strong alignment and stretching of the cytoskeleton actin fibers in different directions. From the acquired z stacks it was observed that cells did not reach heights greater than 10 µm (height of the parallelepipeds) preferring to maximize the contact with the gelatin lateral walls.

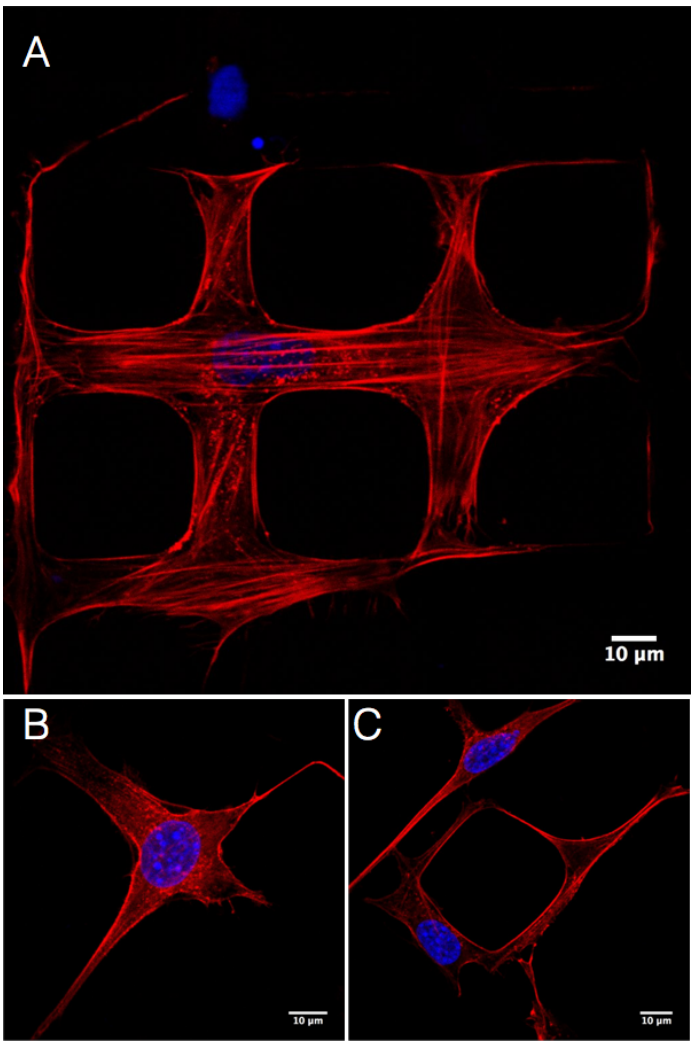

Figure 7: Confocal images of fixed NIH-3T3 seeded on the patterned structures. Scale bars: 10 µm.

To further investigate a more general validity of the lateral topographic pattern on the cell confinement we tested a different cell line (HUVEC). As it is clear from the images (Fig. 8 A-D), also these cells were systematically confined between adjacent blocks.

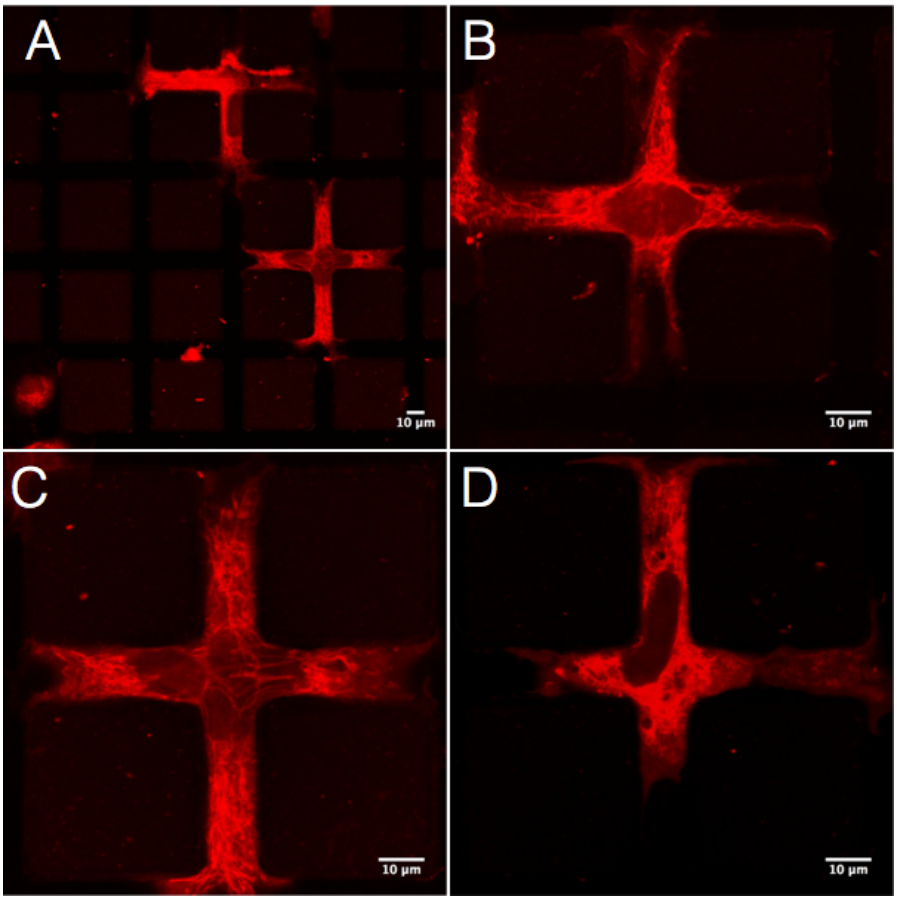

Figure 8: Confocal images of living HUVEC stained with the vital Cell Tracker Deep Red seeded on patterned structures. Scale bars: 10 µm.

3.3.3 Cell Deformation

Once confined, the living cells of Fig. 6C (stained with the vital CellTracker Dip Red) were mechanically and selectively stimulated by photoactuating their surrounding structures. In these experiments structures were exposed for

10 min to a 13 mW multiphoton laser tuned at 700 nm (voxel wavelength 350 nm). The microscope ROI editor prevents undesired effects of UV exposure on living cells by allowing a very accurate light targeting on the regions to be deformed.

Once stimulated, the expansion of the structures could cause the deformation of the cell nucleus (Fig. 9). By analyzing the images, a structure deformation smaller than that registered in the stimulation studies has been observed (≈6.8% instead of ≈10%, see paragraph 3.3.1), even though the same parameters have been used. This result is due to the presence of cells, which limit structure expansion.

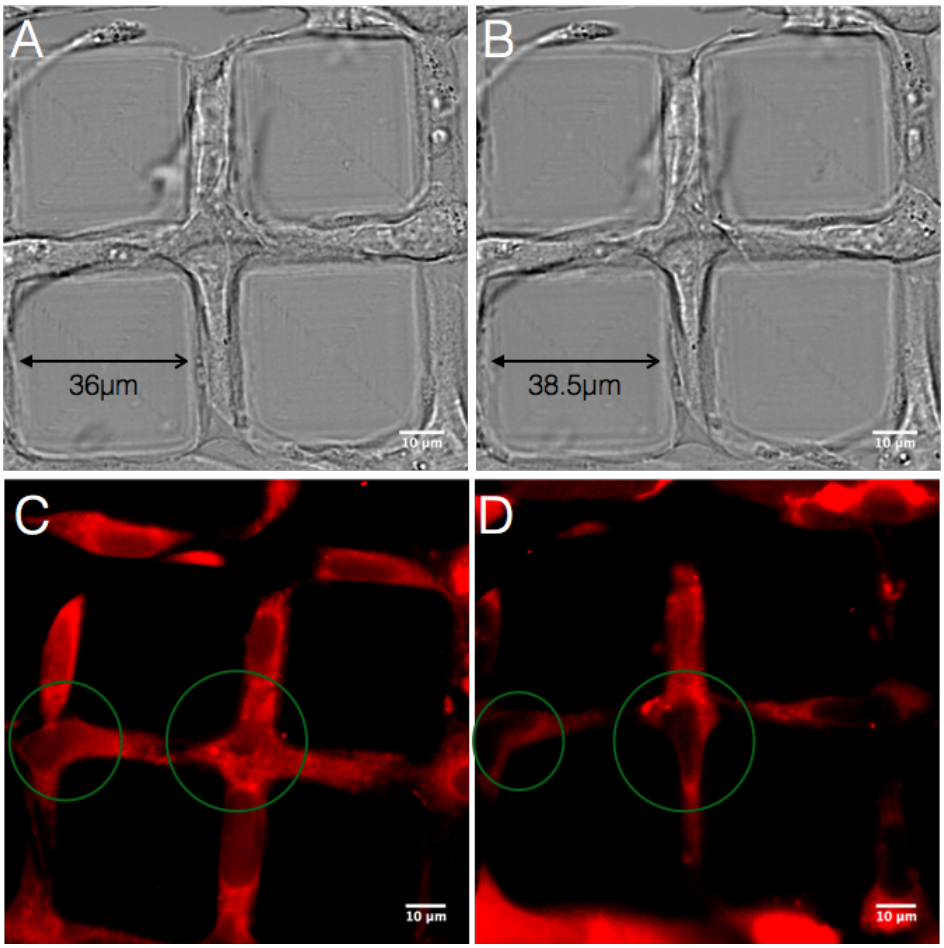

Figure 9: Confocal images of the structures and living cells (NIH-3T3) before (A and C) and after (B and D) the photo-actuation. Scale bars:10 µm.

To systematically study cell reactions to specific mechanical stimuli it is necessary to work on a single cell level to eliminate all the uncontrolled signals provided by the interaction with the surrounding cells. In this case, cell isolation has been obtained by simply decreasing cell seeding density from 140 to 70 cells/mm^2 (Fig.9 A and C).

To evaluate the deformation of living cells a staining treatment with the vital CellTracker Deep Red and with the Hoechst 33342 was performed, to respectively observe during the stimulation the cell body and its nucleus. The photo-stimulation was performed with the same parameters mentioned above and cells were then compressed.

By comparing cell shape before and after the stimulation (Fig.10 A-B and C-D) a decrease of the nucleus area was observed and quantified with ImageJ. From the collected data, a range of deformations between 5 and 13% was registered. The variability of these results is basically due to the cells positioning variability among the gelatin structures (Fig. A and C). Indeed, cells may receive different stimulations by the same structure deformation as a consequence of the different mechanical force they will perceive. To enhance the deformation reproducibility it is fundamental to decrease the cell-positioning variability, which could be dependent from the channel dimensions. More in details we think that a reduction of the channel width represent the key to achieve this goal, and actually we are working on the optimization of this parameter.

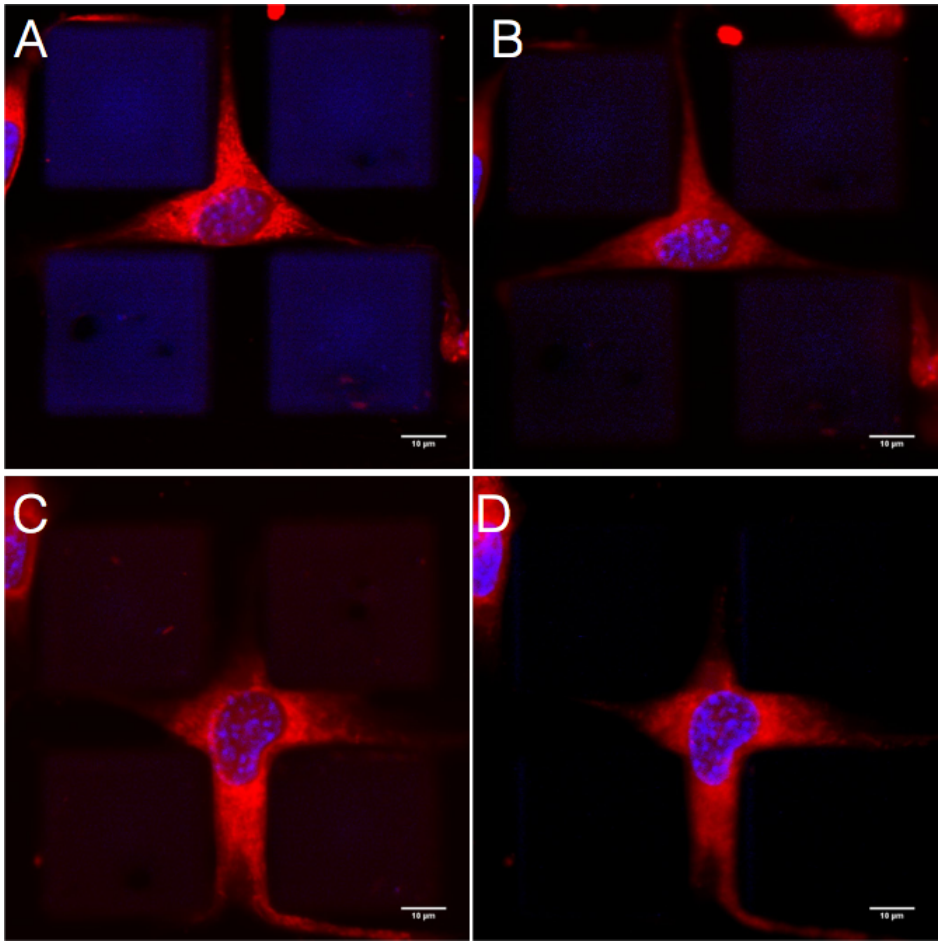

Figure 10: Confocal images of the living cells (NIH-3T3) before (A and C) and after(B and D) the stimulation. Scale bars: 10 µm.

3.4 Conclusion and future perspectives

In this work we have combined the photo-actuation with the contact guidance concept to develop a smart micro-platform able to mechanically stimulate cells down to the single-cell level. To this end we have added an azobenzene molecule to an acrylate photo-crosslinkable gelatin, to fabricate for the first time 3D photo-deformable gelatin microstructures designed to direct apply forces on cells.

Combining the light-sensitivity of the aforementioned gelatin with our capability to micro-fabricate it by means of the 3D lithography, we have built up an instructive platform to deform the nuclei of living cells. More specifically cells have been confined between adjacent structures, either on multiple or single level, and compressed. In our application, moreover, employing a confocal microscope as light source, we have shown the possibility to select the single cell to deform.

For cellular confinement we have introduced a linear topography in the z-direction by means of the 3D lithography; the results evidenced that our approach strongly influence the cell positioning without recurring to complicate fabrication of functionalization steps, paving the way for the development of more complex and efficient cell confinement platforms.

With our positioning method we have precisely controlled the localization of cells between lateral walls. In this way cells could be compressed by photo-stimulating adjacent expanding μstructures . Further characterization of the photo-deformation and of its cyclical changes are under investigation.

Despite to the fact that the platform proposed here can be significantly improved in terms of material properties, it is worth noticing that this is the first example of 3D light-actuator μscaffold which can be a valuable tool for studying and guiding the cell mechano-transduction process.

References

[1] T. Ota, M. Chiba, and H. Hayashi, "Vibrational stimulation induces osteoblast differentiation and the upregulation of osteogenic gene expression in vitro," *Cytotechnology*, vol. 68, no. 6, pp. 2287–2299, 2016.

[2] C. C. Dufort, M. J. Paszek, and V. M. Weaver, "Balancing forces : architectural control of mechanotransduction," *Nat. Publ. Gr.*, vol. 12, no. 5, pp. 308–319, 2011.

[3] B. D. Hoffman, C. Grashoff, and M. a Schwartz, "Dynamic molecular processes mediate cellular mechanotransduction.," *Nature*, vol. 475, no. 7356, pp. 316–323, 2011.

[4] C. Nardini, V. Devescovi, Y. Liu, X. Zhou, Y. Lu, and J. E. Dent, "Systemic Wound Healing Associated with local sub-Cutaneous Mechanical Stimulation," *Sci. Rep.*, vol. 6, p. 39043, 2016.

[5] A. Salameh and S. Dhein, "Effects of mechanical forces and stretch on intercellular gap junction coupling," *Biochim. Biophys. Acta - Biomembr.*, vol. 1828, no. 1, pp. 147–156, 2013.

[6] C. C. DuFort, M. J. Paszek, and V. M. Weaver, "Balancing forces: architectural control of mechanotransduction.," *Nat. Rev. Mol. Cell Biol.*, vol. 12, no. 5, pp. 308–319, 2011.

[7] B. Koch, S. Sanchez, C. K. Schmidt, A. Swiersy, S. P. Jackson, and O. G. Schmidt, "Confinement and deformation of single cells and their nuclei inside size-adapted microtubes," *Adv. Healthc. Mater.*, pp. 1753–1758, 2014.

[8] Z. Alihemmati, B. Vahidi, N. Haghighipour, and M. Salehi, "Computational simulation of static/cyclic cell stimulations to investigate mechanical modulation of an individual mesenchymal stem cell using confocal microscopy," *Mater. Sci. Eng. C*, vol. 70, pp. 494–504, 2017.

[9] R. A. Gould, H. C. Yalcin, J. L. Mackay, K. Sauls, R. Norris, S. Kumar, and J. T. Butcher, “Cyclic Mechanical Loading Is Essential for Rac1-Mediated Elongation and Remodeling of the Embryonic Mitral Valve,” *Curr. Biol.*, vol. 26, no. 1, pp. 27–37, 2016.

[10] E. Huisman, A. Lu, S. Jamil, R. Mousavizadeh, R. McCormack, C. Roberts, and A. Scott, “Influence of repetitive mechanical loading on MMP2 activity in tendon fibroblasts,” *J. Orthop. Res.*, vol. 34, no. 11, pp. 1991–2000, 2016.

[11] A. Tajik, Y. Zhang, F. Wei, J. Sun, Q. Jia, W. Zhou, R. Singh, N. Khanna, A. S. Belmont, and N. Wang, “Transcription upregulation via force-induced direct stretching of chromatin,” *Nat. Mater.*, vol. 15, no. August, pp. 1–20, 2016.

[12] O. Chaudhuri, L. Gu, D. Klumpers, M. Darnell, S. A. Bencherif, J. C. Weaver, N. Huebsch, H.-P. Lee, E. Lippens, G. N. Duda, and D. J. Mooney, “Hydrogels with tunable stress relaxation regulate stem cell fate and activity.,” *Nat. Mater.*, vol. 15, no. November, pp. 326–333, 2015.

[13] N. A. J. S. Niadecki, R. A. V. I. A. D. Esai, S. A. M. I. A. L. O. M. R. Uiz, and C. H. S. C. Hen, “Nanotechnology for Cell – Substrate Interactions,” vol. 34, no. 1, pp. 59–74, 2006.

[14] J. L. Tan, J. Tien, D. M. Pirone, D. S. Gray, K. Bhadriraju, and C. S. Chen, “Cells lying on a bed of microneedles : An approach to isolate mechanical force,” vol. 2002, no. Track II, 2002.

[15] K. Haase, J. K. L. Macadangdang, C. H. Edrington, C. M. Cuerrier, S. Hadjiantoniou, J. L. Harden, I. S. Skerjanc, and A. E. Pelling, “Extracellular Forces Cause the Nucleus to Deform in a Highly Controlled Anisotropic Manner.,” *Sci. Rep.*, vol. 6, no. October 2015, p. 21300, 2016.

[16] M. a C. Stuart, W. T. S. Huck, J. Genzer, M. Müller, C. Ober, M. Stamm, G. B. Sukhorukov, I. Szleifer, V. V Tsukruk, M. Urban, F.

Winnik, S. Zauscher, I. Luzinov, and S. Minko, “Emerging applications of stimuli-responsive polymer materials.,” *Nat. Mater.*, vol. 9, no. 2, pp. 101–113, 2010.

[17] R. Langer, “Bioresponsive materials,” *Nat. Rev. Mater.*, vol. 1, p. 16075, 2016.

[18] J. a Burdick and W. L. Murphy, “Moving from static to dynamic complexity in hydrogel design.,” *Nat. Commun.*, vol. 3, p. 1269, 2012.

[19] A. M. Rosales and K. S. Anseth, “The design of reversible hydrogels to capture extracellular matrix dynamics,” *Nat. Publ. Gr.*, vol. 1, no. February, pp. 1–16, 2016.

[20] M. Guvendiren and J. a Burdick, “Stiffening hydrogels to probe short- and long-term cellular responses to dynamic mechanics.,” *Nat. Commun.*, vol. 3, p. 792, 2012.

[21] D. Kilinc, C. L. Dennis, and G. U. Lee, “Bio-Nano-Magnetic Materials for Localized Mechanochemical Stimulation of Cell Growth and Death,” *Adv. Mater.*, pp. 5672–5680, 2016.

[22] C. Rianna, L. Rossano, R. H. Kollarigowda, F. Formiggini, S. Cavalli, M. Ventre, and P. A. Netti, “Spatio-Temporal Control of Dynamic Topographic Patterns on Azopolymers for Cell Culture Applications,” *Adv. Funct. Mater.*, vol. 26, no. 42, pp. 7572–7580, 2016.

[23] A. A. Abdeen, J. Lee, N. A. Bharadwaj, R. H. Ewoldt, and K. A. Kilian, “Temporal Modulation of Stem Cell Activity Using Magnetoactive Hydrogels,” *Adv. Healthc. Mater.*, vol. 5, no. 19, pp. 2536–2544, 2016.

[24] Z. Mahimwalla, K. G. Yager, and C. J. Barrett, *Azobenzene photomechanics : prospects and potential applications*. 2012.

[25] A. Shishido, “Recent twists in photoactuation and photoalignment control,” *J. Mater. Chem. C Mater. Opt. Electron. devices*, vol. 2, no. 35, pp. 7155–7162, 2014.

[26] A. Natansohn and P. Rochon, “Photoinduced Motions in Azo-Containing Polymers,” 2002.

[27] H. M. D. Bandara and S. C. Burdette, “Photoisomerization in different classes of azobenzene.,” *Chem. Soc. Rev.*, vol. 41, no. 5, pp. 1809–25, 2012.

[28] N. Hosono, H. Furukawa, Y. Masubuchi, T. Watanabe, and K. Horie, “Photochemical control of network structure in gels and photo-induced changes in their viscoelastic properties,” *Colloids Surfaces B Biointerfaces*, vol. 56, no. 1–2, pp. 285–289, 2007.

[29] A. M. Rosales, K. M. Mabry, E. M. Nehls, and K. S. Anseth, “Photoresponsive Elastic Properties of Azobenzene-Containing Poly(ethylene-glycol)-Based Hydrogels,” *Biomacromolecules*, vol. 16, no. 3, pp. 798–806, 2015.

[30] A. A. Beharry and G. A. Woolley, “Azobenzene photoswitches for biomolecules,” *Chem Soc Rev*, vol. 40, no. 8, pp. 4422–4437, 2011.

[31] H. J. Jeon, C. G. Simon, and G. H. Kim, “A mini-review: Cell response to microscale, nanoscale, and hierarchical patterning of surface structure,” *J. Biomed. Mater. Res. - Part B Appl. Biomater.*, vol. 102, no. 7, pp. 1580–1594, 2014.

[32] A. T. Nguyen, S. R. Sathe, and E. K. F. Yim, “From nano to micro: topographical scale and its impact on cell adhesion, morphology and contact guidance.,” *J. Phys. Condens. Matter*, vol. 28, no. 18, p. 183001, 2016.

[33] H. N. Kim, A. Jiao, N. S. Hwang, M. S. Kim, D. H. Kang, D. H. Kim, and K. Y. Suh, “Nanotopography-guided tissue engineering and regenerative medicine,” *Adv. Drug Deliv. Rev.*, vol. 65, no. 4, pp. 536–558, 2013.

[34] X. Yao, R. Peng, and J. Ding, “Cell-material interactions revealed via

material techniques of surface patterning," *Adv. Mater.*, vol. 25, no. 37, pp. 5257–5286, 2013.

[35] Z. A. Cheng, O. F. Zouani, K. Glinel, A. M. Jonas, and M. C. Durrieu, "Bioactive chemical nanopatterns impact human mesenchymal stem cell fate," *Nano Lett.*, vol. 13, no. 8, pp. 3923–3929, 2013.

[36] N. Annabi, K. Tsang, S. M. Mithieux, M. Nikkhah, A. Ameri, A. Khademhosseini, and A. S. Weiss, "Highly elastic micropatterned hydrogel for engineering functional cardiac tissue," *Adv. Funct. Mater.*, vol. 23, no. 39, pp. 4950–4959, 2013.

[37] S. Javaherian, J. P. Soleas, D. Halverson, P. B. Lu, P. W. Zandstra, and A. P. Mcguigan, "A RTICLE A Microgroove Patterned Multiwell Cell Culture Plate for High-Throughput Studies of Cell Alignment," vol. 111, no. 12, pp. 2537–2548, 2014.

[38] H. Zhang, R. Hou, P. Xiao, R. Xing, T. Chen, Y. Han, P. Ren, and J. Fu, "Single cell migration dynamics mediated by geometric confinement," *Colloids Surfaces B Biointerfaces*, vol. 145, pp. 72–78, 2016.

CHAPTER 4
Gelatin building blocks for tissue engineering applications

4.1 Introduction

The aim of tissue engineering is to develop functional 3D constructs that could be implanted *in vivo* to replace or restore damaged tissues. Once implanted, the constructs provide instructive signals that regulate cell functions and behavior required for tissue regeneration; moreover, the ideal functional platform should work as a support for cells, allowing the diffusion of the necessary nutrients and metabolites and then recreating the complex *in vivo* environmental conditions necessary for tissue development [1][2].

In this context, nowadays there are two main strategies for the platforms production: the top-down and the bottom-up approach. In the top-down approach, cells are basically seeded on a scaffold that acts as a temporary template for tissue growth and reorganization. The drawbacks of this approach basically derive from the necessity to control on the microscopic scale the properties of a macroscopic system (area of several cm^2) fabricated with a one-step process: the inability to achieve suitable environmental conditions for cell viability in 3D thick constructs, to accurately reproduce the native tissue architecture and to regulate the cell density are the main limitations of this approach [3].

The bottom up approach is based on the observation for which natural tissues are composed by repeating units with specific micro-architectures and physical and chemical properties that are tissue-dependent; the repeating units (or building blocks) are separately reproduced and then assembled to form the native tissue [4][5][6]. With this method it is theoretically possible

to easier control the construct microscopic features over a broader size range, then overcoming the top-down approach limitations; the development of suitable methodologies for the building blocks assembly actually represents the major challenge and, even though many different strategies have been already presented and important progresses have been done, the complete control over this step has not been achieved yet [5][7][8].

In the reproduction of the living tissues another factor to take into account is the cell alignment, which, in turn, could play a major role in the regulation of several cell functions and in the consequent determination of many tissue properties, such as, for example, the mechanical anisotropy [9]. The formation of highly anisotropic tissues has been obtained by seeding cells on instructive hydrogel fibers [10]; among the many fiber fabrication methods, the microfluidic approach has allowed fabricating the most engineered structures in terms of composition, morphology and cell instructive signals [9][11][12][13]; however, the employment of these types of structures in the bottom-up approach is currently limited to the creation of only pseudo-3D tissues [7].

Reasonably, an intelligent approach to overcome the fiber-related limitations can consist in the fabrication of instructive μscaffolds (building blocks) that promote the alignment of cells for the formation of oriented μtissues and that, once assembled, allow forming oriented macrotissues still preserving the aforementioned advantages of the bottom-up approach.

In this work we have fabricated and tested 3D patterned gelatin-based instructive building blocks for the cell alignment on the bottom up-approach scale. Because of the difficulties in the 3D processing of gelatin, we first optimized the DLW-2PP process as a rapid prototyping technique to test the efficiency of the topographic pattern guidance.

Moreover, we have started to build up a microfluidic platform for the massive production of tubular patterned gelatin μscaffolds. To this end we

have first combined the droplet microfluidic with the gel spinning microfluidic to isolate gelatin emulsions. Briefly, droplet microfluidic is based on the fluid-dynamic interactions between immiscible fluids to produce size-controlled emulsions [14]; in gel spinning microfluidic devices gelatin is fluxed at high temperature in μchannels and cooled at the device exit to freeze instantaneously its shape (avoiding the die swell effect) continuously producing gelatin microfibers [15]. Then, in order to transfer the topography on the gelatin droplet surface, we have performed an in-situ 3D lithography processes aimed at embedding directly in the device microstructures acting as an extrusion micro-head.

4.2 Materials and methods

4.2.1 Cell culture

To seed cells into the plugs, Human dermal fibroblasts (neonatal HDF 106-05n ECACC) were sub-cultured onto 25 mm Petri dishes in culture medium (Eagle's BSS Minimum Essential Medium containing 20% fetal bovine serum, 100 mg/ml L-glutamine, 100 U/ml penicillin/strep- tomycin, and 0.1 mM Non Essential Amino Acids). Cells were maintained at 37 °C in humidified atmosphere containing 5% CO_2. HDF of passages 6-12 were used for all experiments. Before using plugs, they were sterilized by absolute ethanol immersion for 24 h. After that, in order to remove ethanol completely, several washings in calcium-free and magnesium-free phosphate-buffered saline (PBS) were performed. Before cell seeding, PBS was removed and replaced with the culture medium. The Petri dish was shaken onto an orbital shaker and loaded with 20 cells per plug. Culture suspension was stirred intermittently at 30 rpm (5 min stirring and 30 min static incubation) for the first 6 h post-inoculation for cell adhesion, and then continuously agitated at 30 rpm. The growth medium was replenished on the

first day and every 2 days until the end of experiments (7, 17 and 24 days in total).

4.2.2 Cell Imaging

Over the entire dynamic cell culture period, 1 ml aliquots were collected at days 7, 17 and 24 for cell viability as well as for ECM morphology characterization, during human dermal µtissue precursor (HD-µTP) formation and evolution. To this aim samples were investigated by a semi-motorized fluorescence microscope (Olympus BX-53) and by Confocal Leica TCS SP5 II equipped with a Multiphoton laser. Cell viability, proliferation and morphology in the HD-µTPs were assessed by staining the samples with phalloidin tetramethylrhodamine B isothiocyanate (SigmaeAldrich) and SYTOX Green (INVI- TROGEN), the former stains the cell's cytoskeleton the latter cell's nucleic acid. For both analyses, the HD-µTPs were fixed with 4% paraformaldehyde for 20 min at room temperature, rinsed twice with PBS buffer, and incubated with PBS-BSA 0.5% to block unspecific binding. For actin microfilaments and nucleus detections, after fixation, samples were stained with phalloidin tetramethylrhodamine B iso-thiocyanate (phalloidin) and SYTOX Green respectively. In particular, samples were incubated with SYTOX Green stock solution (10 mg/ml in dimethyl sulfoxide) diluted in PBS (1/500 v/v) for 10 min at 37 °C, and after rinsing in PBS, they were stained with phalloidin for 30 min at room temperature. Moreover, two-photon excited fluorescence was used at 840 nm to induce second harmonic generation (SHG) and obtain high-resolution images of unstained collagen structures in the ECM of the HD-µTPs.

4.2.3 Microfluidic Device Fabrication

In this chapter two microfluidic chips were used and fabricated: the first consisted in a simple straight channel that was used for the production of gelatin fiber, while the second device was a T-junction designed for gelatin emulsion production. However, the two chips were fabricated following the same flow-process:

- 2D lithography
- Silicon dry etching
- Replica molding
- Bonding

2D lithography:

For the 2D lithography process we used a mask-less 2D lithography system (Heidelberg DLW-66FS) equipped with a Diode Laser, 405nm, 100mW. The positive tone photoresist AZ-4533 ECI-3012 (Microchemicals GmbH) was first spin-coated on a two inch silicon wafer at 1500 rpm for 40 s; the spin-coater employed was the WS-650 Series (Laurell Technologies Corporation, USA). With these parameters the measured photoresist thickness was 2.5 μm; the thickness was measured with a contact profilometer (Dektak Veeco 150). After the spin coating step, the resist was first soft-baked at 90 °C for 90 s and then exposed with the 2D laser system; the laser power was set to 2.1 mW and the channel area was exposed. Successively, a post exposure bake at 110 °C for 90 s was performed and the sample was then developed in a 4:1 water-developer solution for 60 s, rinsed with water and dried with nitrogen; as developer we used the AZ 351-B (Microchemicals GmbH).

Silicon Dry etching:

The patterned sample was etched with the inductively coupled plasma-reactive ion etching technology (ICP-RIE); the system used here was the PlasmaPro 100 Cobra (OXFORD Instruments).

The sample was fixed on an 8 inches silica wafer by means of high vacuum grease and etched with a Bosh process to obtain vertical walls [16].

After the dry etching, the sample was immersed in acetone for the photoresist stripping, rinsed with 2-propanol and dried with nitrogen. To characterize the etching results the sample was analyzed by SEM (FESEM ULTRAPLUS ZEISS) (Fig.1).

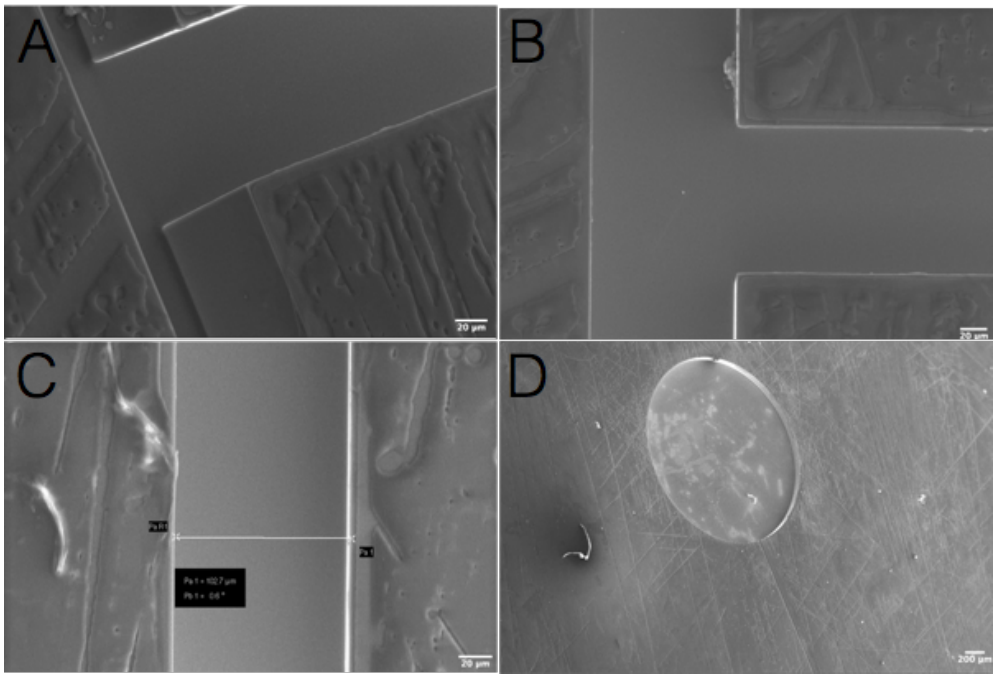

Figure1: SEM images of the silicon master of the T-junction device fabricated with the Bosh process. Scale bars from A to C: 20 µm. Scale bar of image D: 200 µm.

Replica molding:

The final PDMS chip was obtained with a double replica molding procedure. The PDMS pre-polymer (Sylgard 184) was mixed with the cure agent

(mixing ratio 10:1 wt) and degassed to prevent undesired gas bubble entrapping during the curing step. The uncured polymer was then poured on the silicon master; its thickness was controlled with a polymerized PDMS cell (thickness 5 mm). The PDMS was then polymerized transferring the sample in an oven at 100 °C for 2 h. After curing the PDMS was manually peeled off from the silicon master.

The first PDMS replica was then used as a master for a second replica; to this end it was necessary to silanize the PDMS master to prevent the irreversible adhesion of the second replica. The PDMS master was immersed for 3 min in a silanizing solution (95% of water, 3% of 2-propanol, 1% acetic acid and 1% Fluorolink S10 from Acota) and then heated in the oven for 1 h at 120 °C; after this treatment the sample was sonicated in ethanol for 15 min to remove the silanization solution residuals.

After the silanization step, the first replica was then used as a master and another PDMS replica molding was carried out following the procedure previously described. The second replica was cut manually in order to obtain a channel in direct communication with the external ambient.

Bonding:

After the replica molding the PDMS chip was bonded to a second substrate with an oxygen plasma treatment.

The chip designed for the gel spinning process was directly bonded on the Nanoscribe 170 μm thick glass. The chip produced for the plug fabrication was instead bonded on another PDMS surface to obtain the wettability homogeneity required for the droplet generation process; to this end uncured PDMS (10:1 wt prepolymer:curing agent) was spin-coated on the Nanoscribe 170 μm thick glass for 3 min at 6000 rpm and then cured in the oven for 2 h at 100 °C. The PDMS film thickness was evaluated with the profilometer (the same used for the photoresist) and a thickness of 4 μm was measured.

The plasma treatment process was the same for both the devices: surfaces were exposed to oxygen plasma (diener electronic) for 1 min and then put in contact for bonding.

4.2.4 In-chip fabrication lithography

To insert the extrusion micro-head, a 3D lithography process was directly performed on the bonded chip.

Because of the necessity to write in a bonded chip, the oil-immersion writing configuration was used (chapter 2, paragraph 2.2.4). For the lithography process we used the IP-L 780, a negative-tone photoresist specifically optimized for the oil-immersion configuration by Nanoscribe.

The photoresist was manually fluxed in the bonded chip channel with a plastic syringe; once filled with the photoresist, the sample was mounted on the Nanoscribe sample holder and inserted in the system piezo-stage. The process configuration is schematically represented in figure.2. Before the exposure, the lithography system was aligned with the channel to ensure a suitable structure positioning and orientation; more specifically, using the microscope camera of the system, the x-y piezo-coordinates were rotated for matching with those of the channel.

For the development the mr-Dev 600 developer (micro resist technology GmbH) was fluxed in the chip to ensure the complete removal of the non-exposed photoresist; the development was conducted at room temperature for 16 min. After the development the sample was washed with 2-propanol and gently dried with nitrogen to remove all the chemical residuals.

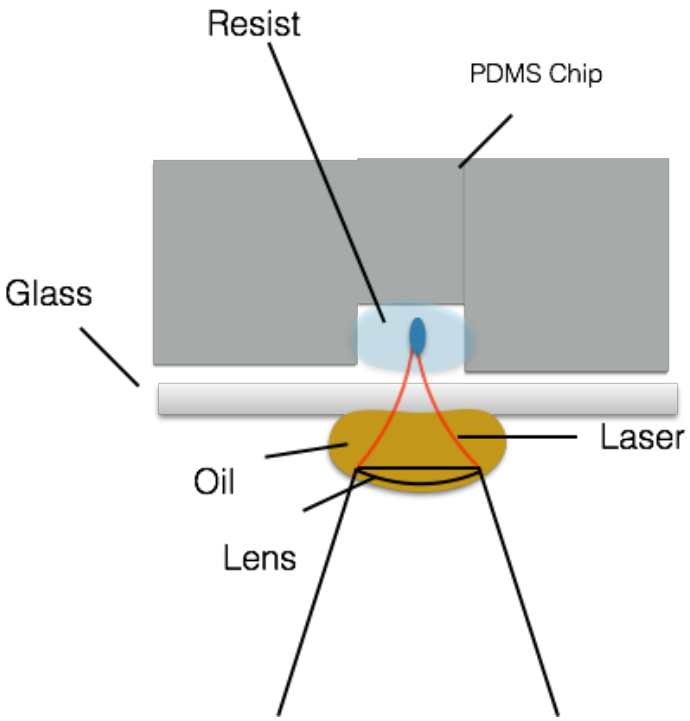

Figure 2: Schematic representation of the in-chip fabrication configuration.

4.2.5 Microfluidic setup

Gelatin A (porcine skin) was prepared dissolving it at 10% wt/v in Milli-Q water at 40 °C for 12 h. Gelatin was then placed in a 2 mL glass syringe and fluxed at 45 °C in the device; a silicon tube was used to connect the syringe with the device. The flow-rate was precisely controlled with the neMESYS syringe pump. To control the gelatin temperature, a flexible heater (BRAINTREE SCIENTIFIC Inc.) was mounted on the syringe and on the silicon tube; the microchip was instead heated at 45 °C with an adhesive heater (RICA heating elements). The temperature control was crucial to ensure the gelatin sol state, a necessary condition to avoid the channel obstruction.

The output of the fiber-spinning device was precisely positioned (schematically represented in Fig. 3) in correspondence of a cold crosslinking

bath (maintained at 0 °C) in order to instantaneously freeze the hot gelatin exiting from the device and then obtain a fiber with a cross section comparable to that of the microfluidic channel. In the crosslinking bath 1-Ethyl-3-(3-dimethylaminopropyl)carbodiimide (EDC) (10 mM) was dissolved in acetone. After 24 h of crosslinking the fiber was collected from the bath and its morphology characterized by SEM analysis. To perform the SEM analysis, gelatin was dried and coated with 6 nm of Au with a sputter coater (CRESSINGTON SPUTTER COATER 208 HR).

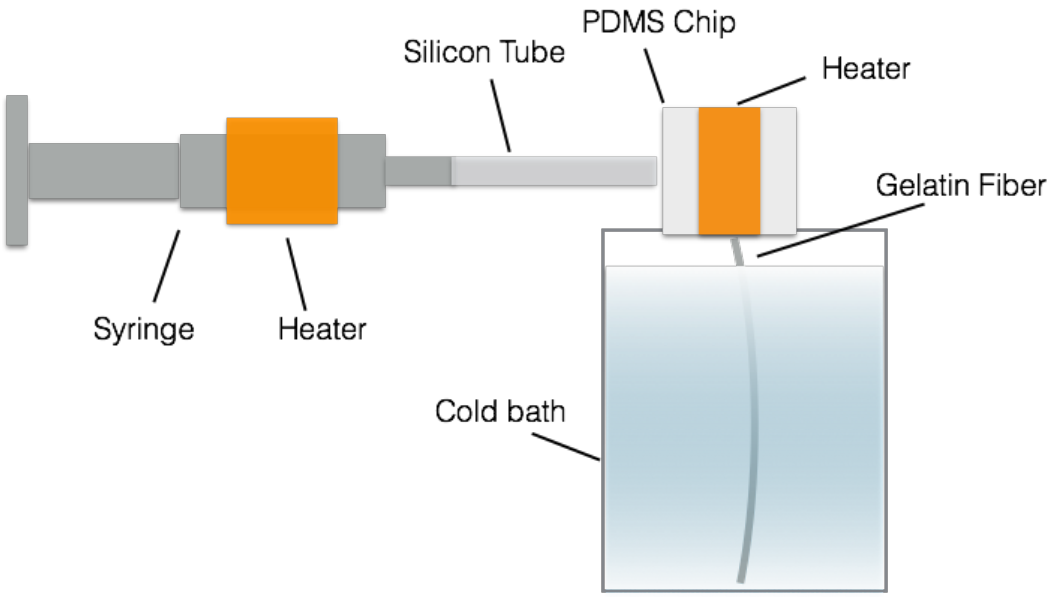

Figure 3: Schematic representation of the configuration of the microfluidic gel-spinning device.

The droplet microfluidic device was instead mounted on the inverted microscope Olympus IX71 to observe and analyze the plug formation; for the visualization a 4X objective was used. The system was heated with the same elements used for the fiber-spinning device. For the emulsion generation the 10% gelatin A solution was used as dispersed phase, while a silicon oil

(viscosity 4 cst) was employed as continuous phase; Span 80 at 10% wt/wt was added to the oil phase for promoting droplet formation.

4.3 Results and discussion

4.3.1 Plug fabrication (Photolithographic Approach)

Patterned hydrogel fibers represent a valid platform to obtain a good 3D cell alignment [9]. To transfer this concept to the bottom up approach scale, here we processed gelatin with a 3D lithography system for the fabrication of instructive tubular μscaffolds.

Even though DLW-2PP offers the possibility to fabricate gelatin as a complex 3D structure with feature sizes influencing cell behavior, it cannot be used for massive production, as required in many tissue engineering applications. The main limitation of this technology is represented by its fabrication time that, as a general rule, dramatically increases whit the resolution. However, because of the difficulties related to the gelatin fabrication on the micrometric scale with other technologies, the DLW-2PP process can be a valid rapid prototyping technique that can be used to quickly test the role of specific topographic signals in the regulation of cell behavior.

The μscaffold designed to evaluate the potentialities of patterned building blocks in the realization of anisotropic micro-tissues is represented in the figure 4; this peculiar shape was designed to maximize the μscaffold-cell surface contact.

The photolithographic process was performed following the protocol described in the chapter 2 (paragraph 2.2.4). The gelatin mixture used here was the same described in the chapter 2: acrylate gelatin at 20% wt/v, Irgacure 369 at 3% wt and the azo-crosslinker at 4% wt dissolved in a phosphate buffer (pH 3.1).

The optimization of experimental parameters aimed to obtain the most stable structure in the shortest time interval, and then to find the highest allowed combination value of output power and scan speed. Especially in the case of hollow structures, the achievement of high crosslinking degree plays a crucial role to get the desired structural stability.

During the optimization of the writing parameters a z-dependent polymerization dose was found. More specifically, because of the material-related optical aberrations (drastically increased in the immersion-oil configuration) [17], the dose required increased with the distance between the region to photocrosslink and the substrate. Therefore, to optimize the writing parameters we divided the structure in a series of modules with a z-thickness of 10 μm (Fig. 4B) and the highest dose of the polymerization range was separately found for each module at each z coordinate.

Precisely controlling the focusing z-position, each module was fabricated with its optimized parameters and then stitched with the successive one following a top-down writing sequence (from the highest to the lowest modulus). The final optimized laser power and scan speed profiles are respectively represented in the figures 4C-D, and their exact value reported in Table 1.

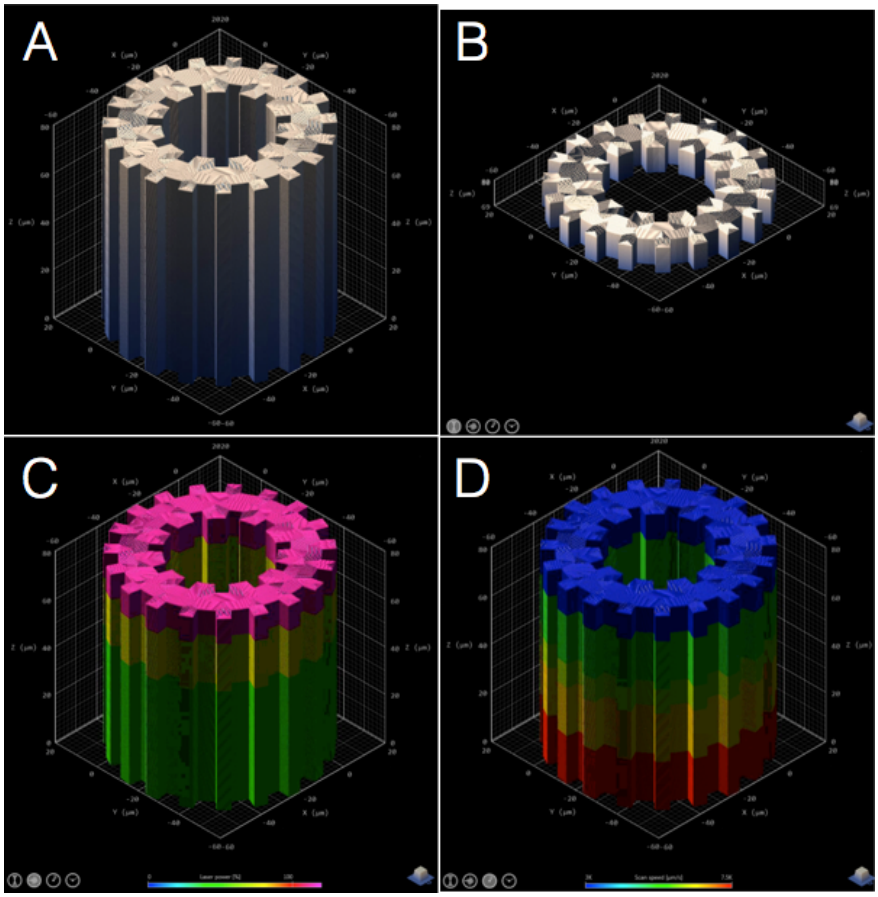

Figure4: Nanoscribe software representation of the entire plug (A) and of the single module (B). In figures C and D the power and speed parameters profiles are respectively reported; here the color legends represent the range of values for respectively output power (C) and Scan Speed (D).

Table 2: Reported data are referred to the Figure 4 C and D. In particular, the value of output power and scan speed are reported for each z coordinate range.

	Output Power (mW)	Scan Speed (µm/s)
70 < z <80	60	3000
60 < z <70	36	5000
50 < z <60	36	5000
40 < z <50	30	6000
30 < z <40	27	6500
20 < z <30	24	7500

10 < z <20	24	7500
0 < z <10	24	7500

Following this fabrication strategy and using the optimized process parameters, stable structures were fabricated (Fig. 5) and each plug was fabricated in about 13 min.

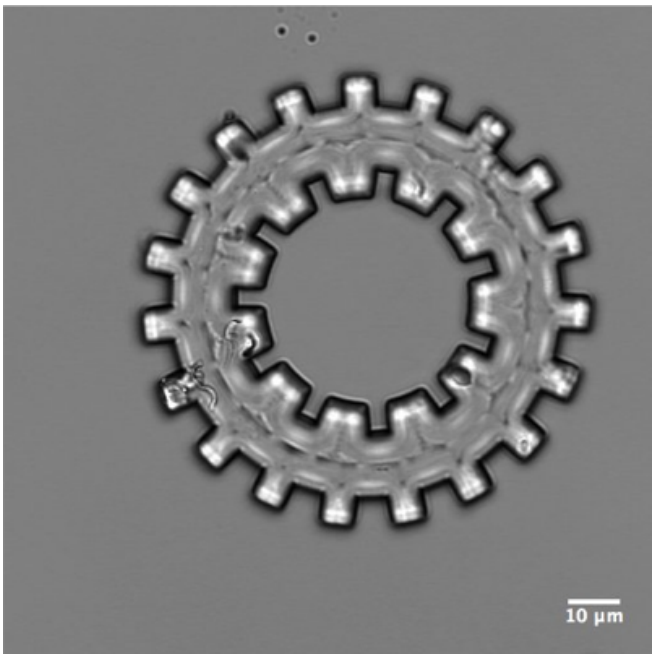

Figure 5: Bright field confocal image of the gelatin plug. Scale bar: 10 µm.

4.3.2 Cell culture

To test our platform potentiality in guiding the cell alignment and the anisotropic µtissue formation, HDF cells were seeded on gelatin µscaffolds as described in the materials and methods section (paragraph 4.2.1).

Cells were observed after 7, 17 and 24 days from the seeding. After 7 days, cells adhered on the plugs surface showing a strong and reproducible alignment along the plug longitudinal direction (Fig. 3 A-B). To prove the

role of the µpattern in the cell alignment, cells were seeded on flat hollow plugs; using the same seeding conditions a very lower cell alignment was observed, further confirming the importance of the topographic signal for our application scope.

Through the multi-photon excitation (see materials and methods, paragraph 4.2.2), the formation of the ECM of the HD-µTPs was monitored and high-resolution images of unstained collagen structures were obtained. Collagen structures assembly was observed only at the 24th day (Fig. 6D) and, such as their cellular counterpart, the mentioned structures were strongly aligned along the plug longitudinal directional.

During the experiment cytotoxic effects were never observed and the cell viability remained unaltered over time.

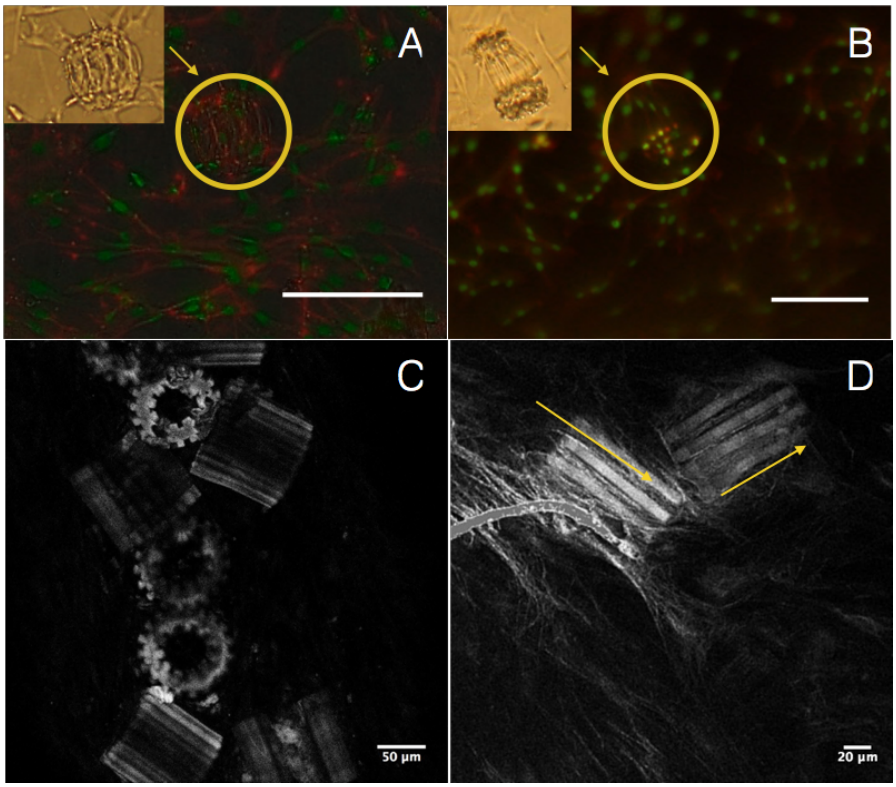

Figure 6: Fluorescence images of HDF seeded on plug (A and B, scale bar 120 and 80 µm); the yellow circles highlight the cell orientation on the µscaffolds. Two-photon excited fluorescence high-resolution images of unstained collagen produced by cells (C and D, scale bars 50 and 20 µm).

4.3.3 Microfluidic Approach

The results relative to the structures fabricated with the 3D lithography indicated that patterned tubular gelatin μscaffolds could be useful tools to produce highly anisotropic micro-tissues. However, as explained in the previous paragraph (4.3.1), the technological specifications of our lithography system limit its use to the rapid prototyping scale.

To produce on a larger scale patterned gelatin μscaffolds, we tried to build up a microfluidic platform combining the droplet microfluidic technology with the gel spinning technique (schematically represented in Fig. 1).

To transfer the topography on the gelatin surface, we were inspired by the work of Shi et al. [9], in which fibers were patterned fluxing the gelatin in a micro-grooved circular PDMS channel; in this work the channel was patterned by integrating into the device a PDMS membrane presenting a specific μtopography. However, following this microfabrication approach it can be extremely hard to modulate the channel shape and topography and, as a consequence, of the extruded fiber.

Therefore, the topography was transferred onto the gelatin surface by following the strategy to integrate 3D μstructures in the microfluidic chip as extrusion μheads; the structures were precisely shaped and positioned with the Nanoscribe system. More specifically, our idea was to insert the structures in correspondence to the channel exit in order to transfer the topography just before gelatin consolidation.

4.3.4 Plug formation

Droplet-microfluidic systems belong to a microfluidic sub-category in which the fluid-dynamic interactions between immiscible fluids are used to isolate little volumes in a controlled way [14]. In this context it is possible to

identify the two immiscible fluids as the continuous and the dispersed phase (the fluid from which the droplet are obtained).

Many droplet formation strategies based on different chip geometries and, then, on different fluid-dynamic interactions were designed [14][18]; among the different geometries here we chose the typical T-junction because of its higher potentialities in the tuning of the droplet aspect ratio (AR) [18].

In this configuration the droplet is formed at the crossing of the two perpendicular channels (fig.7) and is driven by a combination of viscous and interfacial forces, which contribution could be qualitatively valuated with the capillary number Ca:

Equation 1 $$\boldsymbol{Ca} = \mu \boldsymbol{v}/\boldsymbol{\gamma}$$

In the equation μ is the viscosity of the continuous phase, v its velocity and γ the interfacial tension between the two phases.

In the T-junction configuration droplets AR>1 is obtained only in the squeezing regime [19], where the droplet formation driving force is the interfacial tension between the two phases ($Ca<10^{-2}$). In this regime the droplet AR is independent from the fluids viscosity ratio and results proportional to the flow rate ratio Q ($Q= Q_{disp}/Q_{cont}$), as predicted by the Garstecki equation [19].

Here we investigated on the suitable process parameters to obtain stable gelatin plugs with different AR in a T-junction device.

To this end we modulated four parameters:

- % in wt of gelatin
- % of surfactant
- Channels widths ratio
- Flow rates ratio

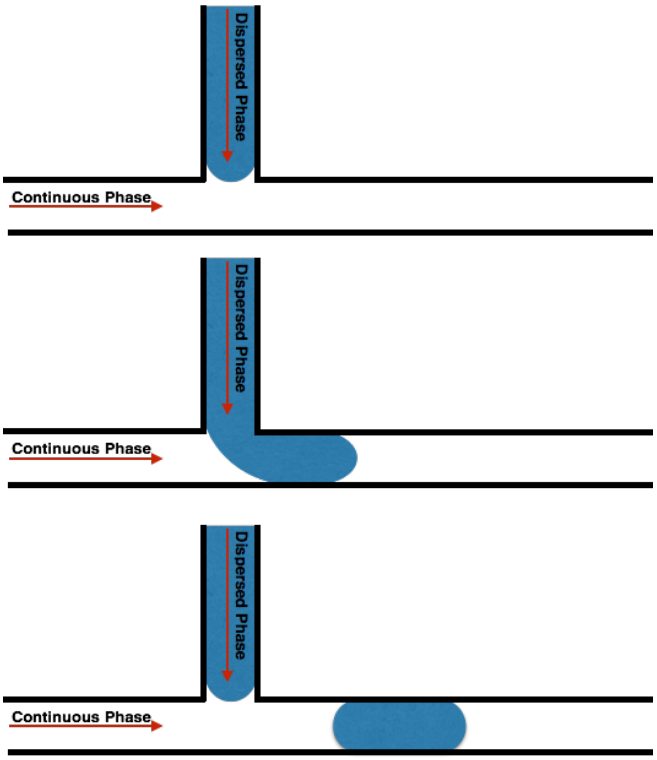

Figure 7: Schematic representation of the plug formation in a T-junction device.

Four different gelatin concentrations were first evaluated; in particular, we tested gelatin A at 5, 10, 15 and 20%. From the experiments, it emerged that using the 15% concentration it was impossible to obtain stable gelatin droplets. We interpreted this result considering the role played by the wettability of the device in the emulsion formation. More specifically, in addition to the immiscibility condition between the two phases, a low device wettability respect to the dispersed phase is required in order to obtain a stable plug formation [20]. Because of the amphiphilic nature of the hydrogel, which increases its hydrophobicity when the polymeric fraction increases, and because of the device (PDMS) hydrophobicity, for higher gelatin fraction, less stable emulsions were produced. On the basis of this

result, we decided to use the 10% gelatin, which showed a better shape-maintaining capability compared to lower concentrations.

For the 10% gelatin the necessary percentage of surfactant to add to the continuous phase was assessed. In general, surfactants promote the droplet formation by decreasing the interfacial tension between two immiscible phases [14]. On the other hand, a decrease in the interfacial tension causes an increase of the capillary number and, then, an exit from the squeezing regime. Starting from these relations it is easy to consider that the best surfactant concentration for the droplet generation is the lowest needed for the stable emulsion production. In our case a 10% of Spun 80 was found as the minimum value to add to the oil phase for a stable gelatin droplet formation.

The third optimized parameter was the channel width ratio Λ, defined as the ratio between the dispersed and continuous channel width. Stable gelatin emulsions were obtained with Λ=2 as also predicted from literature data [21].

With these setup parameters, the plug AR was then evaluated in function of the flow rate ratio; plug AR from 1.9 to 4 were produced (Fig. 8 A-E).

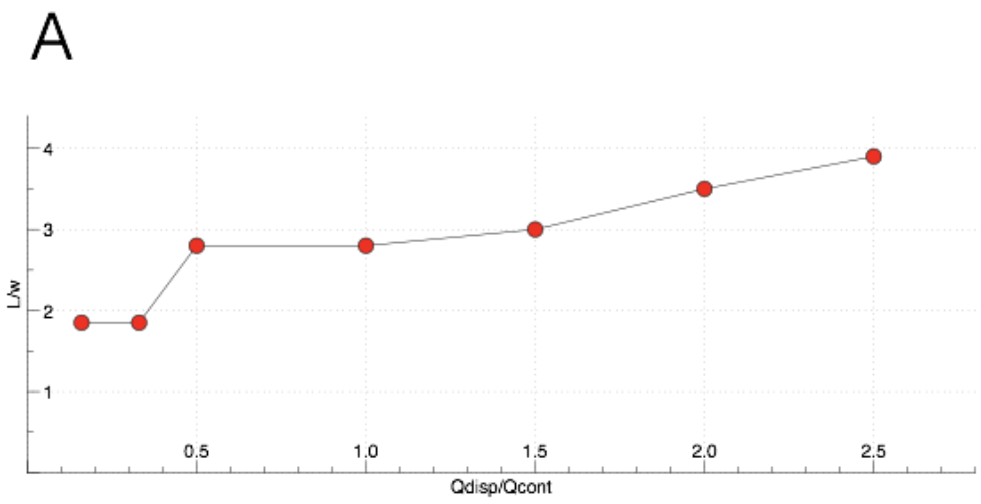

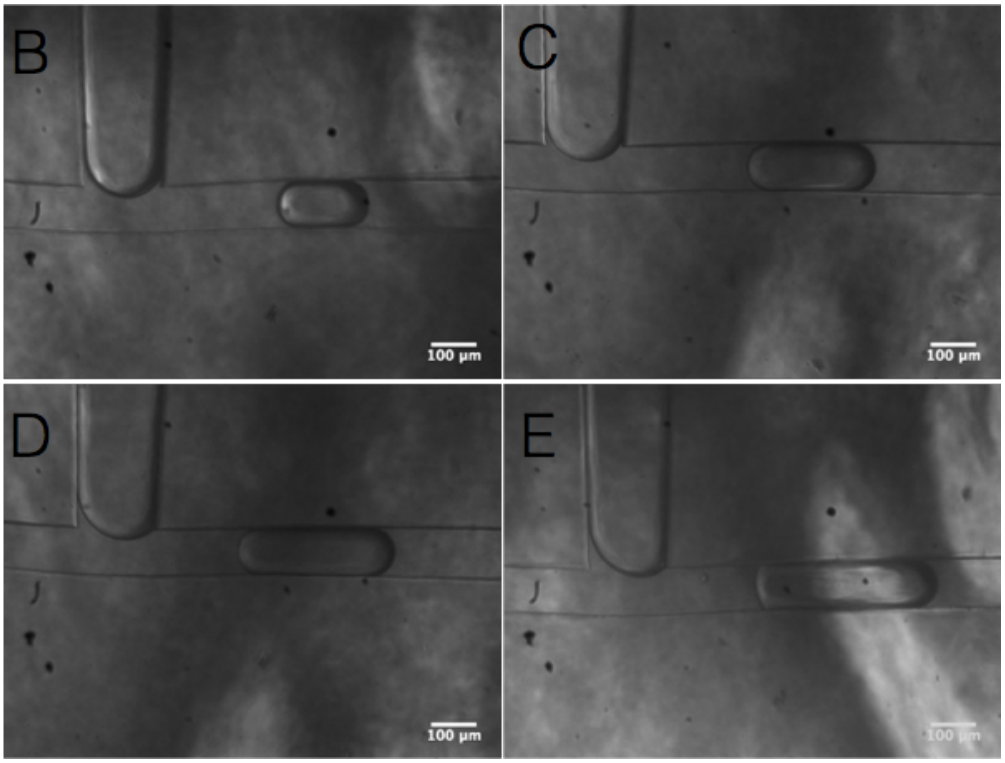

Figure 8: Graphic representing the droplet AR vs Q (A). Bright field images of the droplet formed at Q= 0.1 (B), Q= 0.5 (C), Q= 2 (D) and Q=2.5 (E). Scale bars: 100 µm.

4.3.5 Fiber patterning

To test our capability to transfer topographies onto the gelatin surface adopting the strategy previously described, we inserted with the Nanoscribe a simple structure designed to transfer a single groove on the gelatin fiber surface, as schematically represented in figure 9. Gelatin A was prepared at 10% wt and fluxed at 45 °C in a straight channel with a section of 2500 μm^2. To test the stability of the fabricated extrusion micro-head, gelatin was fluxed up to 500 µl/min; even at the highest velocities the polymerized structures did not detach from the substrate.

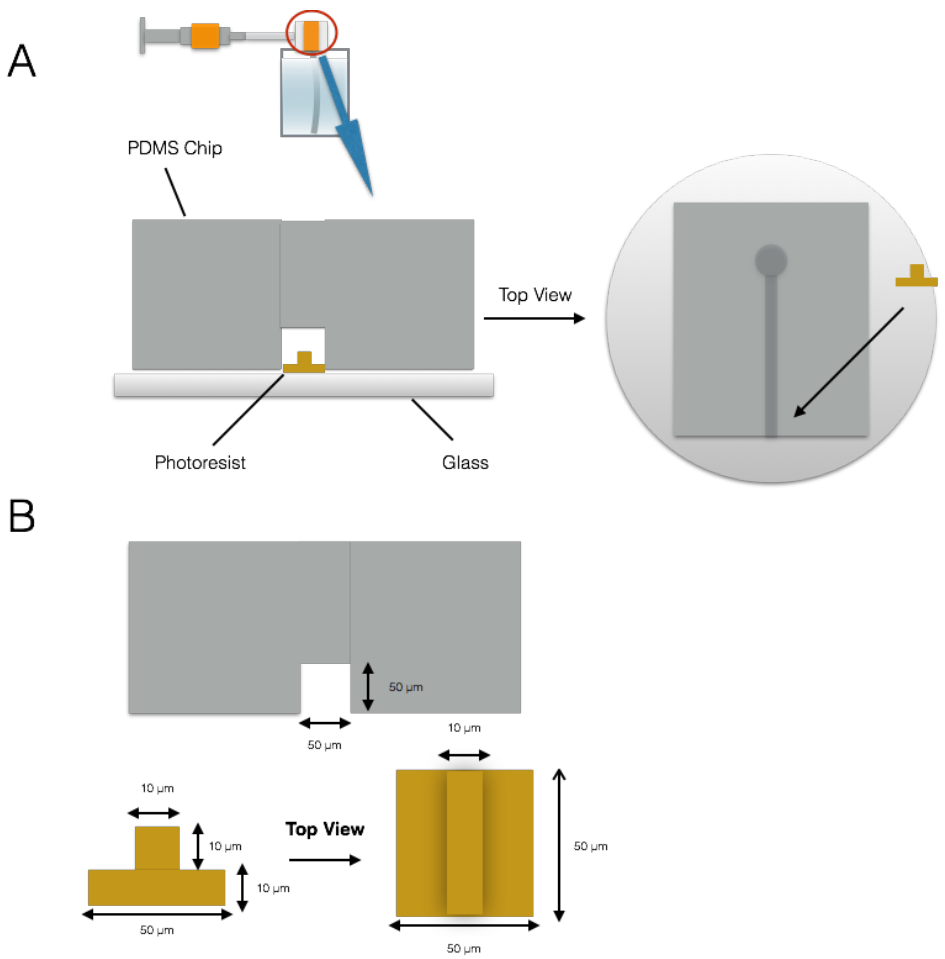

Figure 9: Schematic representation of the system used for the fiber spinning process; the 3D structure fabricated with the Nanoscribe is placed at the exit of the microfluidic channel (A). Schematic representation of the device dimensions**.**

After the chemical crosslinking, the extruded fiber (extrusion flow rate 5 µl/min) surface was characterized by SEM analysis. From the images (Fig. 10 A-C) it is easy to observe on the gelatin fiber the groove presence which was complementary to the integrated protruding microstructure fabricated in the microfluidic device.

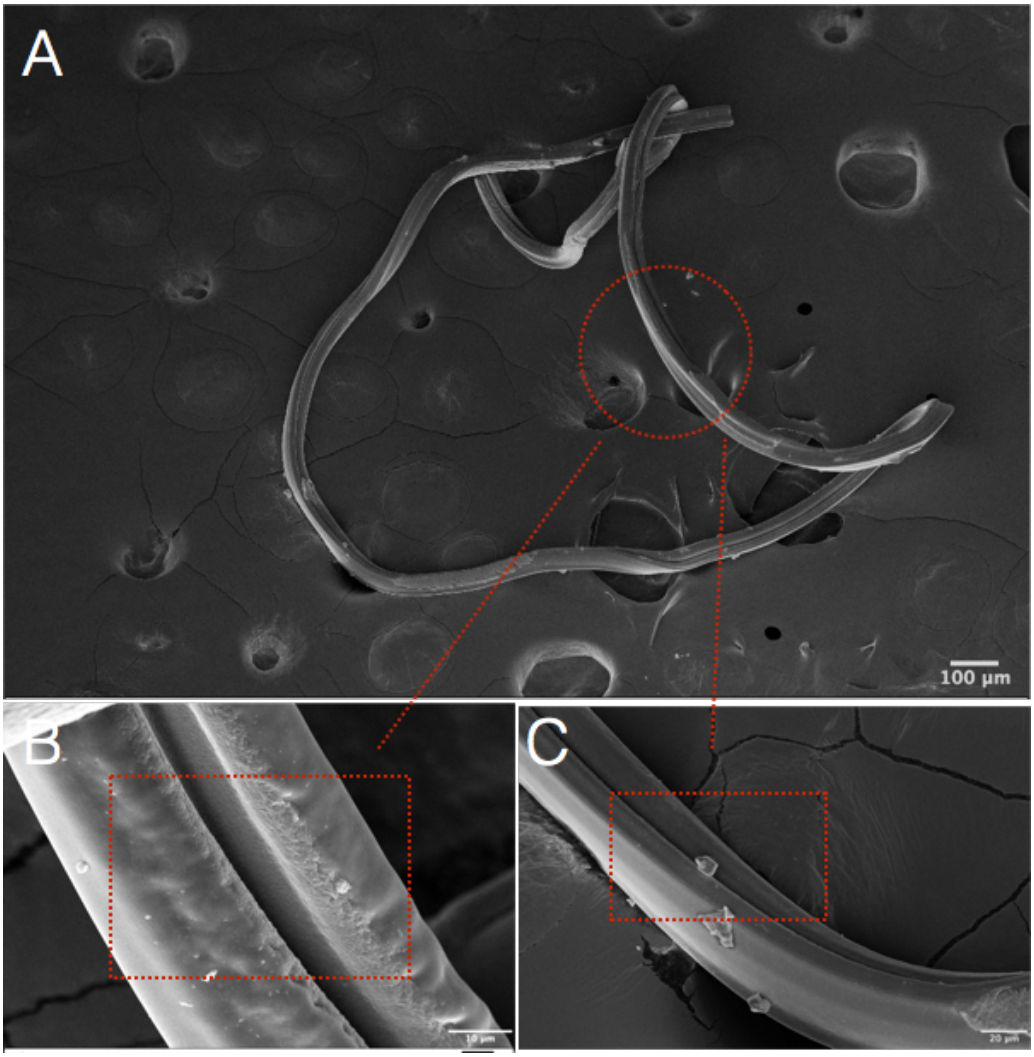

Figure 10: SEM images of the gelatin fiber spinned with the system represented in Figure 9. Scale bars (from A to C): 100, 10, 20 µm.

4.3.6 In-chip extrusion head fabrication

To transfer the topography on the plug surface, an extrusion micro-head was designed and fabricated to occupy the entire channel cross-section of the T-junction device (100x100µm) (figure 11).

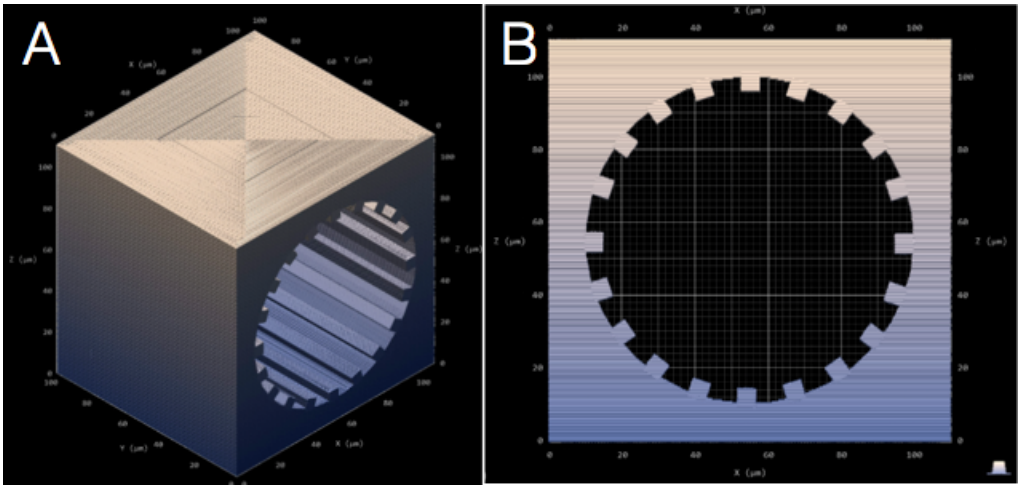

Figure 8: Nanoscribe software representation of the extrusion µhead designed to pattern gelatin plugs.

Because of the structure dimensions and geometrical complexity, an optimization of the process parameters was first conducted on simple glass substrates, to define an appropriate fabrication strategy.

By writing the entire micro-head with a z layer-by-layer approach, a structural collapse was observed (Fig. 12).

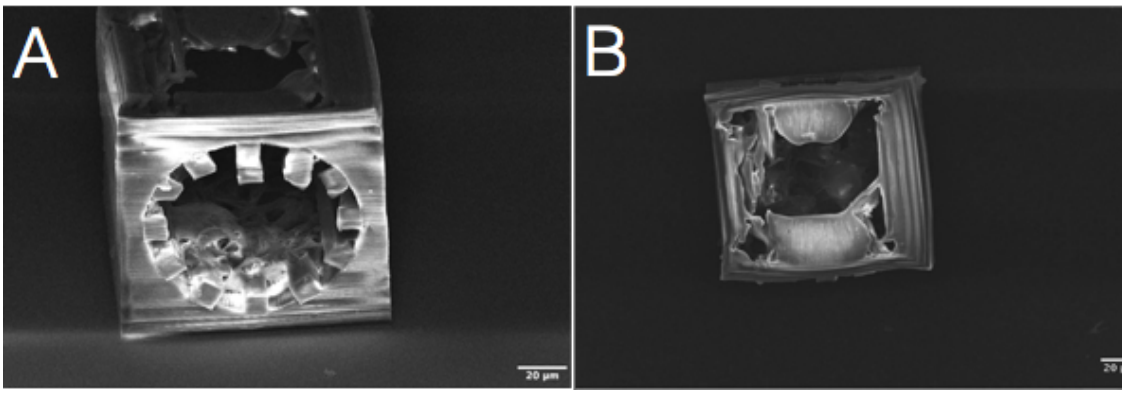

Figure 12: SEM images of the extrusion µhead fabricated with a one-step processa by means of the Nanoscribe. A) Frontal view. B) Top view. Scale bars: 20 µm

To address the collapse problem, we divided the upper part in separate modules, which were stitched and assembled in the xy plane as schematically represented in figure 13.

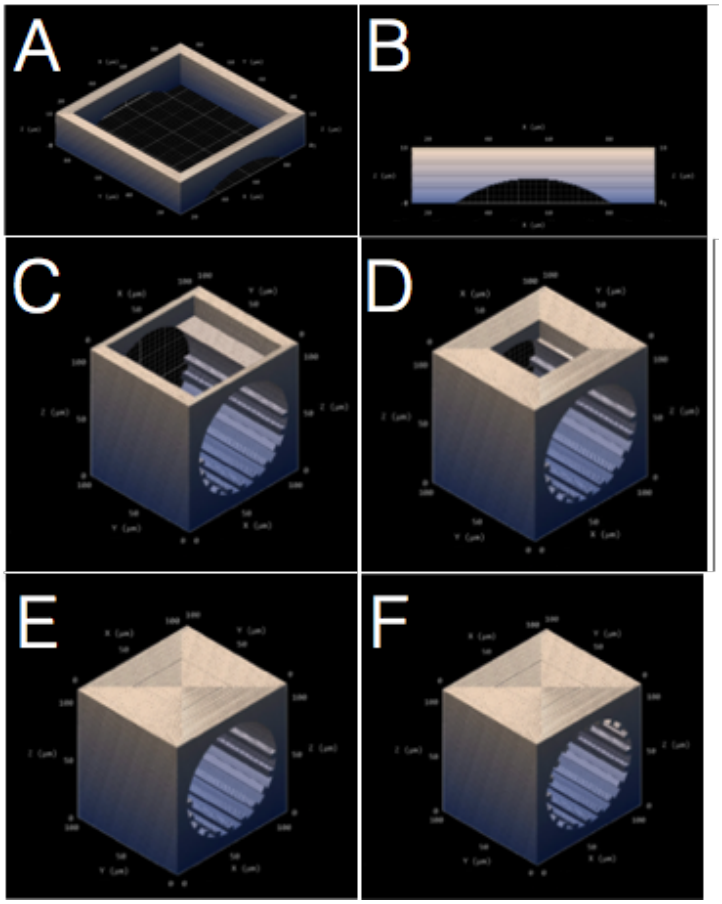

Figure 13: Nanoscribe software representation of the modules composing the upper part of the extrusion μhead (A and B) and of its writing sequence strategy (from C to D).

Following this strategy, the entire structure was integrally fabricated (Fig. 14). The optimized process parameters were: laser output power 40 mW and scan speed 80000 μm/s. Furthermore, we introduced the power-compensation parameter "pspowerslope" at 0.035, to solve the z-dependent power losses associated with the oil immersion configuration, that in our system is observed for z values higher than 30 μm [17]. The fabrication process was completed in about 6 min.

After the microfluidic plug formation and the μhead fabrication optimization, presently we are working on the insertion of the extrusion μhead in the microfluidic device to finally transfer the topography on the plug surface.

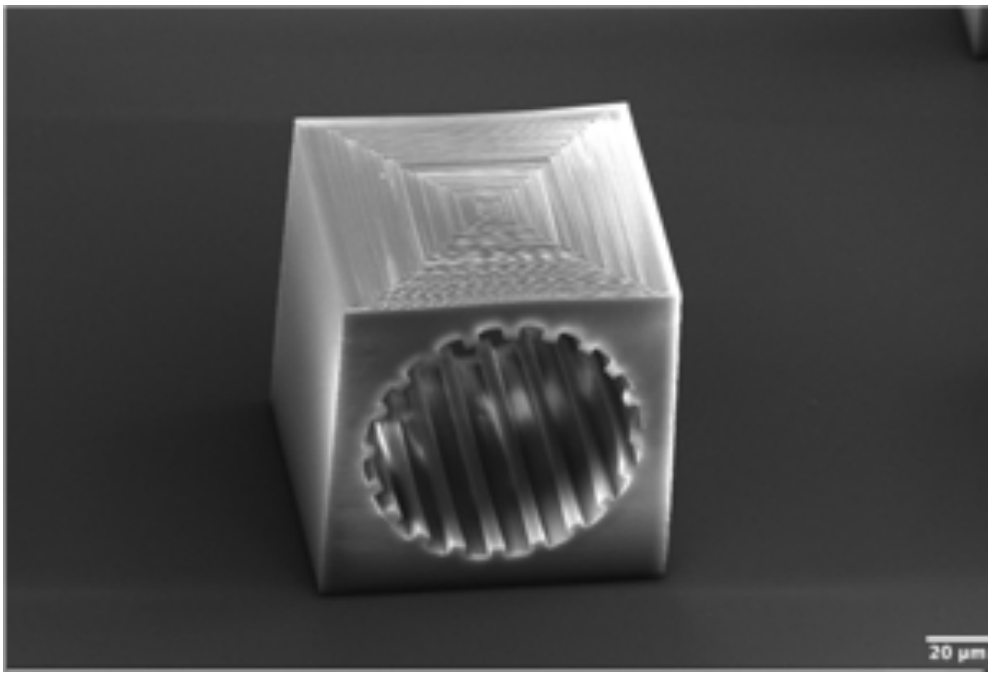

Figure 14: SEM image of the extrusion μhead fabricated with the fabrication strategy represented in Figure 13. Scale bar: 20 μm.

4.4 Conclusion and future perspectives

In this chapter gelatin tubular μscaffolds were fabricated with the Nanoscribe system and subsequently tested to evaluate their potentialities in the production of anisotropic μtissues. From the cell seeding results it was evident that the presence of a linear topography strongly enhances cell alignment and the consequent production of an oriented μtissue.

Starting from this proof of concept we tried to fabricate patterned gelatin μscaffolds on a suitable production scale for tissue engineering applications. To this end, microfluidic μextruder devices, based on the gel spinning

principle, were fabricated. Here an in-chip 3D lithography process was performed for positioning the extrusion μheads in the device. Our strategy successfully allowed the transfer of a simple topography on a gelatin fiber, proving the validity of our approach. In parallel, we have optimized the parameters for obtaining a AR variable gelatin emulsion in a T-junction device. Presently, we are working on the implementation of the extrusion μhead in the device for the massive production of patterned gelatin plug.

References

[1] S. M. Oliveira, R. L. Reis, and J. F. Mano, "Towards the design of 3D multiscale instructive tissue engineering constructs: Current approaches and trends," *Biotechnol. Adv.*, vol. 33, no. 6, pp. 842–855, 2015.

[2] J. W. Nichol and A. Khademhosseini, "Modular tissue engineering: Engineering biological tissues from the bottom up," *Soft Matters*, vol. 5, no. 7, pp. 1312–1319, 2010.

[3] F. Urciuolo, G. Imparato, A. Totaro, and P. A. Netti, "Building a tissue in vitro from the bottom up: Implications in regenerative medicine.," *Methodist Debakey Cardiovasc. J.*, vol. 9, no. 4, pp. 213–217, 2013.

[4] G. Imparato, F. Urciuolo, C. Casale, and P. A. Netti, "The role of microscaffold properties in controlling the collagen assembly in 3D dermis equivalent using modular tissue engineering," *Biomaterials*, vol. 34, no. 32, pp. 7851–7861, 2013.

[5] Y. Du, E. Lo, S. Ali, and A. Khademhosseini, "Directed assembly of cell-laden microgels for fabrication of 3D tissue constructs.," *Proc. Natl. Acad. Sci. U. S. A.*, vol. 105, no. 28, pp. 9522–7, 2008.

[6] A. Khademhosseini and R. Langer, "PERSPECTIVE A decade of progress in tissue engineering," vol. 11, no. 10, pp. 6–9, 2016.

[7] G. H. Lee, J. S. Lee, X. Wang, and S. H. Lee, "Bottom-Up Engineering of Well-Defined 3D Microtissues Using Microplatforms and Biomedical Applications," *Adv. Healthc. Mater.*, vol. 5, no. 1, pp. 56–74, 2016.

[8] Y. Morimoto, A. Y. Hsiao, and S. Takeuchi, "Point-, line-, and plane-shaped cellular constructs for 3D tissue assembly," *Adv. Drug Deliv. Rev.*, vol. 95, pp. 29–39, 2015.

[9] X. Shi, S. Ostrovidov, Y. Zhao, X. Liang, M. Kasuya, K. Kurihara, K.

Nakajima, H. Bae, H. Wu, and A. Khademhosseini, “Microfluidic spinning of cell-responsive grooved microfibers,” *Adv. Funct. Mater.*, vol. 25, no. 15, pp. 2250–2259, 2015.

[10] N. Annabi, A. Tamayol, J. A. Uquillas, M. Akbari, L. E. Bertassoni, C. Cha, G. Camci-Unal, M. R. Dokmeci, N. A. Peppas, and A. Khademhosseini, “25th anniversary article: Rational design and applications of hydrogels in regenerative medicine,” *Adv. Mater.*, vol. 26, no. 1, pp. 85–124, 2014.

[11] R. J. Mcmurtrey, “Patterned and functionalized nano fi ber scaffolds in three-dimensional hydrogel constructs enhance neurite outgrowth and directional control,” vol. 66009.

[12] H. Onoe and S. Takeuchi, “Cell-laden microfibers for bottom-up tissue engineering,” *Drug Discov. Today*, vol. 20, no. 2, pp. 236–246, 2015.

[13] Y. Yu, H. Wen, J. Ma, S. Lykkemark, H. Xu, and J. Qin, “Flexible fabrication of biomimetic bamboo-like hybrid microfibers,” *Adv. Mater.*, vol. 26, no. 16, pp. 2494–2499, 2014.

[14] C. N. Baroud, F. Gallaire, and R. Dangla, “Dynamics of microfluidic droplets,” *Lab Chip*, vol. 10, no. 16, p. 2032, 2010.

[15] Z. Bai, J. M. Mendoza Reyes, R. Montazami, and N. Hashemi, “On-chip development of hydrogel microfibers from round to square/ribbon shape,” *J. Mater. Chem. A*, vol. 2, no. 14, p. 4878, 2014.

[16] B. Wu, A. Kumar, and S. Pamarthy, “High aspect ratio silicon etch: A review,” *J. Appl. Phys.*, vol. 108, no. 5, 2010.

[17] U. Manual, “Photonic Professional,” no. September, 2013.

[18] P. Zhu and L. Wang, “Passive and active droplet generation with microfluidics: a review,” *Lab Chip*, vol. 17, no. online, pp. 34–75, 2017.

[19] P. Garstecki, M. J. Fuerstman, H. a Stone, and G. M. Whitesides,

"Formation of droplets and bubbles in a microfluidic T-junction-scaling and mechanism of break-up.," *Lab Chip*, vol. 6, no. 3, pp. 437–446, 2006.

[20] H. Liu and Y. Zhang, "Droplet formation in a T-shaped microfluidic junction," *J. Appl. Phys.*, vol. 106, no. 3, 2009.

[21] A. Gupta and R. Kumar, "Effect of geometry on droplet formation in the squeezing regime in a microfluidic T-junction," *Microfluid. Nanofluidics*, vol. 8, no. 6, pp. 799–812, 2010.

Chapter 5
Conclusions and future perspectives

In the first part of the thesis an overview of the main 3D micro-fabrication techniques for the production of instructive platforms for cell engineering application is provided, with special emphasis on the principles and main uses of the direct laser writing two-photon polymerization (DLW 2PP) process. The application of this technique to the fabrication of synthetic natural and nature derived hydrogel 3D structures is presented, highlighting its current limitations and potentialities. Special attention is devoted to the versatility of gelatin as biomaterial and its broad spectrum of applications, which is the core subject of this thesis. Indeed we further expanded gelatin use by proposing new approaches for the development of engineered platforms for specific cell culture applications.

In Chapter 2 we defined the composition of an in-house synthetized gelatin-based photoresist to fabricate complex and highly resolute microstructures with our 3D lithography system (Nanoscribe Professional GT); through addition of an azobenzene-based crosslinker, significantly fabrication improvements were observed. Finally, we characterized the polymerized gelatin that has shown physical properties compatible with many cellular applications in terms of elastic modulus and biodegradability. Because of the Nanoscribe laser wavelength (390 nm in the laser focus) we have used the low water-soluble Irgacure 369 as photoinitiator, which in turn has forced the use of an acid buffer solution as solvent. Even though the fabricated 3D constructs have not show cytotoxic effects, the employment of an acid solvent limits the use of the photoresist for some biological applications, such as for example the fabrication of cell laden constructs. To overcome this limitation a possible alternative strategy could be the use of crosslinking

thiolen-based reactions or other water soluble and more biocompatible photoinitiators with an appropriate TPA.

In Chapter 3 we developed a gelatin-based platform for the mechanical stimulation of cells. To this end a strategy in which cells were first precisely positioned and then exposed to mechanical stresses was developed. To control the cell position we used the Nanoscribe to introduce a novel topographic signal that strongly affected the cell adhesion process. Cells were mechanically stimulated by the light induced microstructure deformation due to the azobenzene crosslinker isomerization. To get a higher comprehension of the photo-deformation, the material mechanical properties were monitored after the light exposure revealing that a viscous deformation takes place, which in turn prevents the structures cyclical deformations; to address this issue, we think that the introduction of more elastic crosslinker moieties could be a suitable solution. However with our approach we were able to selectively deform living cells down to the single-cell level.

In Chapter 4 we fabricated gelatin cell-instructive building blocks for modular tissue engineering applications. These structures were indeed able to guide, with specific topographic patterns, the production of anisotropic oriented micro-tissue. To this end, first of all the Nanoscribe was used as a rapid prototyping technique to test the efficiency of the engineered modules. Finally, we tried to build up a droplet microfluidic device for the massive production of tubular gelatin patterned emulsions. More specifically, to pattern the gelatin surface, we performed an in-chip 3D lithography process to insert specific 3D extrusion micro-heads strategically positioned into the device; adopting this strategy a patterned gelatin fiber was obtained, while the process for the patterning of the gelatin emulsions is actually under development.

Engineering gelatin in combination with an extensive use of DLW-2PP technology has been shown to be a powerful method to specifically guide

cells and to explore cell-material interactions; however we think that there are still unexplored potentialities that can be developed to further control the material properties and, thus, enhance the platform performance.